St. Anthony Falls Hydraulic Laboratory
University of Minnesota
Mississippi River at Third Avenue S.E.
Minneapolis, Minnesota 55414

Project Report No. 255

INTAKE HYDRAULIC MODEL STUDY FOR THE ST. CLOUD HYDROELECTRIC PROJECT

by

John S. Gulliver

Warren Q. Dahlin

and

Judson Woods

Prepared for

Warzyn Engineering
Minneapolis, Minnesota

and

M. A. Mortenson Co.
Minneapolis, Minnesota

April 1987

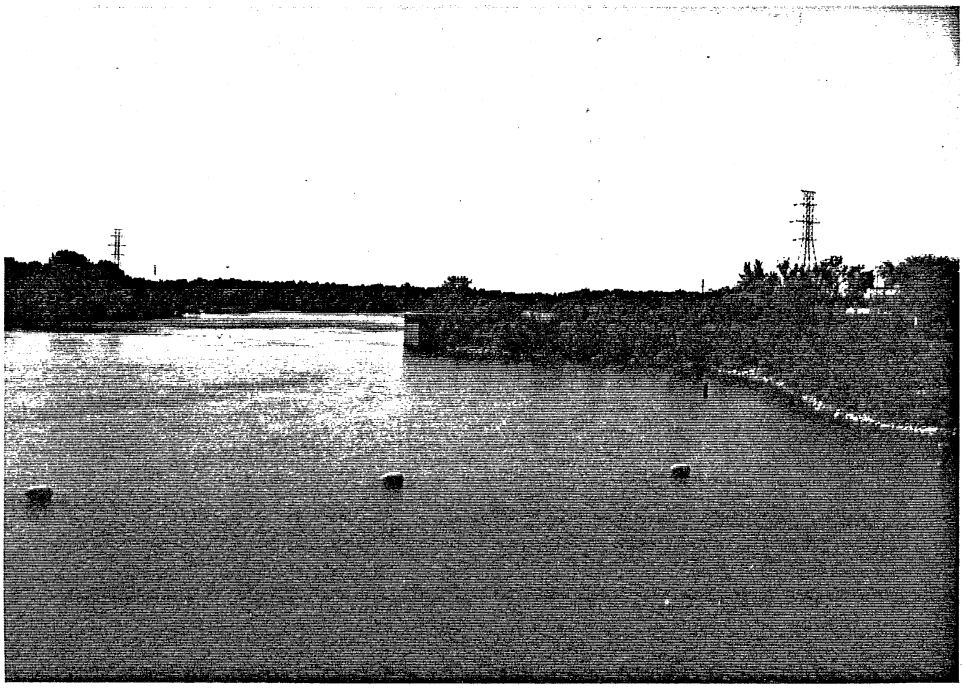

FRONTISPIECE 1

View from upstream showing the proposed location of the powerhouse on the right bank.

FRONTISPIECE 2

Type A9, Q_p = 6500 cfs, Q_{GS} = 3300 cfs, Q_{MS} = 3000 cfs, H.W. = 981 ft. The model showing the same area with powerhouse and gated spillway in operation.

TABLE OF CONTENTS

I. INTRODUCTION

This report describes a hydraulic model study of the intakes and related approach flow regions for the St. Cloud Hydroelectric Project. The study was conducted for Warzyn Engineering and the M. A. Mortenson Company. The hydroelectric facility will be composed of two 4-Mw pit turbine/generator units utilizing approximately 17 ft of head with a design flow of 3,250 cfs each. The objectives of the model study were as follows:

(1) Reduce head losses in the intake region to the extent economically feasible. With only 17 ft of head, any reduction in head losses would significantly increase plant output and income. The Mississippi River near St. Cloud is very shallow and wide. The transition from an approximately 6 ft deep channel to the 50 ft deep intakes was of special concern in the model.

(2) Intake vortices were a distinct possibility as indicated by the design guidelines of Gulliver, Rindels, and Lindblom [1]. Flow improvements in the hydraulic model study are a cost effective means of eliminating vortex problems.

(3) The pit turbine units each have a vertical generator pit separating the flow into two channels shortly after it enters the intake. The velocity distribution on both sides of the generator pit should be close to equal or the turbine will not operate efficiently. Velocity profiles taken in a hydraulic model can be used to determine this difference between the two sides of the generator pit, and indicate at an early stage if there will be difficulty in meeting the turbine manufacturer's guidelines. In addition, velocity profiles may be taken in the gate slots, at the same location as those which will be used for turbine acceptance. These velocity profiles may provide guidance for field acceptance, and resolve problems in the manufacturer's warranty.

II. CONCLUSIONS AND RECOMMENDATIONS

As a result of the hydraulic model study, the following conclusions and recommendations are made:

(1) The approach flow region should have additional excavation (dredging) to the topography given in Fig. 35, with dredging to El. 975, a 1:9.5 slope into the intake region, and a straight shoreline on the right bank.

(2) A submerged grid, shown in Fig. 9, is recommended as an anti-vortex device.

(3) It is recommended that the trashrack support beams be boxed in, as shown in Fig. 9. Although the improvement in headloss is small, the additional cost is probably not great. No additional streamlining is required for the trashrack support beams.

(4) Operation at headwater El. 979 is acceptable, considering the reservoir elevation will only be at this level for a small percent of the year. Significant bed erosion may occur when the gated spillway is open and the headwater is at El. 979. Riprap is therefore recommended near the large pier separating the gated spillway from the main spillway.

(5) Water surface flow-patterns for the final recommended design indicate a smooth approach flow without separation along the shoreline. With a full turbine discharge of 6,500 cfs, all velocities in the approach flow were below 5 ft/sec. When the gated spillway is open, surface flow is across the intakes from right to left. The flow into the intakes, however, is relatively straight at depths greater than 2 ft. If the surface flow in this region is perceived to be an operation problem, a slotted wall at the pier between the intakes and gated spillway is recommended.

(6) Surface flow patterns for the two flow conditions with the highest near-shore velocities are given in Figs. 51 and 52. These may be used for riprap design.

(7) With the recommended design, there is no measurable difference between the pressure heads (and intake headlosses) of one-unit versus two-unit operation, as indicated in Table 1. Before additional dredging was recommended (Type A9) the difference was between 0 (right unit) and 0.275 ft (left unit), or 1.6%, assuming a head difference of 17 ft across the turbines.

(8) The measured flow distribution and velocity profiles on the two sides of each generator pit were virtually identical, as shown

in Figs. 54 and 56. Velocities in the gate slots upstream, however, indicate that the flow is sensing the nose of the pit, slowing down directly in front of the pit, and dividing around either side of the pit, as shown in Figs. 57 and 58.

(9) Headlosses were calculated for the trashracks from measured flow angles and the literature because the trashracks were not included in the model.

(10) Estimated headlosses through the intakes are given in Table 2 for full design flow, and two additional flows which are anticipated to be close to those of the field acceptance test for the turbines. Most of the headloss occurs before the gate slots. These head losses are an upper limit of the true value, estimated by assuming the correction factor for velocity head is equal to 1.00.

(11) The model results were insensitive to the distribution of the flow into the diffusers.

(12) It is impossible for any model to perfectly simulate the topography of the full scale prototype because point measurements are an incomplete description of topography. This adds some uncertainty in transferring the model results to the prototype.

III. SITE CHARACTERISTICS AND FUTURE HYDROELECTRIC FACILITIES

The St. Cloud Dam MN 00506 is located on the Mississippi River within the City of St. Cloud, Minnesota, approximately 500 ft below the 10th Street Bridge, as shown in Fig. 1. The dam consists of a concrete, fixed crest spillway 19.5 ft high and 550 ft long centered on the river, as shown in Photo 1. It is flanked on the right bank by an earth embankment approximately 420 ft long with a top width of 28 ft and an elevation 12.5 ft higher than the spillway crest. Frontispiece 1 gives an upstream view of the earth embankment. On the left bank, a concrete wall and earth embankment extend from the spillway a distance of 200 ft to high ground. The top of the wall is 16 ft above the spillway crest. Training walls extend from the spillway crest to a point approximately 180 ft downstream, thus confining the width of flow to 550 ft immediately below the dam [2].

A plan view and typical cross sections of the existing dam are given in Figs. 2 and 3. The reservoir lies in a deep, wooded valley that varies in width from 500 to 1000 ft, and extends from the dam to a point 2.6 miles upstream. Water power was produced at the dam from 1882 until 1967, when the original powerhouse was taken out of commission. The present dam was constructed in 1972. The main component of the dam is the unregulated ogee spillway crest, shown in Photo 1 and Fig. 3. Located approximately 1-1/2 miles upstream from the dam is the water supply intake for the City of St. Cloud. Water supply and recreation are two of the major purposes of the dam at the present time. Photographs of the existing ogee spillway, earth embankment, and proposed powerhouse locations are given in Frontispiece 1 and Photo 1.

Plan and section views of the preliminary hydroelectric facility design are given in Figs. 4, 5, and 6. A powerhouse and taintergate spillway will replace the earth embankment on the west side of the river (Frontispiece 1 and 2). Headwater elevation will be maintained at El. 981 ft above msl when possible. Two ft high trip gates will be placed on the main spillway. After these gates trip, during floods, headwater elevation can go to El. 979 ft before the trip gates are reset.

The mean velocity in the intakes will vary from approximately 3 ft/sec through the trashracks to 10 ft/sec just before the end of the generator pit.

IV. HYDRAULIC MODEL DESIGN, CONSTRUCTION, AND CALIBRATION

The intakes and upstream section were modeled with Froude scaling, which is based upon the ratio of inertial and gravity forces.

$$F_r = \frac{V_m}{\sqrt{gL_m}} = \frac{V_p}{\sqrt{gL_p}}$$

where Fr = Froude number,
V_m = velocity in the model,
V_p = full scale velocity, corresponding to V_m.
g = acceleration due to gravity,
L_m = a length in the model, and
L_p = full scale length, corresponding to L_m.

If the scale is not distorted, L_m/L_p is a constant value equal to the model scale at every location. The model scale of the St. Cloud Hydroelectric Project is 1:24, meaning that 1 inch in the model corresponds to 2 ft in the prototype.

The size (or scale) of the model was determined such that other forces, such as friction, do not significantly alter the results, e.g. produce scale effects. The criteria to be used were recently reviewed by Lindblom [3], who concluded the following:

(1) To avoid viscous scale effects on intake vortices, the intake height must be greater than 5 inches [4], and the radial Reynolds number, $Q/\upsilon S$), should be greater than 10^5. Here, Q is discharge (ft^3/sec), υ is kinematic viscosity of the water (ft^2/sec), and S is intake submergence (ft). When no vortices are present, such as after modifications to the intake, the radial Reynolds number may be as low as 10^4 [4]. The radial Reynolds number for the St. Cloud model was approximately $1.5x10^5$. The vertical opening of the intakes was 12 inches.

(2) To avoid scale effects due to surface tension, the Weber number, $W = \rho V^2 D/\sigma$, should be greater than 600 [4]. If there are no intake vortices, however, no scale effect due to surface tension has been observed at Weber numbers as low as 100 [4]. Here, ρ = liquid density, V = velocity in the intake throat, D = throat diameter, and σ = surface tension of the liquid. D = 4 times the hydraulic radius may be used if the throat is not circular.

For the St. Cloud model, the Weber number was approximately 370. Which is acceptable because any free surface intake vortices will be eliminated.

(3) The Reynolds number in the approach flow should be greater than 10^4 at all locations to avoid laminar flow and properly simulate the approach flow. Here $Re = 4Vh/\upsilon$, where V = velocity, and h = depth, each taken at the same location. The depth at the upstream end of the excavation region is shallow in the prototype, between 1 ft and 6 ft. The velocities are approximately 5 ft/sec. This shallow depth dictated the 1:24 scale of the model, which corresponds to an upstream depth of between 0.5 and 3 inches, and an approximate velocity of 1 ft/sec. The upstream Reynolds number in the model varied between 1.6×10^4 and 10^5 according to preliminary calculations.

The 1:24 scale and the available space meant that half of the existing spillway could be included in the model. This is shown in Fig. 7, where the model outline is juxtaposed on a site plan. It was felt that this would be sufficient if the flow was properly distributed around the outside of the model. Measurements were to be taken only in the region near the intakes, and all that was desired of the remainder of the basin was an approach flow that adequately simulated the prototype.

A proper distribution of the flow was accomplished by placing two diffuser pipes on the outside of the model basin, as shown in Fig. 4. An electric analogue was used to determine the distribution of flow into the two pipes. The outline of the channel is painted on conductive paper with a silver paint which has no significant resistance to electricity. A voltage is then applied is applied between the two banks of the channel, and the voltage increments in between indicate flow streamlines. The electric analogue assumes a frictionless flow in a channel of constant depth, and does not work well near the intake. It is a relatively good approximation for the flow in the center of the stream under various operating conditions. Fig. 7 gives the results of the electric analogue with all of the flow going through the powerhouse and gated spillway. This figure was used to determine that in this operating condition, 60% of the flow should be through the upstream diffuser and 40% through the side diffuser. This 60-40 distribution is slightly more conservative than the 70-30 distribution indicated by the electric analogue, the reason being that the actual depth increases towards the side diffuser. With the main spillway in full operation, 100% of the flow was distributed through the upstream diffuser.

The powerhouse was constructed to the 1:24 model scale according to drawings provided by Warzyn Engineering, which are partially duplicated on Figs. 5 and 6, and show the extent of the powerhouse modeled. The powerhouse was fabricated in the Laboratory shop mostly from transparent sheet plastic, as shown in Photo 2. The transparent plastic or lucite is readily machined to close tolerances, and flow conditions inside the structure can be observed. The invert of the powerhouse is at elevation 938.85 ft, the crown at elevation 963.15 ft, and the top of the structure at 995.0 ft (Fig. 6). In Photo 2 the trash rack support beams and upstream ends of the generator-turbine housings can be seen. The powerhouse was provided with pressure taps and velocity ports at locations

numbered 1 through 14 in Figs. 5 and 6. The completed powerhouse was taken to the model area and installed as shown in Photo 3 and Fig. 4. The gated spillway (with gates provided) and main spillway were modeled up to the crests as shown in Fig. 4.

The topographic features upstream of the structure were molded of non-erodible lightweight concrete to the contours shown on Fig. 4. These contours were derived from information provided by Warzyn Engineering. Most of the information was from previous projects in the same area. To better define the area immediately upstream of the powerhouse and gated spillway, soundings were taken in the Mississippi River by Warzyn, along the right bank between the bridge and proposed structure. The soundings showed that considerable deposition had occurred in this area and the model was molded accordingly. This area is from elevation 975 to 981 ft along the right bank as shown in Fig. 4. This area was previously thought to be all at El. 975 ft. Sheet metal templates were cut to the contours and anchored to the floor at intervals of 2 or 4 ft depending on the complexity of the topography. As the model is over 2 ft high, fill material such as blocks and sand was placed between the templates up to about 2 inches below the final contours. The final 2 inches of the model was then molded from the lightweight concrete, as shown in Photo 3. The cementing was done in alternate strips so the construction could continue without interruption, as indicated by the different shadings in Photo 3. After the cementing was completed and cured, a coat of paint was applied, completing the model, as shown in Photo 4. Bridge piers were placed in the model showing the location of the bridge with respect to the dam (Photo 4).

Photos 5 and 6 show the installed powerhouse and gated spillway, and the riprap protected area immediately upstream. The 12 inch size riprap to be used in the prototype was represented by one-half inch material in the model. A 6 inch manifold was placed along the left side of the model basin and a 12 inch manifold along the upstream end of the basin, as shown in Fig. 4. Both were connected to the Laboratory's water supply for a continuous flow. Each manifold contained a flow control valve and orifice meter so that the flows could be adjusted individually to the specified distribution for each manifold. The 6 inch manifold contained a 4 inch orifice meter, and the 12 inch manifold an 8 inch orifice. Both were calibrated before installation by utilizing the Laboratory's weighing tanks, which have an accuracy of about 0.25 percent. Each manifold was provided with a series of holes along the upstream side for the water to be discharged. Over each hole an adjustable metal flap was provided so the flow adjustments could be finely tuned. Deflector plates were placed along both manifolds to direct the flow into the model, and mesh baffle was placed along the upstream 12 inch manifold to further reduce the turbulence and eliminate crossflow, as shown in Fig. 4.

The model was then put in operation, as shown in Photo 7. The first procedure was to calibrate the model. In the absence of prototype flow information, the flow into the model was adjusted to be slightly more conservative than the flow distribution determined in the electric analog study presented in Fig. 7 and described earlier. This was accomplished by

adjusting the flow in the two manifolds, the sliding plates over the exit holes in the manifolds, the deflectors, and the mesh baffle. Adjustments were made and the flow patterns visually observed by paper confetti thrown on the water surface. After a series of these adjustments, an acceptable flow pattern was achieved and the model testing program initiated.

V. FLOW IMPROVEMENT STUDY

The flow improvement study proceeded from the upstream towards the downstream end of the model, with cost effective improvements to the flow. Flow improvements which required a major change in the model were performed last.

Three design flow conditions were considered to be important for the flow improvement study, all at reservoir elevation 981 ft msl:

(a) Powerhouse only at full design flow, Q_p = 6,500 cfs.

(b) Powerhouse (Q_p) and gated spillway (Q_{GS}) at full design flow.

(c) Powerhouse (Q_p) gated spillway (Q_{GS}), and existing main spillway (Q_{MS}) at full design flow.

The full design flow of the gated spillway and main spillway will vary somewhat, depending upon angle of approach flow.

The following flow visualization techniques were utilized as desired throughout the flow improvement study:

(1) Photographs and observation of the water surface, illustrating any potential flow problems such as separation zones, surface waves, and vortices.

(2) Time-exposure photography of surface particles to give streaklines. These streaklines were used in a qualitative manner to indicate where high flow velocities were located. The photos from directly overhead were also used to measure surface flow velocities.

(3) Dye was released from various points in the flow field to indicate flow problems which are not apparent from visualization of the water surface.

(4) Yarn placed on the end of a point gage was used to indicate the angle of the flow, and observe any unusual turbulence in the flow such as that produced by a separation zone.

In addition, the following measurements were made as desired throughout the flow improvement study and documentation of final design.

(1) Water surface profiles were taken upstream. The location of the profiles taken are given on Fig. 8. Three profiles were taken across the front of the powerhouse, profiles A-A, B-B, and C-C.

One profile was taken directly out from the powerhouse, profile D-D, up to the bridge.

(2) Headwater pressure was measured at a location upstream of the intake on the far side of the large pier as shown in Fig. 4. In addition, the water surface was set in a stilling well at this location to be either El. 981 or 979.

(3) Pressures were measured at 14 locations inside the intakes, as shown in Fig. 5 and 6. Pressure taps 1 and 14 were located upstream of the gate slots, in the side walls. Taps 2, 5, 8, and 11 were located in the intake roof, upstream of the gate slots. Taps 3, 6, 9, and 12 were located in the intake roof, just after the flow splits around the generator pit. Taps 4, 7, 10, and 13 are located towards the end of the pit, just upstream of the turbine, near the end of the model. The large number of pressure taps was required to indicate any difference in head due to a poor distribution of flow. The pressure taps were connected to a manometer bank to give steady state pressure readings. Each reading is accurate to ± 0.1 ft in the full scale prototype. The three pressure measurements of one bay, however, may be compared with the same measurements of a previous run to approximately ± 0.06 ft, assuming that the difference in pressure readings are all caused by the same event, such as an improved inflow condition. The six pressure measurements of one unit may be similarly compared with a previous run to approximately ± 0.04 ft. All pressure measurements and comparisons are accurate to ± 0.1 ft except where noted.

(4) Velocities were measured at the tail end of the generator pit, very near pressure taps 4, 7, 10, and 13, by means of a pitot tube. These velocity measurements are accurate to ± 0.3 fps. The mean of the velocity measurements in each bay is accurate to ± 0.09 fps.

(5) Velocities and the direction of flow were also measured at the gate slot, because this is the location of velocity measurements for the field acceptance tests of the turbine/generator units. These velocities were measured with a Marsh-McBirney two-component electromagnetic flow meter, accurate to within 2%.

Because the velocity profiles are only taken in the center of each pit, they could not be used to estimate the velocity head available at that location. The velocity head is given by

$$a\ V^2/2g$$

where V = cross-sectional mean flow velocity (ft/sec)
$= Q/A$
Q = flow rate (ft^3/sec)
A = cross-sectional area (ft^2)
g = acceleration of gravity (ft/sec^2), and
a = a velocity correction factor.

$$a = \frac{1}{A} \int_A \left(\frac{v}{V}\right)^3 dA$$

where v = local velocity.

It is anticipated that the correction factor, a, is between 1.05 and 1.25. This cannot be determined from the velocity measurements in the pit. The correction factor, a, will be assumed to be 1.0, giving an estimate of the minimum velocity head at each location. Head losses are determined by subtracting the pressure head and velocity head at a given location from the water surface elevation in the stilling well upstream on the far side of the large pier. Thus, head losses estimated herein are an upper limit of the true value.

A. Type A, Original Design

The original design is shown in Photos 4, 5, and 6, and in Figs. 4, 5, and 6. The overall flow in the model is shown in Photo 7. The most detrimental characteristic of the flow was the high velocities and separation zones in the approach to the excavated region. This is shown in Photo 8, where surface tracers and time exposure photography are used to indicate velocities. The high velocities across the large pier to the left and the separation zone (with backflow) in the foreground are apparent. Not as apparent in the photo, but very visible in the model, are intake vortices in the right corner of each intake. These vortices would intermittently pull trash from the water surface into the intake. They would not be classified as an air core vortex, the most severe, but may cause some loss of turbine performance and intake clogging problems.

Photo 9 shows another ramification of the high approach velocity: surface waves (and associated head loss) at the beginning of the excavation region caused by a rapid transition from a high velocity to a lower velocity.

B. Type A1. Reduced Pier Noses

Before documentation of Type A was complete, Warzyn Engineering and M. A. Mortenson decided to reduce concrete volume by cutting back and stoping the piers separating the intakes. This is shown in Fig. 9, where the new pier noses are slightly tilted back, rather than vertical. The measurements for flow conditions a), b), and c) are documented in Figs. 10 through 17 and in the first three rows of Table 1. Figs. 10, 13, and 16 indicate a water surface drawdown in the approach flow region that was particularly severe for conditions b) and c), when the gated spillway was open. The velocity profiles, shown in Fig. 12, are fairly uniform except that there are higher velocities in the leftmost bay . Surface velocities for the worst condition, (b): powerhouse and gated spillway, are shown in

Fig. 15. This indicates relatively high velocities away from the powerhouse near the large pier, and low velocity, recirculating flows near the shoreline. The reason for the high velocities is the shallow depth of the reservoir and the recirculating zone, which eliminates approximately one-third of the cross-section for flow entering the intakes.

Head loss was estimated, as mentioned earlier, by the relation

$$\text{Headloss} = \text{Headwater Elevation} - \text{Pressure Head} - \frac{V^2}{2g}$$

Figure 11 and Table 1, row 1 indicate that the headloss with only the turbines in operation (excluding trash racks) was 0.46 ± 0.07 ft in the right unit (Bays 1 and 2) and 0.66 ± 0.07 ft in the left unit (Bays 3 and 4).

C. Type A2, Sloped Excavation

In an effort to eliminate some of the headloss and flow problems, a sloped rather than abrupt transition in the excavated region was installed. This would reduce the required excavation, so any benefit would be an added plus. The revised geometry is given in Fig. 18, where a 1:9.5 slope replaces a horizontal excavation zone with a 1:2 slope at the upstream end. The water surface profiles are given in Figs. 19, 20, and 21. The improvement in water surface elevation over Type A1 is small (within the measurement error). Photo 10 gives the flow pattern and indicates that the surface waves, although reduced somewhat, were still present.

D. Type A3, Trashrack Support Beams Removed

In order to determine the headloss created by the trashrack support beams, they were removed. Measurements then taken were compared with those of Type A1, the difference being attributed to a decrease in headloss. Pressure and velocity measurements are given in Table 1, row 4 and Fig. 22. Some pressure head measurements were 0.1 ft higher and some velocity measurements were slightly higher than those in Table 1, row 1 and in Figs. 11 and 12. Although small, the trend in measurements was always in the same direction and averaged 0.05 ± 0.03 ft. The difference in head was small because the flow into the intake was fairly straight, and nearly normal to the supports (normal to the top of the I).

E. Types A4, A5, and A6, Anti-Vortex Devices

Although difficult to identify in the photographs, intermittant, trashpulling intake vortices were observed in the model. Three separate anti-vortex devices were used in an attempt to eliminate these vortices, and all three were successful. They are shown together in Fig. 9.

Type A4 is with the installation of a curtain wall across the front of the intake piers to El. 977. Pressure and velocity measurements of this type are given in Table 1, row 5 and Fig. 23.

Type A5 is the installation of an 11 ft wide horizontal hood above the intakes at El. 977. Pressure and velocity measurements are given in Table 1, row 6 and Fig. 24.

Type A6 is a submerged grid, fixed at a bottom elevaton of 975. The grid has 1 ft x 1 ft spacings, is 1 ft high, and 10 ft long. Pressure and velocity measurements for this device are given in Table 1, row 7 and Fig. 25.

All of the anti-vortex devices eliminated the intermittent trashpulling vortices at a headwater elevation of 981. The trend in headloss for all three devices appears to be a reduction by 0.09 ± 0.03 ft in Bay 1, by 0.041 ± 0.03 ft in Bay 2, by 0.1 ± 0.03 ft in Bay 3, and an increase by 0.13 ± 0.03 ft in Bay 4. At a headwater elevation of 979, however, intake vortices were present for both the curtain wall and the hood. Thus, the submerged grid was chosen as the anti-vortex device to be used in the remainder of the model test program, and is recommended for the prototype. The flow is shown in Photo 11. The performance of the submerged grid was not visibly affected when an opening of 2 ft was left for an automatic trashrack cleaning device.

F. Types A7 and A8, Comparison of Unboxed and Boxed Trashrack Support Beams

It was believed that the unboxed trashrack support beams, shown in Fig. 9, would create a headloss due to interaction of the fluid inside the I-section with the flow into the intake. Type A7, I-beam supports, and Type A8, boxed beam support were compared because the incremental cost of boxing in the beams was small. Table 1, rows 8 and 9, and figures 26 and 28 also indicate that the benefits are not great. The small improvement in both pressures (taps 10 and 12) and velocities, however, was deemed sufficient to propose boxed trashrack support beams for the prototype. Overall, the improvement was 0.03 ± 0.03 ft in reduced headloss. The boxed support is indicated by a dashed line in Fig. 9. It was previously anticipated that more streamlining of the beams may be required. This, however, was not the case. Each of the remaining flow improvements include a boxed trashrack support beam.

G. Type A8, Further Documentation, Including Two-Unit versus One-Unit Performance

The measurements taken on Type A8 are given in Table 1, rows 9 through 13 and Figs. 27 through 34. Of particular interest is a comparison of row 9 with rows 12 and 13, relating to the two-unit versus one-unit guarantee for the type A8 design. There is no measureable difference (± 0.07 ft) in headloss with the right unit operating (Bays 1 and 2) versus both units. With the left unit operating (Bays 3 and 4), there is approximately 0.275 ± 0.07 ft less of headloss with one unit operating than with two. If we assume a headwater-tailwater difference of 17 ft, the difference would be between 0% (right unit) and 1.6% (left unit).

H. Type A9, Increased Excavation in the Flow Approach Region

The most obvious flow problem in the hydraulic model study was the high velocities in the reservoir prior to the excavated zone. This was caused primarily by the separation behind the point on the shoreline, (just upstream of the proposed riprap), and by the shallow water depths upstream of the excavation zone. These high velocities are the reason for the surface waves and some of the headlosses in the flow approach region. This flow improvement was saved until the end of the study because it required that the model morphology upstream be altered, which requires, in turn, that the model be dry for at least one week.

The flow improvement was accomplished by eliminating the point on the shoreline upstream of the excavation zone and by increasing the excavation to El. 975 upstream to the bridge. This is shown in Fig. 35, and Photo 12. The additional zone of excavation is within the rope line in Photo 12.

Water surface flow patterns are shown in Photos 13, 14, and 15 for the powerhouse operating at design flow. The separation zone near the shoreline has been eliminated. There is still a separation zone behind the large pier, and flow from right to left across the front of the powerhouse. This flow from right to left occurs only at the surface. Below a depth of 2 ft, the flow is straight into the intakes. It would be expensive to eliminate the separation zone behind the large pier in the prototype. This was not attempted since no operation problem associated with this flow could be identified.

The measurements are documented in Table 1, rows 14, 15, and 16, and in Figs. 36 through 41. The improvement in water surface levels (ultimately less headloss) can be seen by comparing Figs. 27 with 36, Figs. 29 with 38, and Figs. 31 with 40. The improvement is approximately 0.2 ft with only the powerhouse operating and 0.4 ft with the powerhouse and gated spillway in operation. The flow over the gated spillway has increased by 300 cfs because of the higher water surface. The flow over the main spillway has increased by 600 cfs because the crossflow velocities on the spillway as the flow approached the powerhouse have been significantly reduced.

With the powerhouse alone operating, the pressure heads at the tail end of the generator pit had previously varied from El. 979.2 to 979.6 from left to right bay, as can be seen from Table 1, row 9. In the A9 improvement, this has been improved to a range of 979.4 to 979.6, a maximum difference of only 0.2 ft. This is an indication that the flow will be evenly distributed around the generator pits and between each turbine/generator unit. The same is true for the other flows tested, as can be seen from Table 1, rows 15 and 16. In addition, there is no significant difference between the velocity profiles given in Figs. 37, 39, and 41. All are fairly uniform, within the measurement accuracy of the pitot tube.

VI. DOCUMENTATION OF RECOMMENDED DESIGN

A. Sensitivity to Flow Distribution in Diffuser System

The sensitivity of the results to flow distribution between the two diffusers was tested. Originally, the flow split was 60% in the upstream diffuser and 40% in the side diffuser. The 40% represents flow coming from the portion of the river channel not included in the model. Two additional flow distributions were chosen for a sensitivity case: a 40-60 and a 20-80 split between the upstream and side diffusers, respectively. The 20-80 distribution is the absolute worst case, assuming the specific discharge (discharge per unit width) is linearly proportional to depth right up to the main spillway. In other words, the 20-80 distribution assumes no increase in velocity on the west bank due to the draw of the hydropower facility.

Table 1, rows 17 and 18, and the measurements on the two additional flow distributions are given in Figs. 42 through 45. They show no measurable difference between the 40-60 sensitivity test and the chosen 60%-40% flow distribution. A small difference, a mean of 0.07 ± 0.03 ft, was noticed between the 20-80 sensitivity test and the chosen 60-40 flow distribution. Thus, the model results are fairly insensitive to even this extreme flow distribution.

B. Operation at Lower Headwater Elevation

In the normal mode of operation, the headwater elevation would go down to El. 979 when the trip gates on the spillway are being reset. For this reason, the model was run at a headwater elevation of 979. Photos 16 through 18 compare the water surface flow patterns without and with the gate spillway in operation. Some surface waves are apparent in Photo 16, but these are not considered to be significant for hydroplant operation. In Photo 18, the surface waves are much larger because the flow upstream is close to critical. Supercritical upstream flow with the corresponding hydraulic jump were noted at slightly lower elevations. It is likely that some bed erosion may occur at headwater El. 979 with the gated spillway in operation. This may be of importance near the large pier, where riprap will be required.

Water surface profiles and pressure measurements are documented in Table 1, rows 19 and 20, and Figs. 46 through 47. These show no unexpected results that would affect hydroplant operation. Measurements indicate 0.25 ± 0.07 ft of additional headloss in the left unit with only the powerhouse in operation, and somewhat more with the gated spillway and the powerhouse in operation.

C. Water Surface Flow Patterns and Velocities

Water surface flow patterns and velocities were measured for the three test conditions near the intake, as shown in Figs. 48, 49, and 50. These were taken from time exposure photographs of particles on the water surface. Velocities were measured by taking the distance traveled from a particle streak and dividing by the exposure time. The surface flow direction and velocities should be fairly representative of the flow at other depths except very near the intakes, where the surface flow is across the intakes from right to left and flow at greater depths (2 ft or more) is directly into the intake.

Under normal operation, Q_p = 6,500 cfs, as indicated in Fig. 48, velocities in the approach flow were all below 5 ft/sec. In fact, there was only a small region where velocities were greater than 5 ft/sec. The large separation zone near the shoreline has been eliminated, and there is only one small separation near the cellular walls, which is to be expected. A comparison of Fig. 49 and Fig. 15, under similar flow conditions, indicates the vast improvement in flow due to the additional excavation (A9). The large region of velocities greater than 6 ft/sec in Fig. 15 has been reduced to a relatively small region flowing over the gated spillway in Fig. 49. Figure 50 indicates that the flow near the powerhouse does not change greatly with flow over the main spillway.

No operational problem has been identified which would be caused by the surface flow across the front of the intakes, from right to left. If an operational problem is identified, this surface crossflow can be greatly reduced with a 10 ft slotted wall placed to El. 977; parallel to the pier between the gated spillway and the powerhouse as shown in Photo 21. The slotted wall is composed of alternating vertical boards, 1 ft in width, with 1 ft of opening, for a porosity of 50%.

Time exposure photos were also taken upstream to be used for riprap design. An example is given in Photo 19. These photos were of the operation which gave the highest velocities in the shoreline region. Figure 51 gives surface velocities at headwater El. 981 with flow through the powerhouse and over both spillways. Figure 52 gives water surface velocities at headwater El. 979 with flow through the powerhouse and over the gated spillway.

D. One-Unit versus Two-Unit Operation

Measurements taken on the right and left turbine/generator units operating individually are given in Table 1, rows 21 and 22, and figs. 53 through 56. The water surface streaklines, given in Photo 20, indicate a smooth approach flow. The data of these figures should be compared with that of Table 1, row 14 and Figs. 36 and 37, to indicate the expected performance of one unit versus two units. The water surface is drawn down approximately 0.3 ft more in front of the intakes with both units in operation, and the pressure head at the tail end of the generator pits is between 0.1 ft and zero ft lower for both units in operation as can be seen by comparing taps 4, 7, 10, and 13 in Table 1, rows 14, 21, and 22 The velocity head for the three cases would be equivalent. Thus, within the accuracy of measurements, $\pm$ 0.1 ft, there is no difference in the upstream head available for two unit versus one unit operation.

E. Velocities and Flow Distribution around Generator Pit

Velocities at the tail end of the generator pits were measured along the centerline of each flow channel, and are not a complete representation of the entire cross section. However, it is seen from Figs. 54 and 56 that these velocity profiles are virtually identical on each side of the generator pit. This is a strong indication that the flow is properly distributed and relatively uniform on the two sides of the pit. The difference in mean velocity between the two sides of each pit were only 0.02 ± 0.09 ft/sec.

Velocities were also measured in the gate slots upstream with a two-component electromagnetic flow meter to indicate what flow velocities and directions could be expected in the field acceptance tests of the prototype. The results, given in Fig. 57 and 58 for each unit, indicate that the flow is sensing the nose of the pit, slowing down directly in front of the pit, and dividing around the pit on each side. Flow angles as great as 32° were found at one location near the bottom of the intake in each unit. *The flow angles in the gate slots are significantly greater than those in the intake, which are given in Fig. 59.*

F. Operation at Partial Turbine Discharge

Pressure head was measured at single unit discharges of 2,120 cfs and 1,300 cfs, the approximate discharge of field acceptance tests in the prototype. They are given in Table 1, rows 23 through 26. All measurements were as expected.

G. Trashrack Head Losses

The trashracks were not included in the model because the head losses are not likely to scale properly (spacing of 3-3/4 inch prototype and .156 inch model) from model to prototype. The headloss is therefore calculated from velocity and flow angle across the trashrack herein. The velocity across the trashracks is assumed to be uniform, 3.72 ft/sec for full turbine discharge. The angle of the approach flow was measured from yarn, accurate to ± 1.0°, and is given in Fig. 59. Headloss coefficients for the trashracks were taken from Idelchik [5], and doubled because velocity is not uniform but is actually accelerating into the intake. The headloss is then given as

$$h_L = 2k\ V^2/2g$$

where k = headloss coefficient, taken as the weighted average of those across the trashrack, with a uniform velocity,
V = Q/A
A = cross-sectional area, and
Q = discharge.

Across the right unit, calculations give 2k = 0.489. Across the left unit, calculations give 2k = 0.652. Headloss at full discharge (Q = 3,250 cfs) is therefore approximately 0.105 ft for the right unit and 0.140 ft for the left. The headloss is greater in the left unit because the angles of flow across the trashracks are generally greater.

H. Headloss through Intakes

The total headloss through the intakes was calculated based upon the pressure head elevations measured in the model study and the trashrack headloss calculated in Section VI.G. Thus, estimated headloss at each location is

$$h_L = \begin{matrix}\text{headwater} \\ \text{elevation}\end{matrix} - \begin{matrix}\text{pressure head} \\ \text{elevation}\end{matrix} - a\frac{V^2}{2g} + \begin{matrix}\text{calculated trashrack} \\ \text{headloss}\end{matrix}$$

where a = 1.0 was used for these estimates. A slightly higher 'a' value would result in less headloss. These figures are therefore conservative, and the head loss estimate should be slightly high. The headloss from the headwater to the locations behind the trashracks, behind the gate slots, and at the tail end of the pit (Figs. 5 and 6) are given in Table 2. This table indicates that most of the headloss occurs befor the first pressure taps, located behind the trashracks.

VII. REFERENCES

1. Gulliver, J. S., A. J. Rindels, and K. C. Lindblom, "Designing Intakes to Avoid Free Surface Vortices," International Water Power and Dam Construction, Vol. 38, September 1986.

2. U. S. Army Corps of Engineers, St. Paul District, "Mississippi River Dam, St. Cloud, National Dam Safety Program Inspection Report," Dept. of Natural Resources, State of Minnesota, 1978.

3. Lindblom, K. L. C., "Hydraulic Modeling Techniques for Intake Vortices," M.S. Thesis, University of Minnesota, Minneapolis, MN, 1987.

4. Cambell, N. J., "Modeling Free Surface Vortices in Vertical Pumping Pits," M.S. Thesis, Utah State University, Logan, Utah, 1983.

5. Idelchik, I. E., "Handbook of Hydraulic Resistance," Hemisphere Publishing, Second Edition, 1986.

TABLE 1. Full scale piezometric pressure heads from measurements taken in hydraulic model

Row	Type	HW Elev.	Q_{PL} cfs	Q_{PR} cfs	Q_{GS} cfs	Q_{MS} cfs	Right Wall Tap 1	Bay 1 2	Bay 1 3	Bay 1 4	Bay 2 5	Bay 2 6	Bay 2 7	Bay 3 8	Bay 3 9	Bay 3 10	Bay 4 11	Bay 4 12	Bay 4 13	Left Wall Tap 14
1	A1	981	3250	3250	0	0	980.4	980.4	979.8	979.5	980.4	979.8	979.5	980.1	979.4	979.3	980.3	979.4	979.3	980.3
2	A1	981	3250	3250	3000	0	980.4	980.3	979.7	979.5	980.3	979.7	979.5	980.0	979.5	979.4	980.4	979.5	979.3	980.4
3	A1	981	3250	3250	3000	2400	980.0	979.9	979.3	979.1	979.9	979.3	979.1	979.8	979.2	979.2	980.2	979.2	979.1	980.1
4	A3	981	3250	3250	0	0	980.6	980.5	979.8	979.6	980.6	979.8	979.6	980.1	979.4	979.3	980.2	979.5	979.2	980.3
5	A4	981	3250	3250	0	0	980.6	980.6	979.9	979.7	980.6	979.8	979.7	980.2	979.5	979.4	980.4	979.6	979.4	980.3
6	A5	981	3250	3250	0	0	980.7	980.5	979.9	979.7	980.6	979.9	979.7	980.2	979.5	979.4	980.4	979.6	979.3	980.4
7	A6	981	3250	3250	0	0	980.6	980.6	979.9	979.7	980.6	979.8	979.7	980.2	979.5	979.4	980.3	979.6	979.3	980.3
8	A7	981	3250	3250	0	0	980.6	980.5	979.8	979.6	980.5	979.8	979.6	980.1	979.3	979.2	980.2	979.4	979.2	980.3
9	A8	981	3250	3250	0	0	980.6	980.5	979.8	979.6	980.5	979.8	979.6	980.1	979.3	979.4	980.2	979.5	979.2	980.3
10	A8	981	3250	3250	3000	0	980.6	980.4	979.8	979.5	980.4	979.8	979.5	979.9	979.2	979.3	980.3	979.3	979.2	980.4
11	A8	981	3250	3250	3000	2400	980.0	979.9	979.2	979.1	979.9	979.2	979.1	979.8	979.2	979.2	980.1	979.2	979.1	980.2
12	A8	981	0	3250	0	0	980.5	980.4	979.9	979.6	980.4	979.8	979.6	—	—	—	—	—	—	980.7
13	A8	981	3250	0	0	0	980.9	—	—	—	—	—	—	980.4	979.7	979.6	980.4	979.7	979.5	980.5
14	A9	981	3250	3250	0	0	980.6	980.5	979.8	979.6	980.4	979.9	979.6	980.3	979.5	979.5	980.3	979.6	979.4	980.5
15	A9	981	3250	3250	3300	0	980.7	980.5	979.8	979.7	980.5	979.9	979.7	980.3	979.6	979.6	980.6	979.7	979.6	980.6
16	A9	981	3250	3250	3300	3000	980.5	980.3	979.7	979.5	980.2	979.7	979.5	980.2	979.5	979.5	980.4	979.6	979.4	980.5
17	A9*	981	3250	3250	0	0	980.6	980.5	979.8	979.6	980.4	979.8	979.6	980.3	979.6	979.5	980.4	979.6	979.4	980.5*
18	A9**	981	3250	3250	0	0	980.6	980.5	979.9	979.7	980.5	979.9	979.7	980.3	979.6	979.6	980.4	979.7	979.4	980.5**
19	A9	979	3250	3250	0	0	980.6	978.5	977.7	977.6	978.4	977.8	977.6	978.1	977.4	977.2	978.2	977.5	977.2	978.3
20	A9	979	3250	3250	2200	0	980.5	978.4	977.7	977.4	978.4	977.7	977.5	977.9	977.2	977.1	978.2	977.3	977.1	978.2
21	A9	981	0	3250	0	0	980.5	980.4	979.7	979.5	980.3	979.8	979.6	—	—	—	—	—	—	980.8
22	A9	981	3250	0	0	0	980.9	—	—	—	—	—	—	980.4	979.6	979.5	980.4	979.6	979.4	980.5
23	A9	981	0	2120	0	0	980.8	980.8	980.5	980.4	980.7	980.5	980.4	—	—	—	—	—	—	980.9
24	A9	981	2120	0	0	0	980.9	—	—	—	—	—	—	980.7	980.4	980.4	980.7	980.4	980.3	980.8
25	A9	981	0	1300	0	0	980.8	980.8	980.7	980.6	980.5	980.7	980.6	—	—	—	—	—	—	980.9
26	A9	981	1300	0	0	0	980.9	—	—	—	—	—	—	980.8	980.7	980.7	980.8	980.7	980.6	980.9

*Sensitivity Test: 40%/60%
**Sensitivity Test: 20%/80%

TABLE 2. Estimated headloss through intakes (ft) assuming a = 1.0. Headlosses are cumulative and accurate to ± 0.1 ft.

Discharge (cfs)		Behind Trashracks				Behind Gate Slots				At End of Pit			
	Bay:	4	3	2	1	4	3	2	1	4	3	2	1
Q_{PL}	Q_{PR}												
3250	3250	0.60	0.60	0.47	0.37	0.60	0.70	0.27	0.37	0.70	0.60	0.47	0.47
3250	—	0.50	0.50			0.60	0.60			0.70	0.60		
—	3250			0.57	0.47			0.37	0.47			0.37	0.47
2120	—	0.24	0.24			0.26	0.26			0.22	0.42		
—	2120			0.14	0.24			0.14	0.14			0.20	0.20
1300	—	0.18	0.18			0.17	0.17			0.16	0.26		
—	1300			0.18	0.18			0.17	0.17			0.25	0.25

LIST OF PHOTOGRAPHS

Photograph No.

11 Type A7, Q_p = 6500 cfs, Q_{GS} = 0 cfs, Q_{MS} = 0 cfs, H.W. = 981 ft. The flow pattern with vortices over the intake eliminated by a submerged grid.

12 Type A9, the revised model showing the area excavated to elevation 975 ft. Proposed final design.

13 Type A9, Q_p =6500 cfs, Q_{GS} = 0 cfs, Q_{MS} = 0 cfs, H.W. = 981 ft. The flow pattern.

14 Type A9, Q_p = 6500 cfs, Q_{GS} = 0 cfs, Q_{MS} = 0 cfs, H.W. = 981 ft. The flow pattern showing a smooth approach flow with no upstream separation zone.

15 Type A9, Q_p = 6500 cfs, Q_{GS} = 0 cfs, Q_{MS} = 0 cfs, H.W. = 981 ft. The flow pattern.

16 Type A9, Q_p = 6500 cfs, Q_{GS} = 0 cfs, Q_{MS} = 0 cfs, H.W. = 979 ft. The flow pattern.

17 Type A9, Q_p = 6500 cfs, Q_{GS} = 3300 cfs, Q_{MS} = 0 cfs, H.W. = 981 ft. The flow pattern.

18 Type A9, Q_p = 6500 cfs, Q_{GS} = 2200 cfs, Q_{MS} = 0 cfs, H.W. = 979 ft. The flow pattern.

19 Type A9, Q_p = 6500 cfs, Q_{GS} = 3300 cfs, Q_{MS} = 3000 cfs, H.W. = 981 ft. The flow pattern upstream along the bank.

20 Type A9, Q_{PL} = 3250 cfs, Q_{GS} = 0 cfs, Q_{MS} = 0 cfs, H.W. = 981 ft. The flow pattern.

21 Type A10, Q_p = 6500 cfs, Q_{GS} = 3300 cfs, Q_{MS} = 0 cfs, H.W. = 981 ft. The flow pattern with a 10 ft slotted wall extending from one pier to reduce surface cross flow.

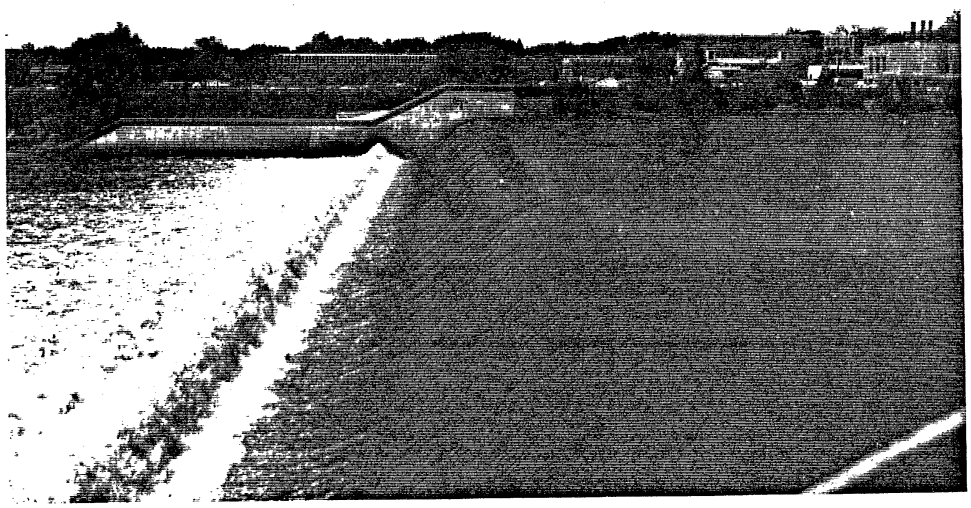

PHOTO 1 - View from the left bank showing the main spillway and the location of the proposed powerhouse on the right bank.

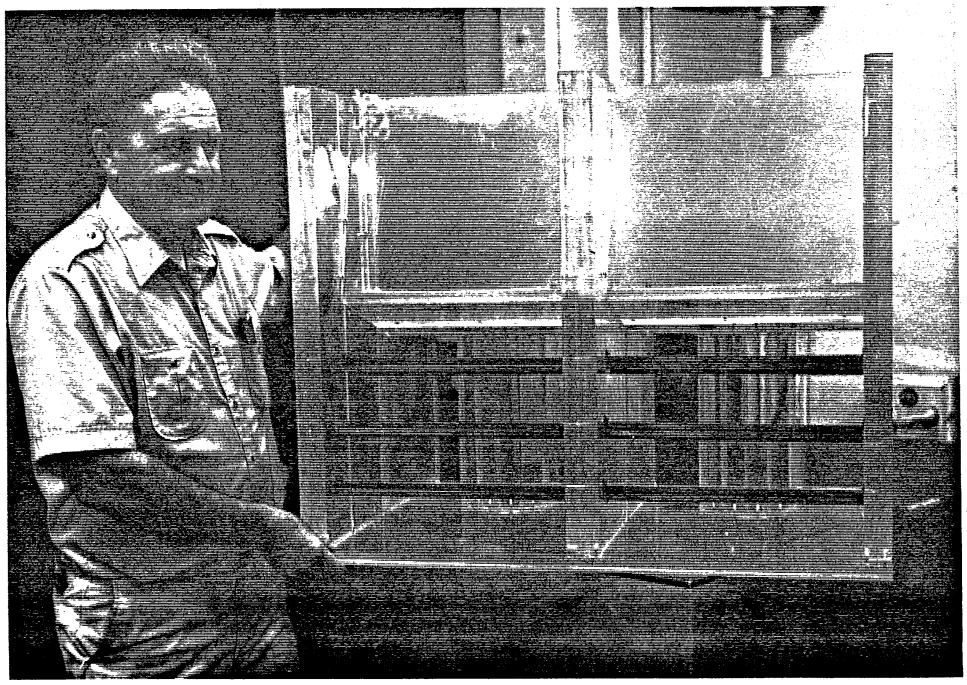

PHOTO 2 - The completed powerhouse in the Laboratory shop.

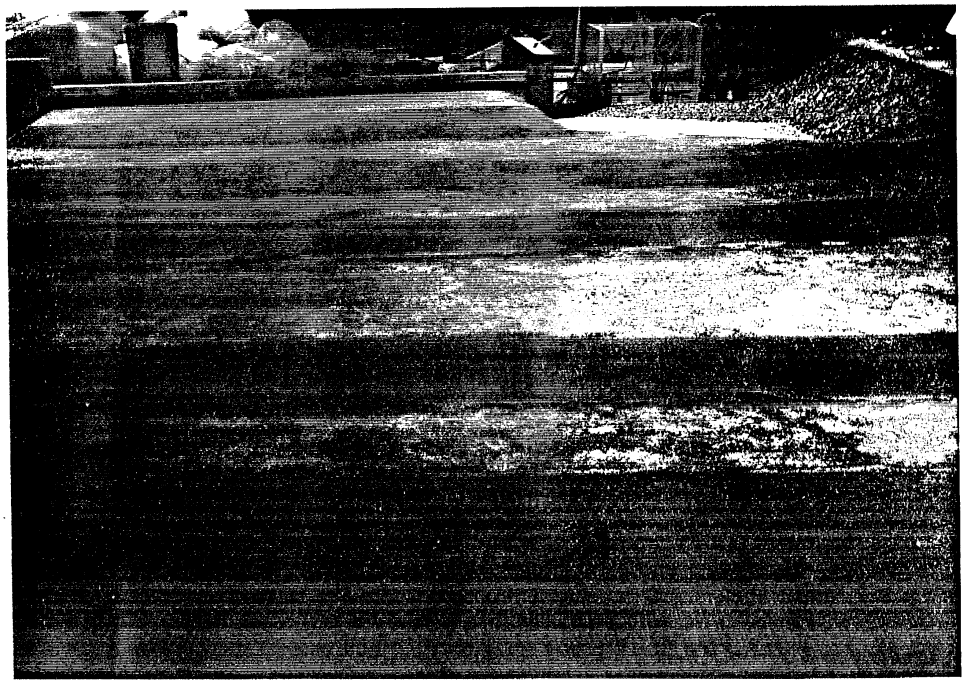

PHOTO 3 - The model under construction.

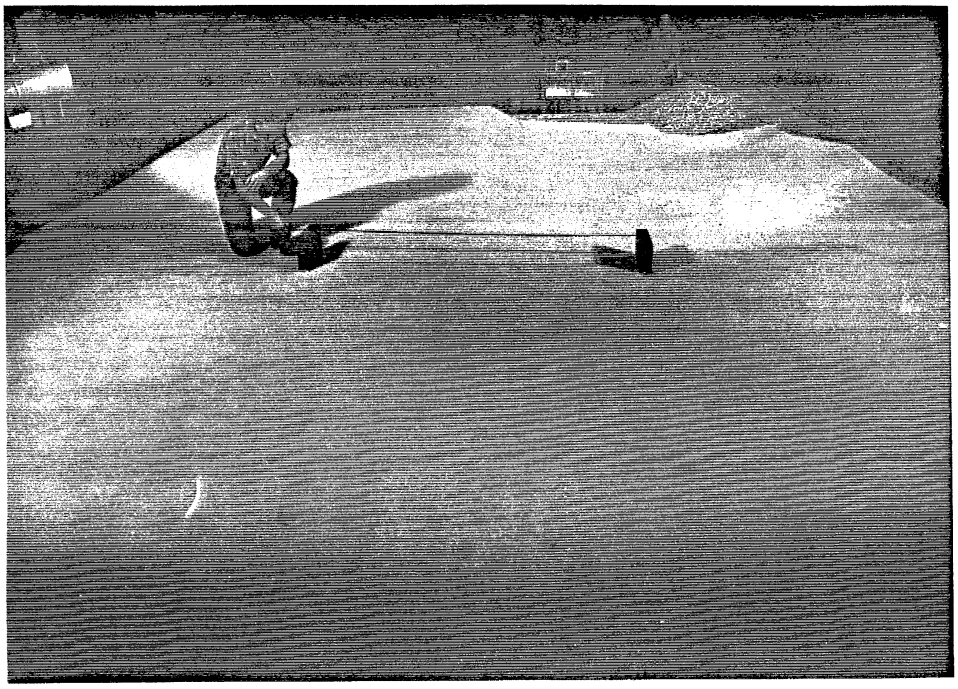

PHOTO 4 - Type A, the completed model. Tenth Street Bridge piers in foreground.

PHOTO 5 - Type A, the completed model and some of the personnel responsible for its construction. Models of 13 ft automobiles ındicate scale.

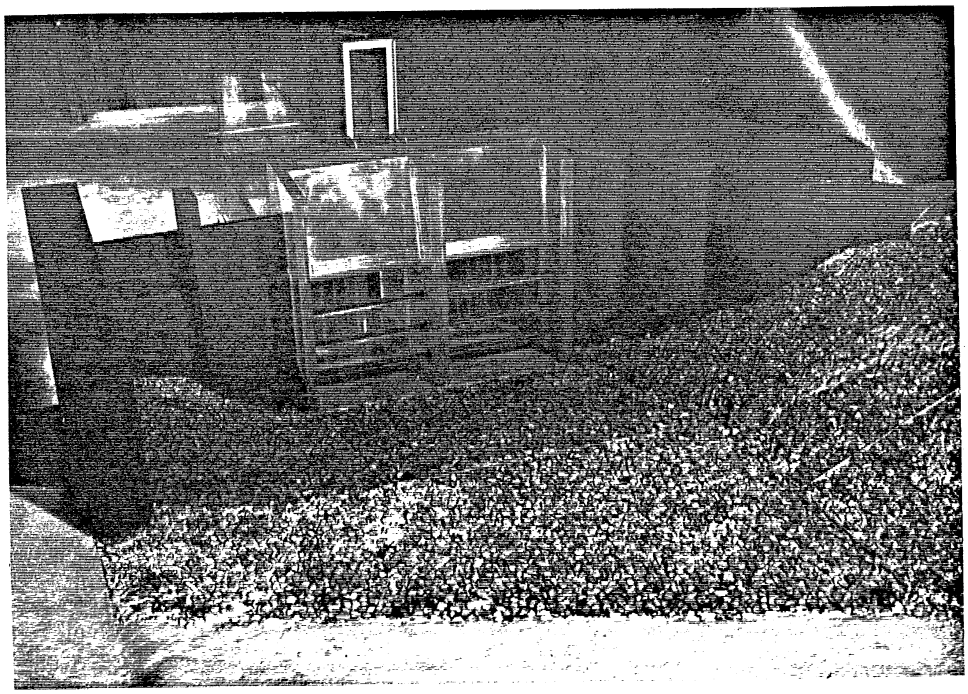

PHOTO 6 - Type A, the approach to the powerhouse and gated spillway.

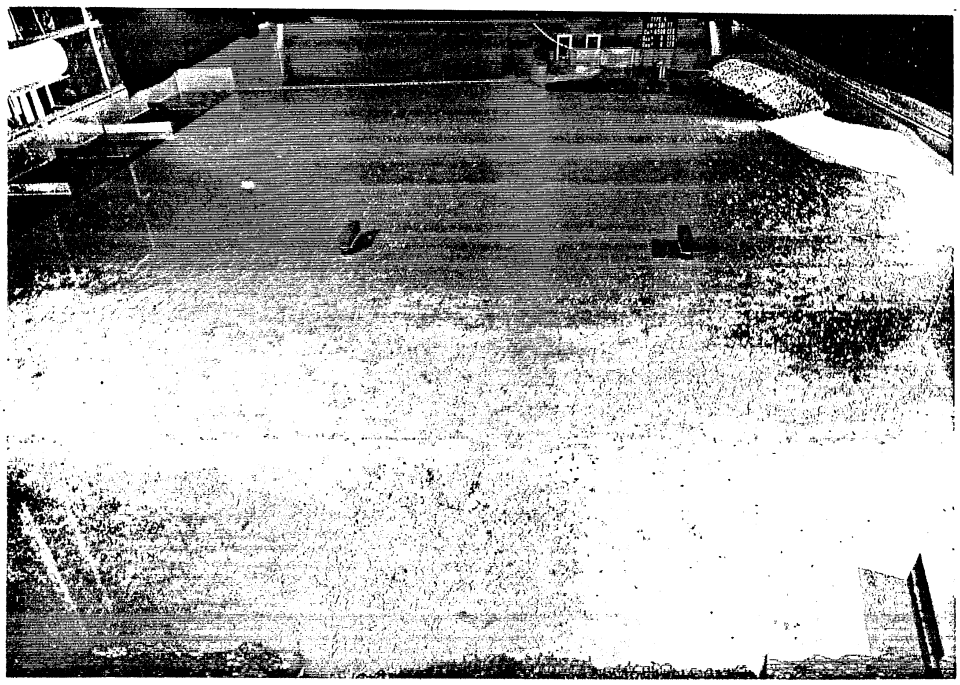

PHOTO 7 - Type A, Q_p = 6500 cfs, Q_{GS} = 0 cfs, Q_{MS} = 0 cfs, H.W. = 981 ft. The model in operation.

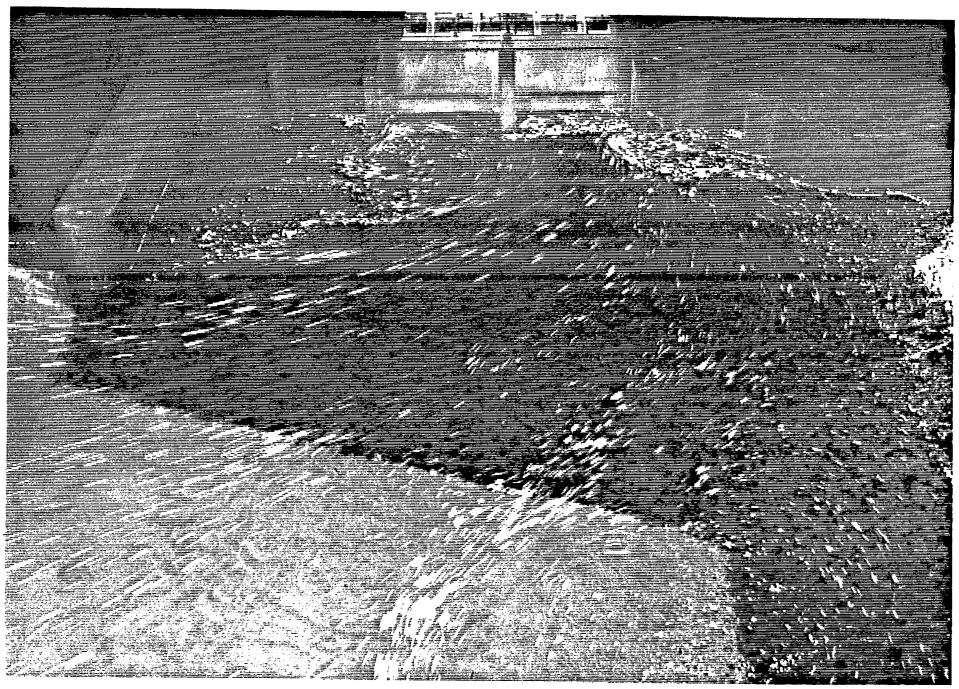

PHOTO 8 - Type A, Q_p = 6500 cfs, Q_{GS} = 0 cfs, Q_{MS} = 0 cfs, H.W. = 981 ft. Flow pattern indicates large separation zone in foreground and vortices over intake.

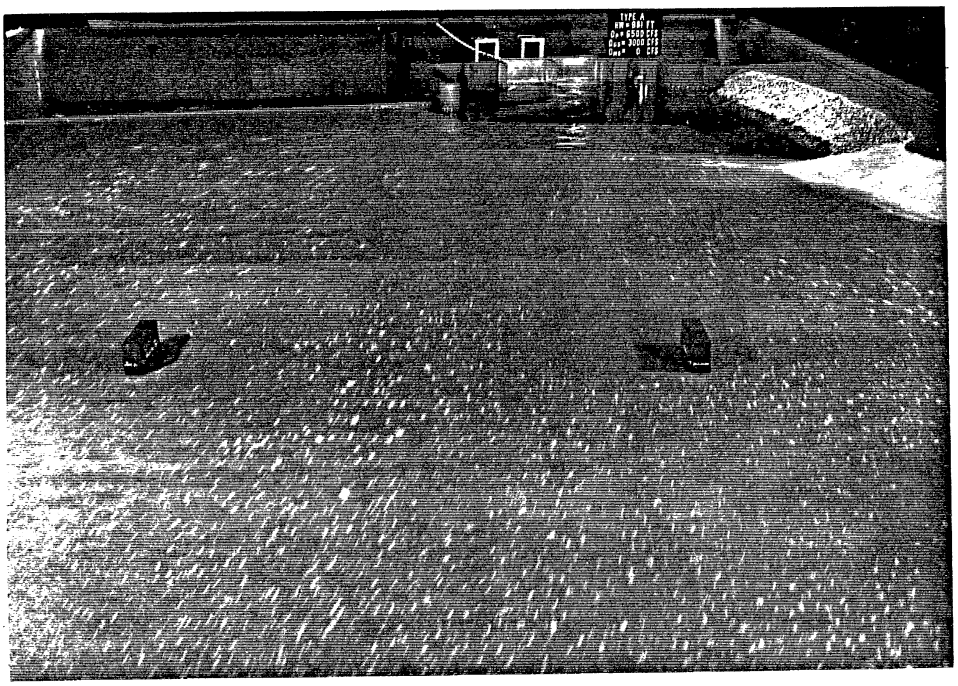

PHOTO 9 - Type A, Q_p = 6500 cfs, Q_{GS} = 3000 cfs, Q_{MS} = 0 cfs, H.W. = 981 ft. The flow pattern.

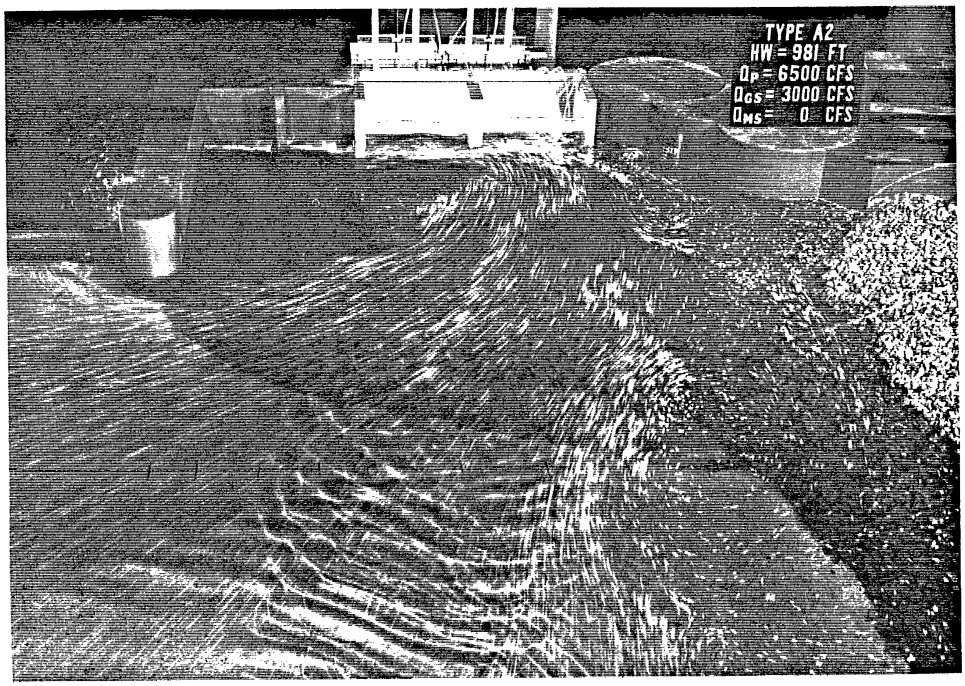

PHOTO 10 - Type A2, Q_p = 6500 cfs, Q_{GS} = 3000 cfs, Q_{MS} = 0 cfs, H.W. = 981 ft. The flow pattern. Note surface waves at beginning of excavation zone.

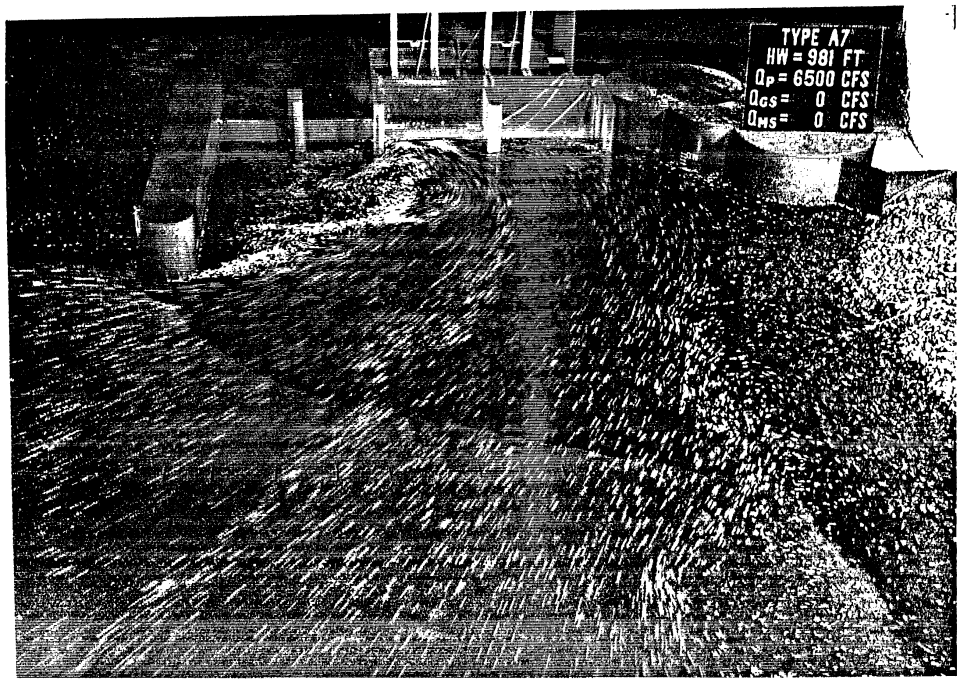

PHOTO 11 - Type A7, Q_P = 6500 cfs, Q_{GS} = 0 cfs, Q_{MS} = 0 cfs, H.W. = 981 ft. The flow pattern with vortices over the intake eliminated by a submerged grid.

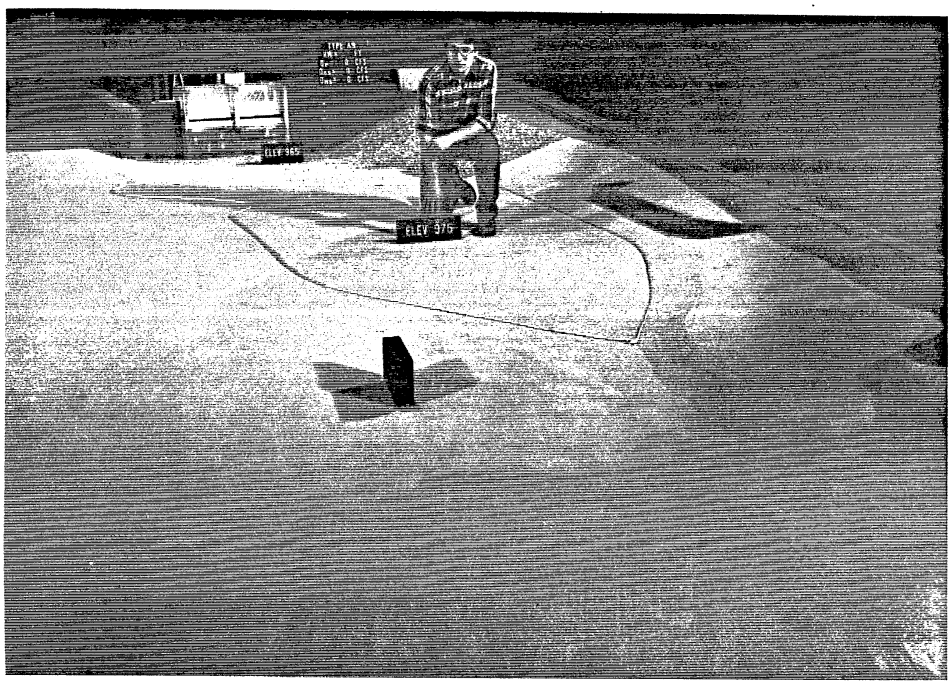

PHOTO 12 - Type A9, the revised model showing the area excavated to elevation 975 ft. Proposed final design.

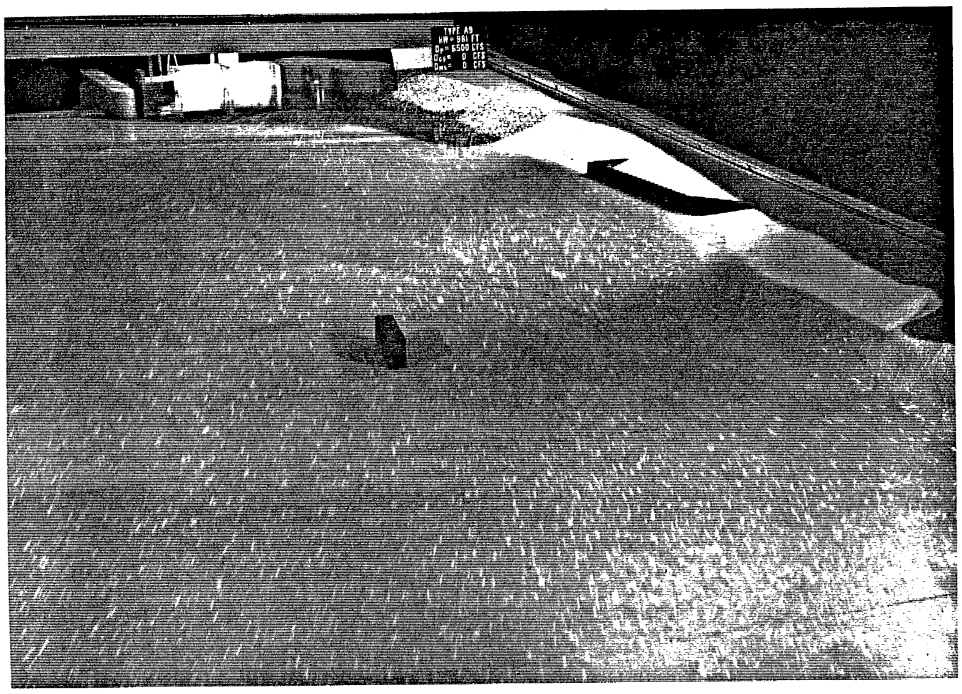

PHOTO 13 - Type A9, Q_p = 6500 cfs, Q_{GS} = 0 cfs, Q_{MS} = 0 cfs, H.W. = 981 ft. The flow pattern.

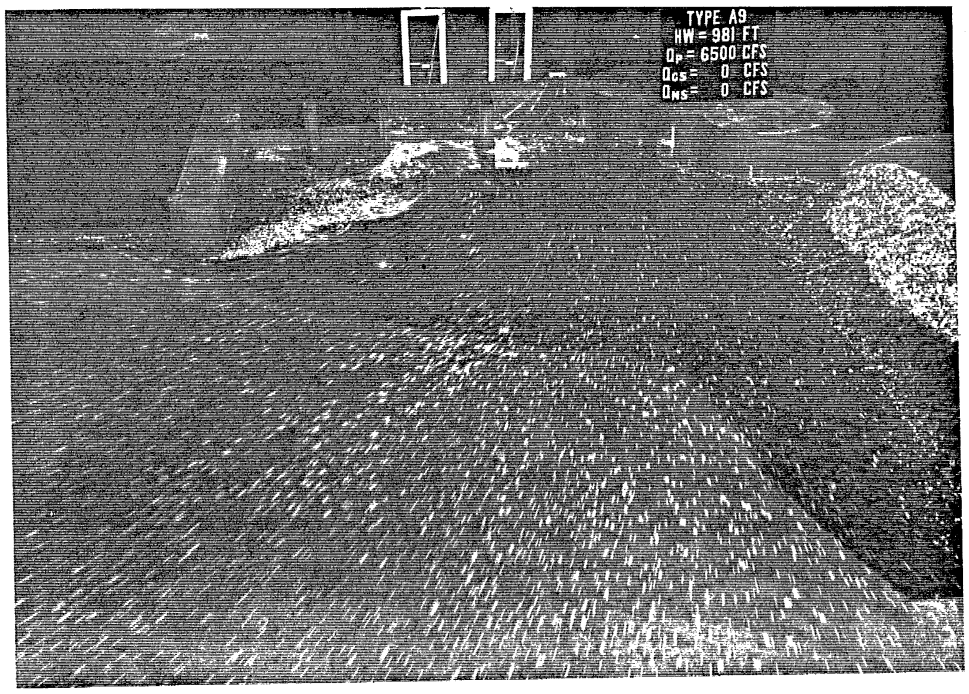

PHOTO 14 - Type A9, Q_p = 6500 cfs, Q_{GS} = 0 cfs, Q_{MS} = 0 cfs, H.W. = 981 ft. The flow pattern showing a smooth approach flow with no upstream separation zone.

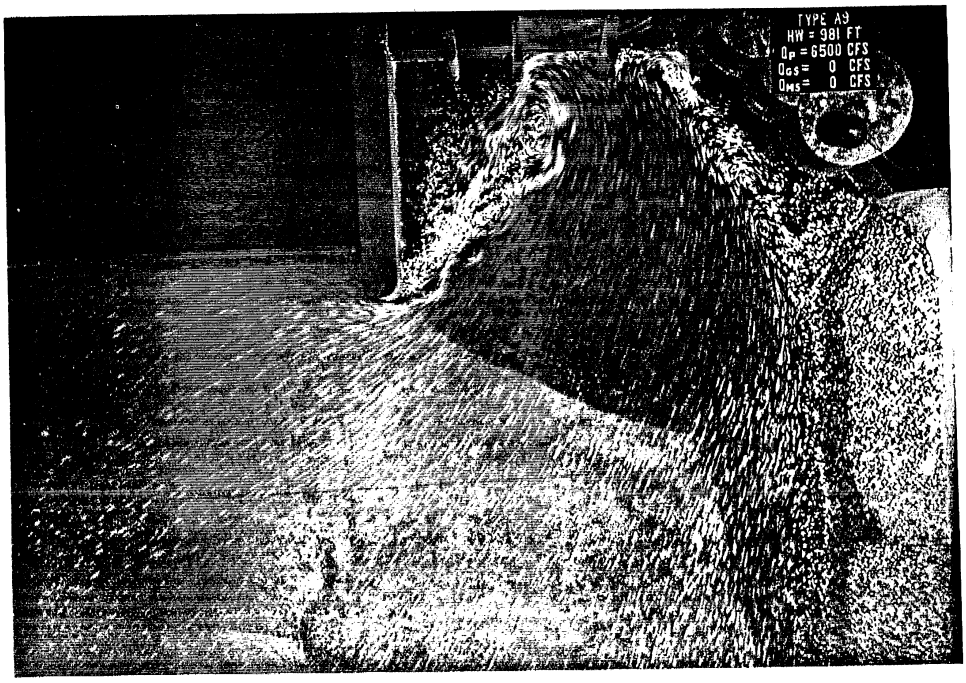

PHOTO 15 - Type A9, Q_p = 6500 cfs, Q_{GS} = 0 cfs, Q_{MS} = 0 cfs, H.W. = 981 ft. The flow pattern.

PHOTO 16 - Type A9, Q_p = 6500 cfs, Q_{GS} = 0 cfs, Q_{MS} = 0 cfs, H.W. = 979 ft. The flow pattern.

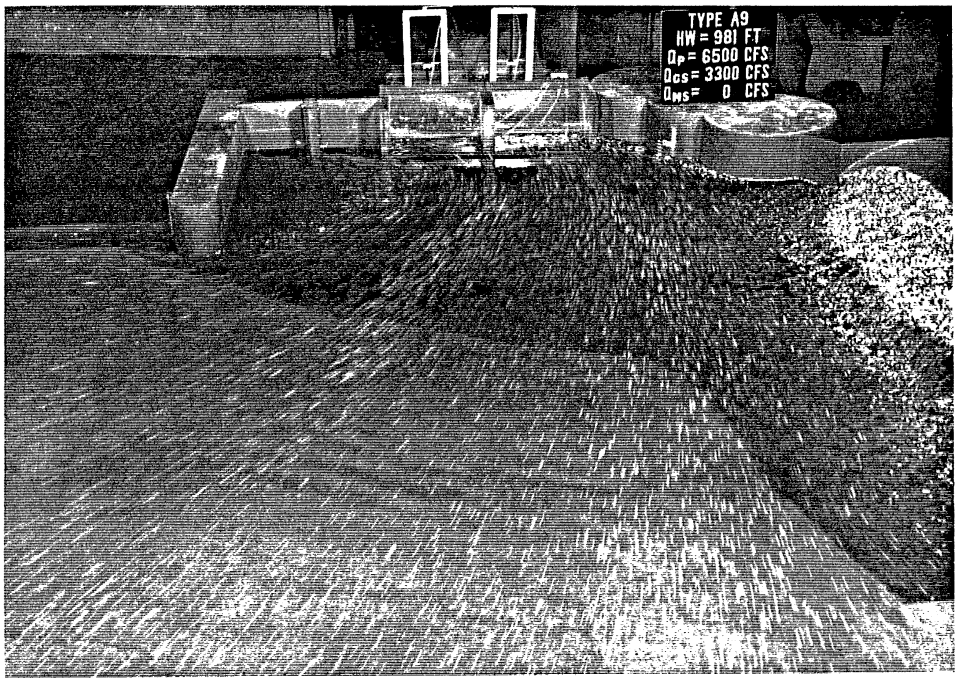

PHOTO 17 - Type A9, Q_p = 6500 cfs, Q_{GS} = 3300 cfs, Q_{MS} = 0 cfs, H.W. = 981 ft. The flow pattern.

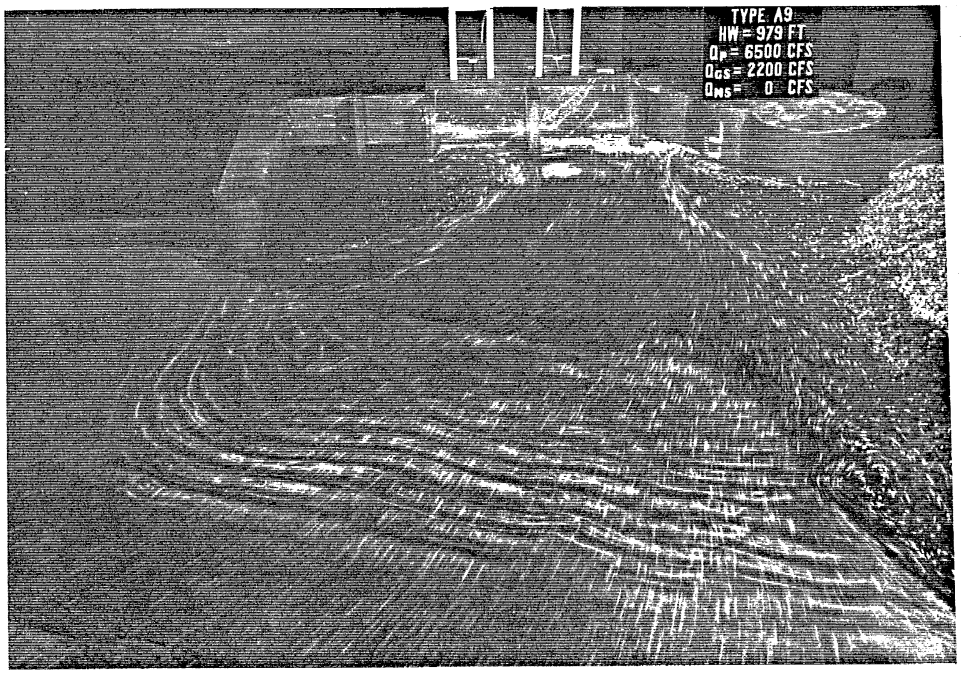

PHOTO 18 - Type A9, Q_p = 6500 cfs, Q_{GS} = 2200 cfs, Q_{MS} = 0 cfs, H.W. = 979 ft. The flow pattern.

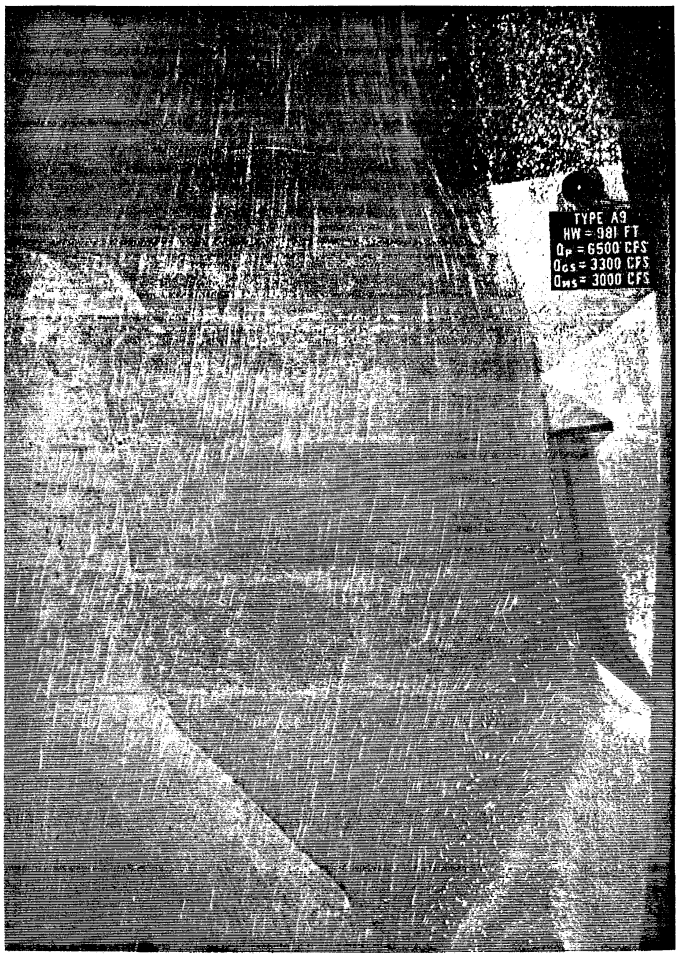

PHOTO 19 - Type A9, Q_p = 6500 cfs, Q_{GS} = 3300 cfs, Q_{MS} = 3000 cfs, H.W. = 981 ft. The flow pattern upstream along the bank.

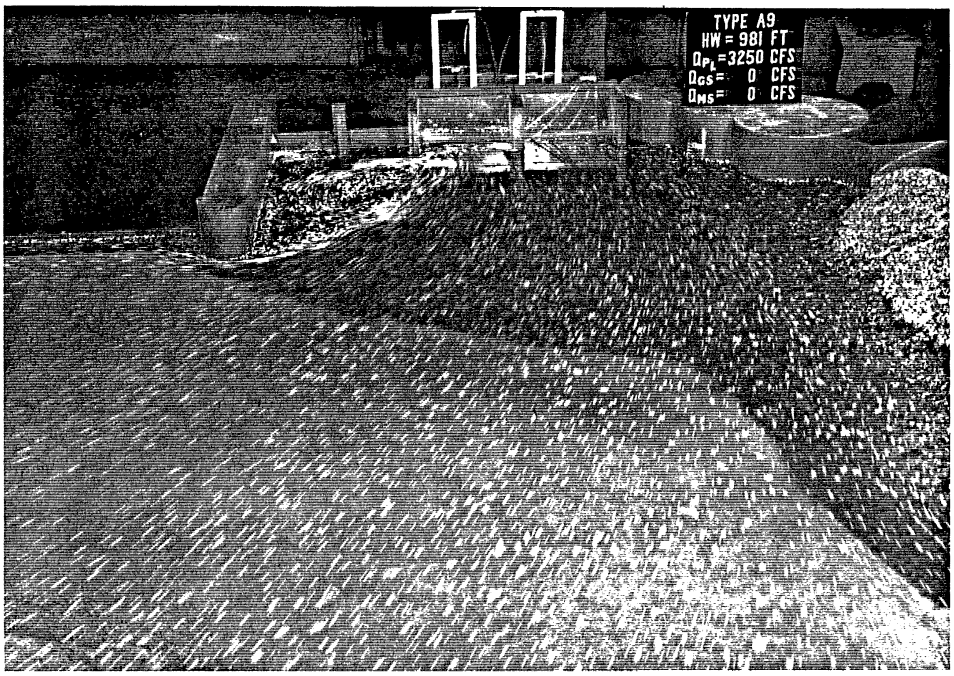

PHOTO 20 - Type A9, Q_{PL} = 3250 cfs, Q_{GS} = 0 cfs, Q_{MS} = 0 cfs, H.W. = 981 ft. The flow pattern.

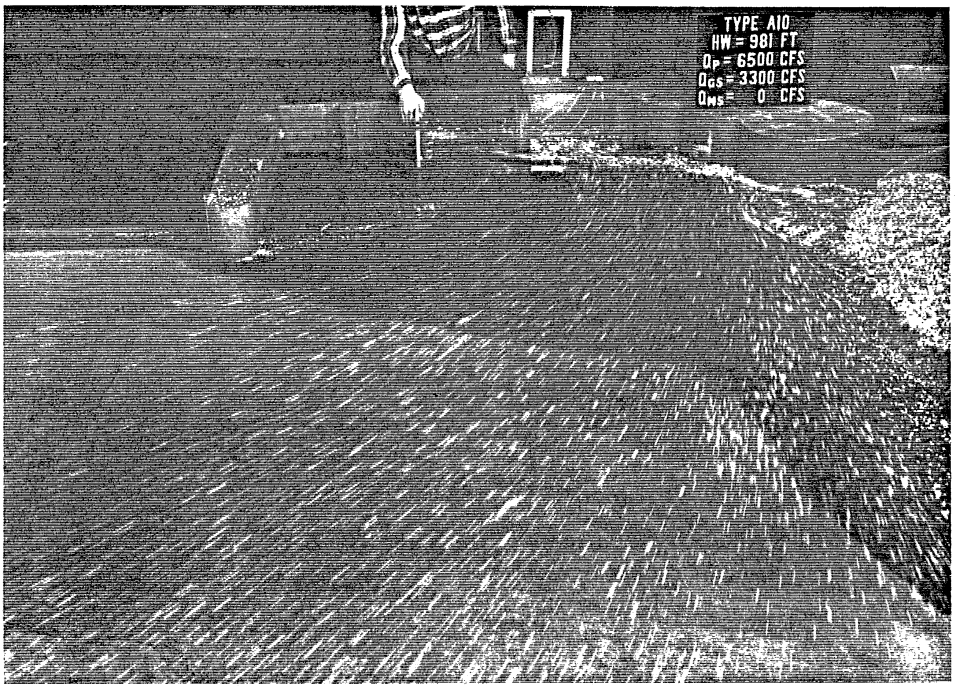

PHOTO 21 - Type A10, Q_P = 6500 cfs, Q_{GS} = 3300 cfs, Q_{MS} = 0 cfs, H.W. = 981 ft. The flow pattern with a 10 ft slotted wall extending from one pier to reduce surface cross flow.

LIST OF FIGURES

17 Type A1, Q_p = 6,500 cfs, Q_{GS} = 3,000 cfs, Q_{MS} = 2,400 cfs, H.W. = 981 ft. Typical velocity profiles.

18 Type A2, revised geometry.

19 Type A2, Q_p = 6,500 cfs, Q_{GS} = 0 cfs, Q_{MS} = 0 cfs, H.W. = 981 ft. Typical water surface traverses.

20 Type A2, Q_p = 6,500 cfs, Q_{GS} = 3,000 cfs, Q_{MS} = 0 cfs, H.W. = 981 ft. Typical water surface traverses.

21 Type A2, Q_p = 6,500 cfs, Q_{GS} = 3,000 cfs, Q_{MS} = 2,400 cfs, H.W. = 981 ft. Typical water surface traverses.

22 Type A3, Q_p = 6,500 cfs, Q_{GS} = 0 cfs, Q_{MS} = 0 cfs, H.W. = 981 ft. Typical velocity profiles.

23 Type A4, Q_p = 6,500 cfs, Q_{GS} = 0 cfs, Q_{MS} = 0 cfs, H.W. = 981 ft. Typical velocity profiles.

24 Type A5, Q_p = 6,500 cfs, Q_{GS} = 0 cfs, Q_{MS} = 0 cfs, H.W. = 981 ft. Typical velocity profiles.

25 Type A6, Q_p = 6,500 cfs, Q_{GS} = 0 cfs, Q_{MS} = 0 cfs, H.W. = 981 ft. Typical velocity profiles.

26 Type A7, Q_p = 6,500 cfs, Q_{GS} = 0 cfs, Q_{MS} = 0 cfs, H.W. = 981 ft. Typical velocity profiles.

27 Type A8, Q_p = 6,500 cfs, Q_{GS} = 0 cfs, Q_{MS} = 0 cfs, H.W. = 981 ft. Typical water surface traverses.

28 Type A8, Q_p = 6,500 cfs, Q_{GS} = 0 cfs, Q_{MS} = 0 cfs, H.W. = 981 ft. Typical velocity profiles.

29 Type A8, Q_p = 6,500 cfs, Q_{GS} = 3,000 cfs, Q_{MS} = 0 cfs, H.W. = 981 ft. Typical water surface traverses.

30 Type A8, Q_p = 6,500 cfs, Q_{GS} = 3,000 cfs, Q_{MS} = 0 cfs, H.W. = 981 ft. Typical velocity profiles.

31 Type A8, Q_p = 6,500 cfs, Q_{GS} = 3,000 cfs, Q_{MS} = 2,400 cfs, H.W. = 981 ft. Typical water surface traverses.

32 Type A8, Q_p = 6,500 cfs, Q_{GS} = 3,000 cfs, Q_{MS} = 2,400 cfs, H.W. = 981 ft. Typical velocity profiles.

33 Type A8, Q_{pR} = 3,250 cfs, Q_{GS} = 0 cfs, Q_{MS} = 0 cfs, H.W. = 981 ft. Typical velocity profiles. Right powerhouse in operation only.

34 Type A8, Q_{pL} = 3,250 cfs, Q_{GS} = 0 cfs, Q_{MS} = 0 cfs, H.W. = 981 ft. Typical velocity profiles. Left powerhouse in operation only.

35 Types A9, A10, revised geometries.

36 Type A9, Q_p = 6,500 cfs, Q_{GS} = 0 cfs, Q_{MS} = 0 cfs, H.W. = 981 ft. Typical water surface traverses.

37 Type A9, Q_p = 6,500 cfs, Q_{GS} = 0 cfs, Q_{MS} = 0 cfs, H.W. = 981 ft. Typical velocity profiles.

38 Type A9, Q_p = 6,500 cfs, Q_{GS} = 3,300 cfs, Q_{MS} = 0 cfs, H.W. = 981 ft. Typical water surface traverses.

39 Type A9, Q_p = 6,500 cfs, Q_{GS} = 3,300 cfs, Q_{MS} = 0 cfs, H.W. = 981 ft. Typical velocity profiles.

40 Type A9, Q_p = 6,500 cfs, Q_{GS} = 3,300 cfs, Q_{MS} = 3,000 cfs, H.W. = 981 ft. Typical water surface traverses.

41 Type A9, Q_p = 6,500 cfs, Q_{GS} = 3,300 cfs, Q_{MS} = 3,000 cfs, H.W. = 981 ft. Typical velocity profiles.

42 Type A9, Q_p = 6,500 cfs, Q_{GS} = 0 cfs, Q_{MS} = 0 cfs, H.W. = 981 ft. Typical water surface traverses. Sensitivity test.

43 Type A9, Q_p = 6,500 cfs, Q_{GS} = 0 cfs, Q_{MS} = 0 cfs, H.W. = 981 ft. Typical velocity profiles. Sensitivity test.

44 Type A9, Q_p = 6,500 cfs, Q_{GS} = 0 cfs, Q_{MS} = 0 cfs, H.W. = 981 ft. Typical water surface traverses. Sensitivity test.

45 Type A9, Q_p = 6,500 cfs, Q_{GS} = 0 cfs, Q_{MS} = 0 cfs, H.W. = 981 ft. Typical velocity profiles. Sensitivity test.

46 Type A9, Q_p = 6,500 cfs, Q_{GS} = 0 cfs, Q_{MS} = 0 cfs, H.W. = 979 ft. Typical water surface traverses.

47 Type A9, Q_p = 6,500 cfs, Q_{GS} = 2,200 cfs, Q_{MS} = 0 cfs, H.W. = 979 ft. Typical water surface traverses.

48 Type A9, Q_p = 6,500 cfs, Q_{GS} = 0 cfs, Q_{MS} = 0 cfs, H.W. = 981 ft. Flow patterns and velocities at the water surface.

49 Type A9, Q_p = 6,500 cfs, Q_{GS} = 3,300 cfs, Q_{MS} = 0 cfs, H.W. = 981 ft. Flow patterns and velocities at the water surface.

50 Type A9, Q_p = 6,500 cfs, Q_{GS} = 3,300 cfs, Q_{MS} = 3,000 cfs, H.W. = 981 ft. Flow patterns and velocities at the water surface.

51 Type A9, Q_p = 6,500 cfs, Q_{GS} = 3,300 cfs, Q_{MS} = 3,000 cfs, H.W. = 981 ft. Flow patterns and velocities at the water surface along shoreline.

52 Type A9, Q_p = 6,500 cfs, Q_{GS} = 2,200 cfs, Q_{MS} = 0 cfs, H.W. = 979 ft. Flow patterns and velocities at the water surface along shoreline.

53 Type A9, Q_{pR} = 3,250 cfs, Q_{GS} = 0 cfs, Q_{MS} = 0 cfs, H.W. = 981 ft. Typical water surface traverses. Right powerhouse in operation only.

54 Type A9, Q_{pR} = 3,250 cfs, Q_{GS} = 0 cfs, Q_{MS} = 0 cfs, H.W. = 981 ft. Typical velocity profiles. Right powerhouse in operation only.

55 Type A9, Q_{pL} = 3,250 cfs, Q_{GS} = 0 cfs, Q_{MS} = 0 cfs, H.W. = 981 ft. Typical water surface traverses. Left powerhouse in operation only.

56 Type A9, Q_{pL} = 3,250 cfs, Q_{GS} = 0 cfs, Q_{MS} = 0 cfs, H.W. = 981 ft. Typical velocity profiles. Left powerhouse in operation only.

57 Type A9, Q_{pR} = 3,250 cfs, Q_{GS} = 0 cfs, Q_{MS} = 0 cfs, H.W. = 981 ft. Typical velocities and flow directions in right unit. Right powerhouse in operation only.

58 Type A9, Q_{pL} = 3,250 cfs, Q_{GS} = 0 cfs, Q_{MS} = 0 cfs, H.W. = 981 ft. Typical velocities and flow directions in left unit. Left powerhouse in operation only.

59 Type A9, Q_{p} = 6,500 cfs, Q_{GS} = 0 cfs, Q_{MS} = 0 cfs, H.W. = 981 ft. Typical flow directions.

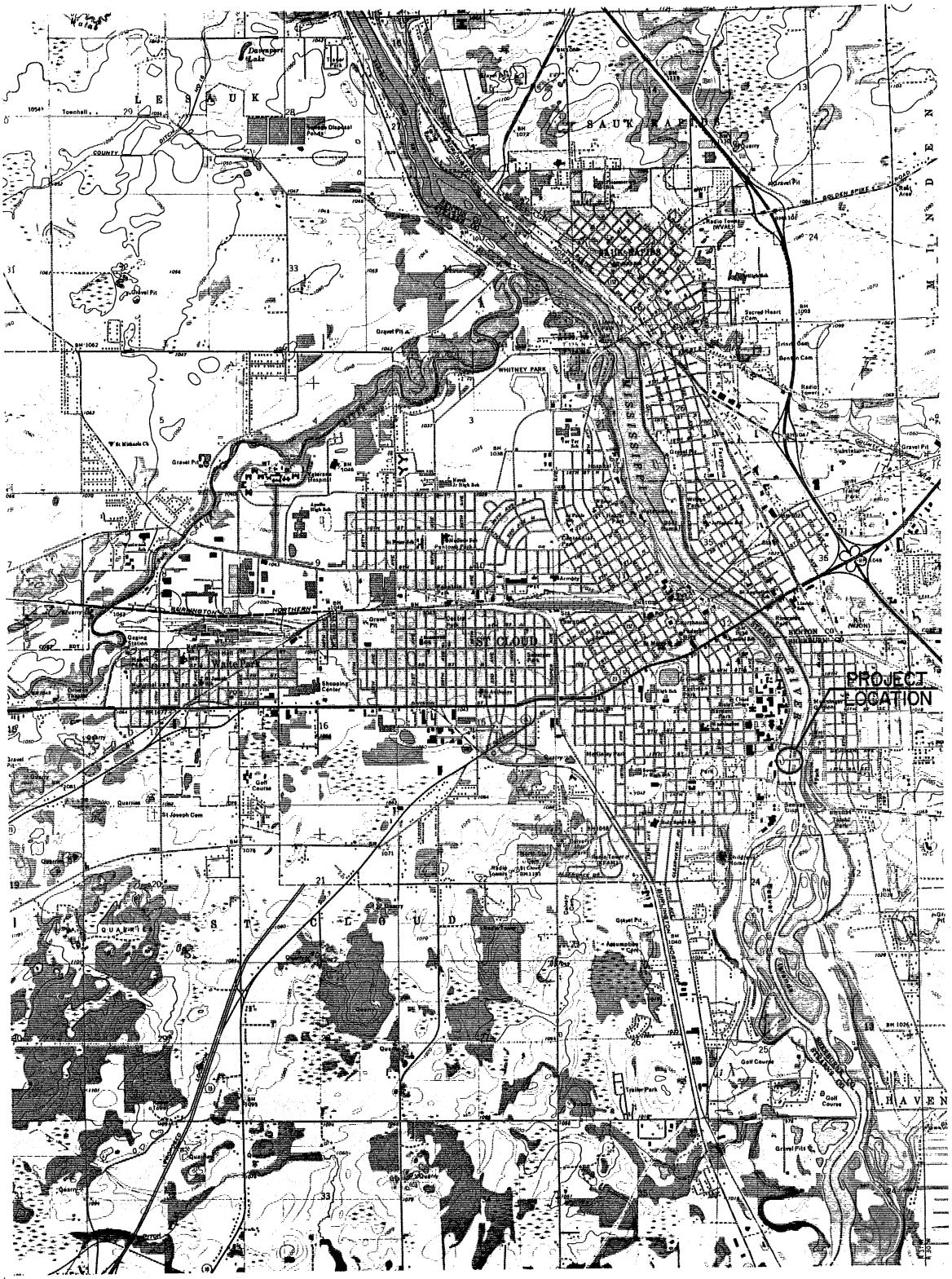

Fig. 1. Project location.

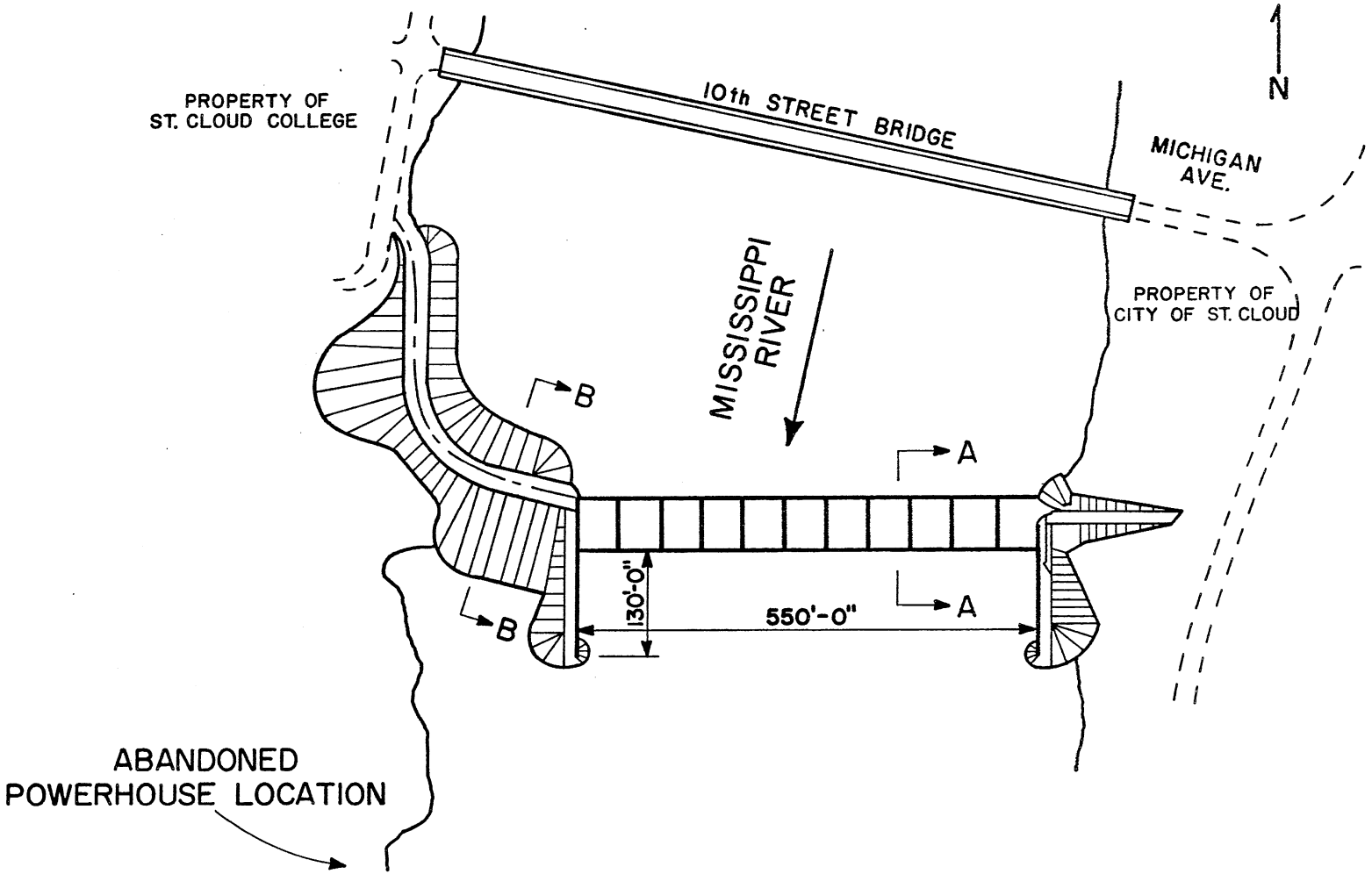

Fig. 2. Plan of Mississippi River at St. Cloud Dam.

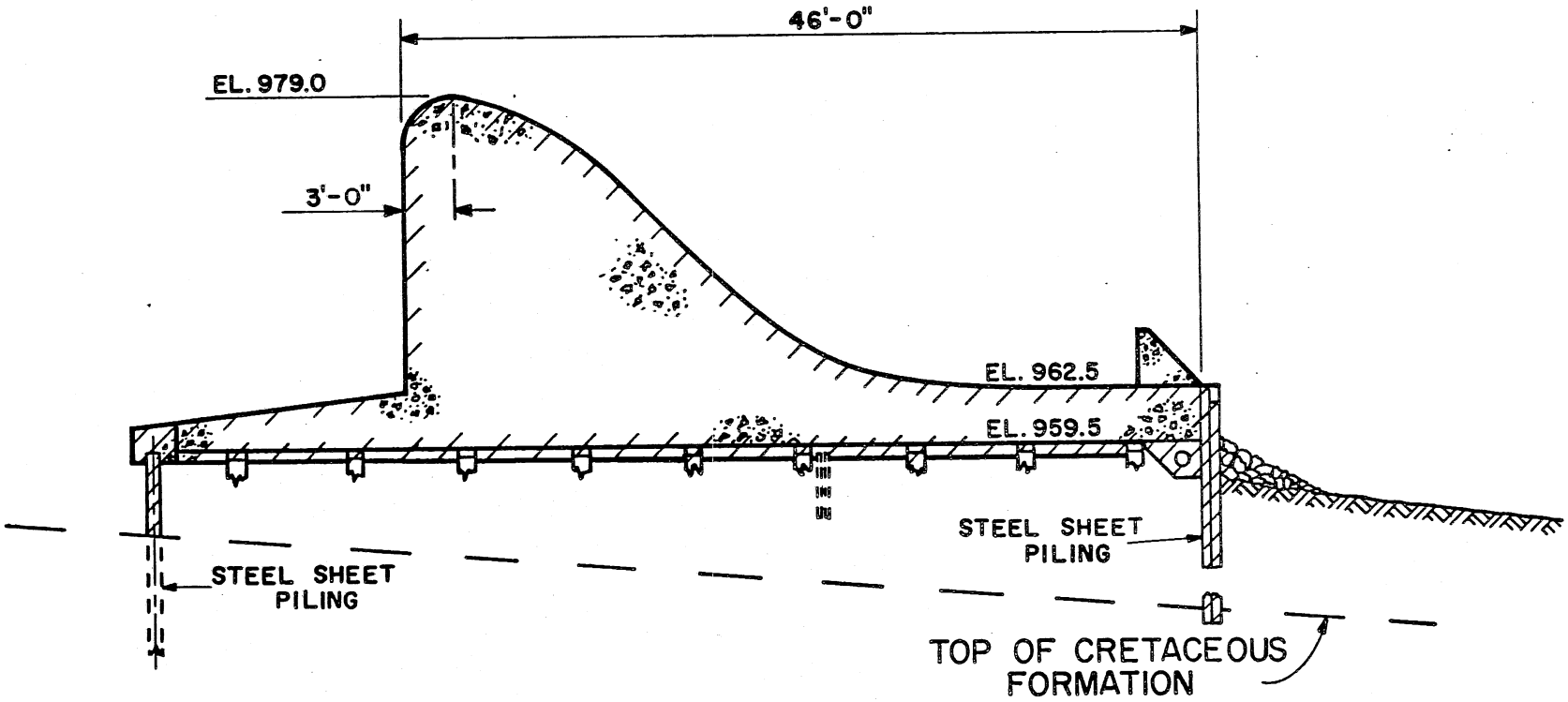

Fig. 3. Section A-A Through Ogee Spillway Crest.

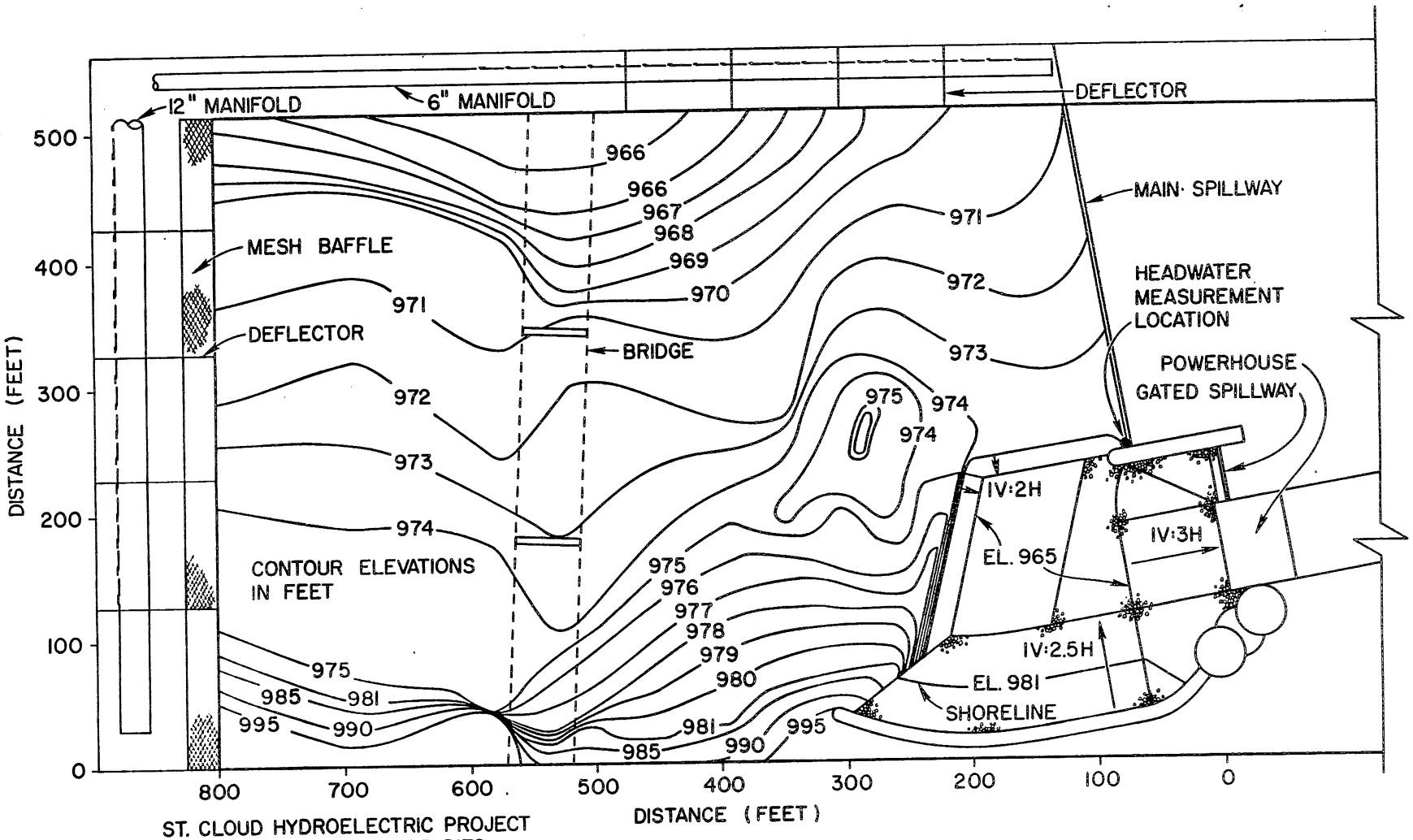

ST. CLOUD HYDROELECTRIC PROJECT
HYDRAULIC MODEL STUDIES
MODEL SCALE 1:24
TYPE A - ORIGINAL MODEL GEOMETRY

Figure 4

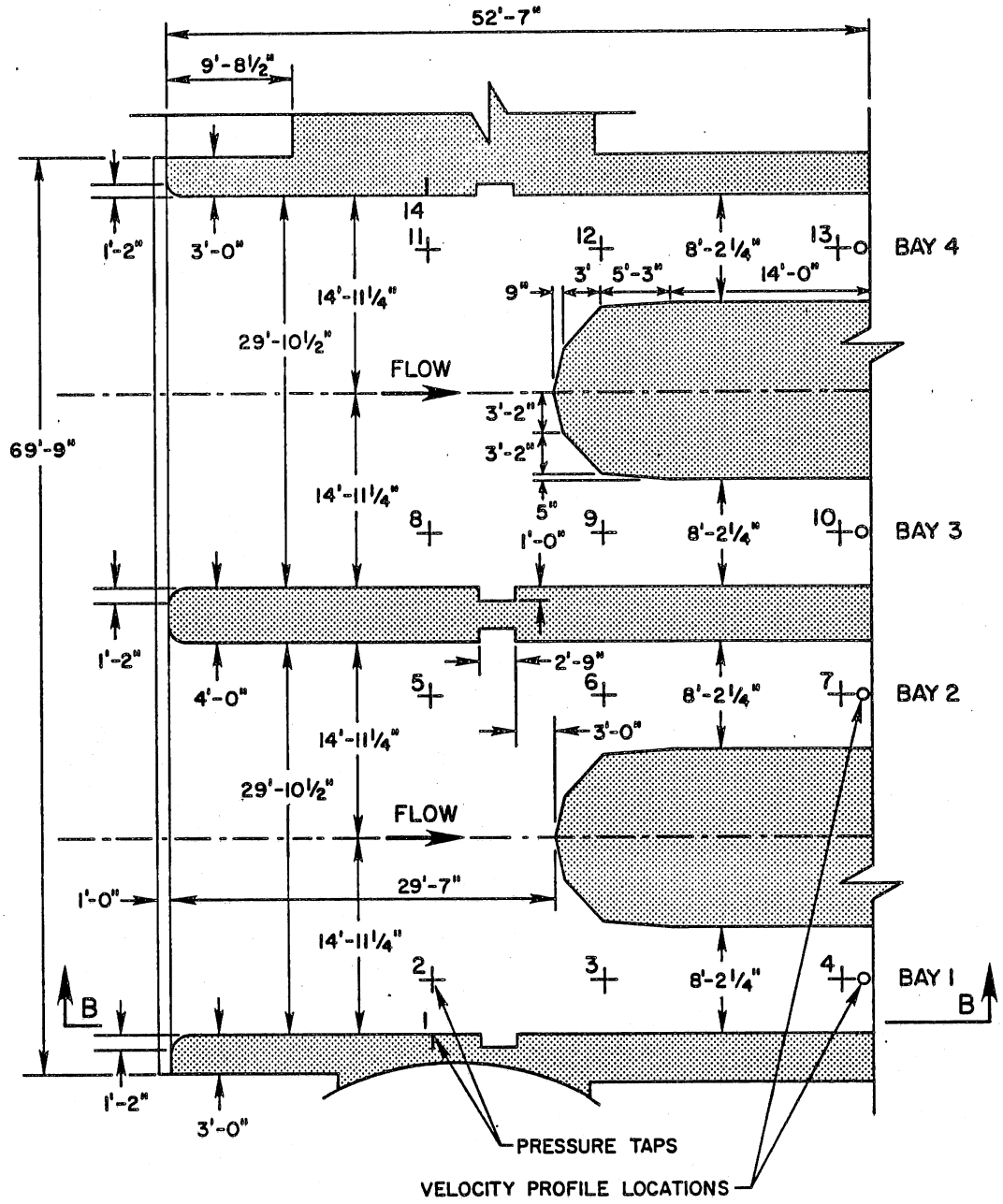

SECTION A-A

ST. CLOUD HYDROELECTRIC PROJECT
HYDRAULIC MODEL STUDIES
MODEL SCALE 1:24
TYPE A - ORIGINAL MODEL GEOMETRY

Figure 5

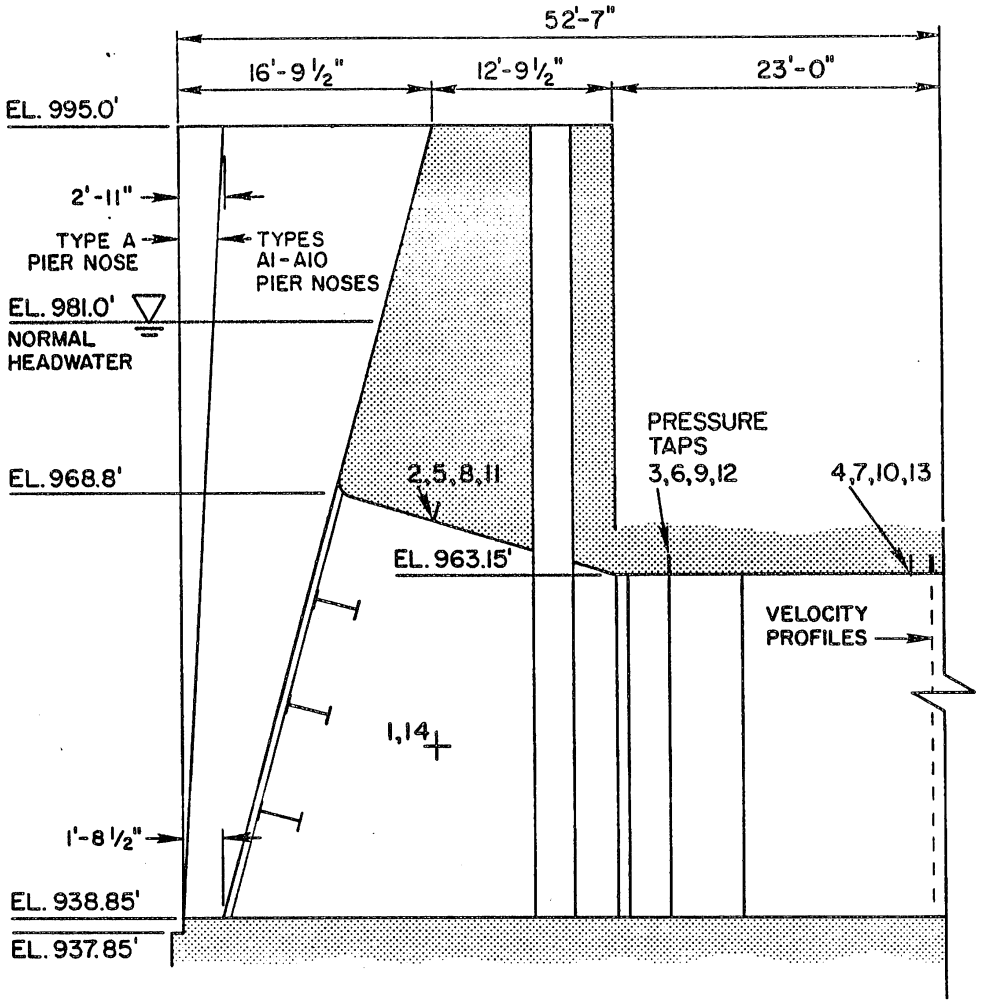

SECTION B-B

ST. CLOUD HYDROELECTRIC PROJECT
HYDRAULIC MODEL STUDIES
MODEL SCALE 1:24
TYPE A - ORIGINAL MODEL GEOMETRY

Figure 6

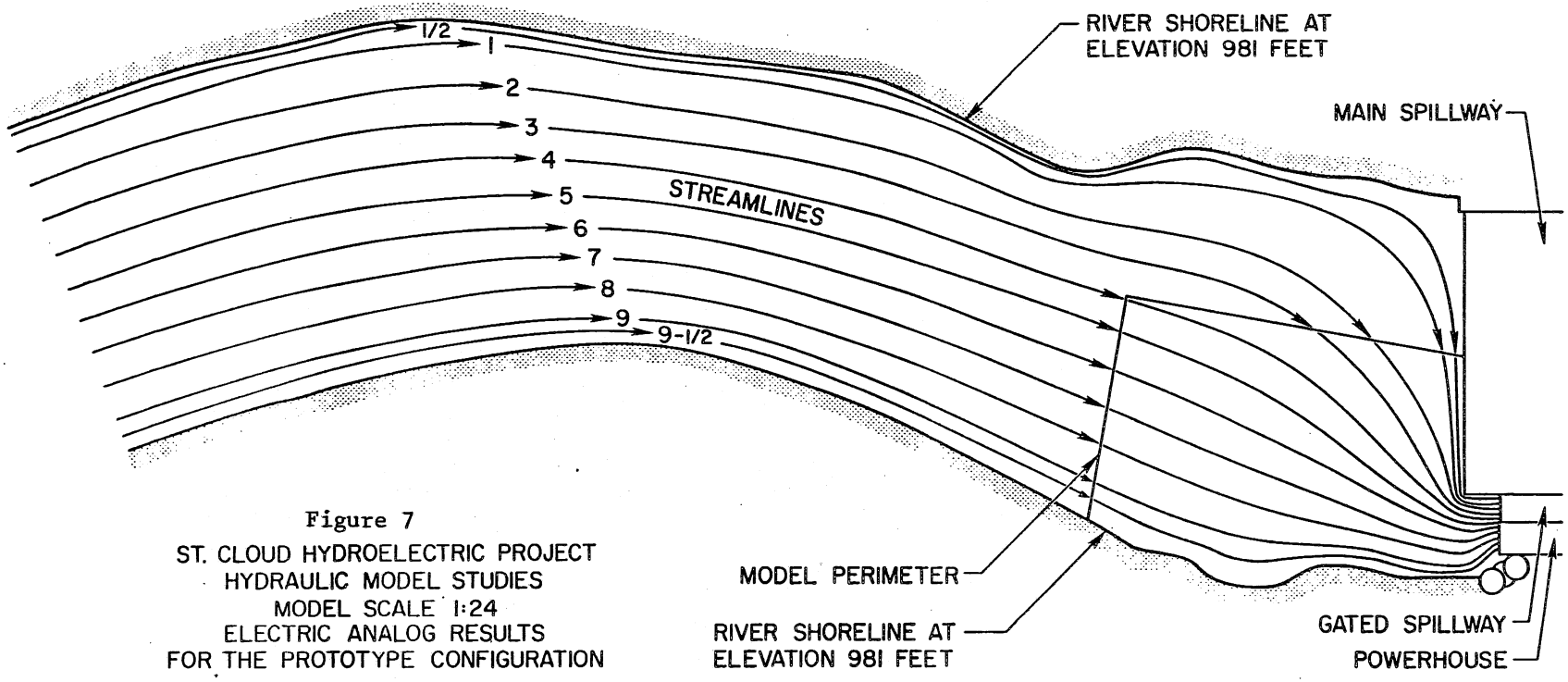

Figure 7
ST. CLOUD HYDROELECTRIC PROJECT
HYDRAULIC MODEL STUDIES
MODEL SCALE 1:24
ELECTRIC ANALOG RESULTS
FOR THE PROTOTYPE CONFIGURATION

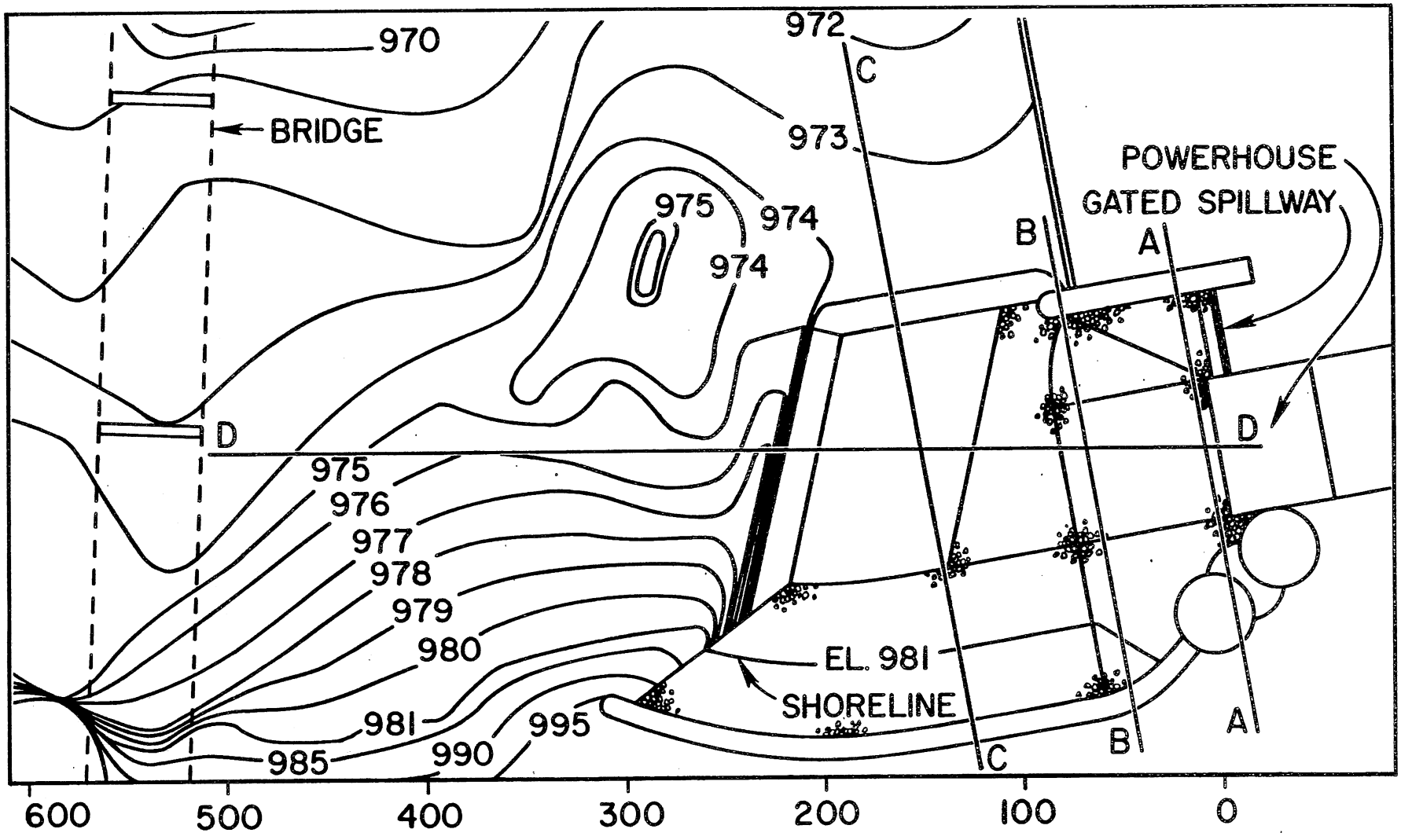

Figure 8

ST. CLOUD HYDROELECTRIC PROJECT
HYDRAULIC MODEL STUDIES
TYPES A-AIO MODEL SCALE 1:24
LOCATION OF WATER SURFACE TRAVERSES

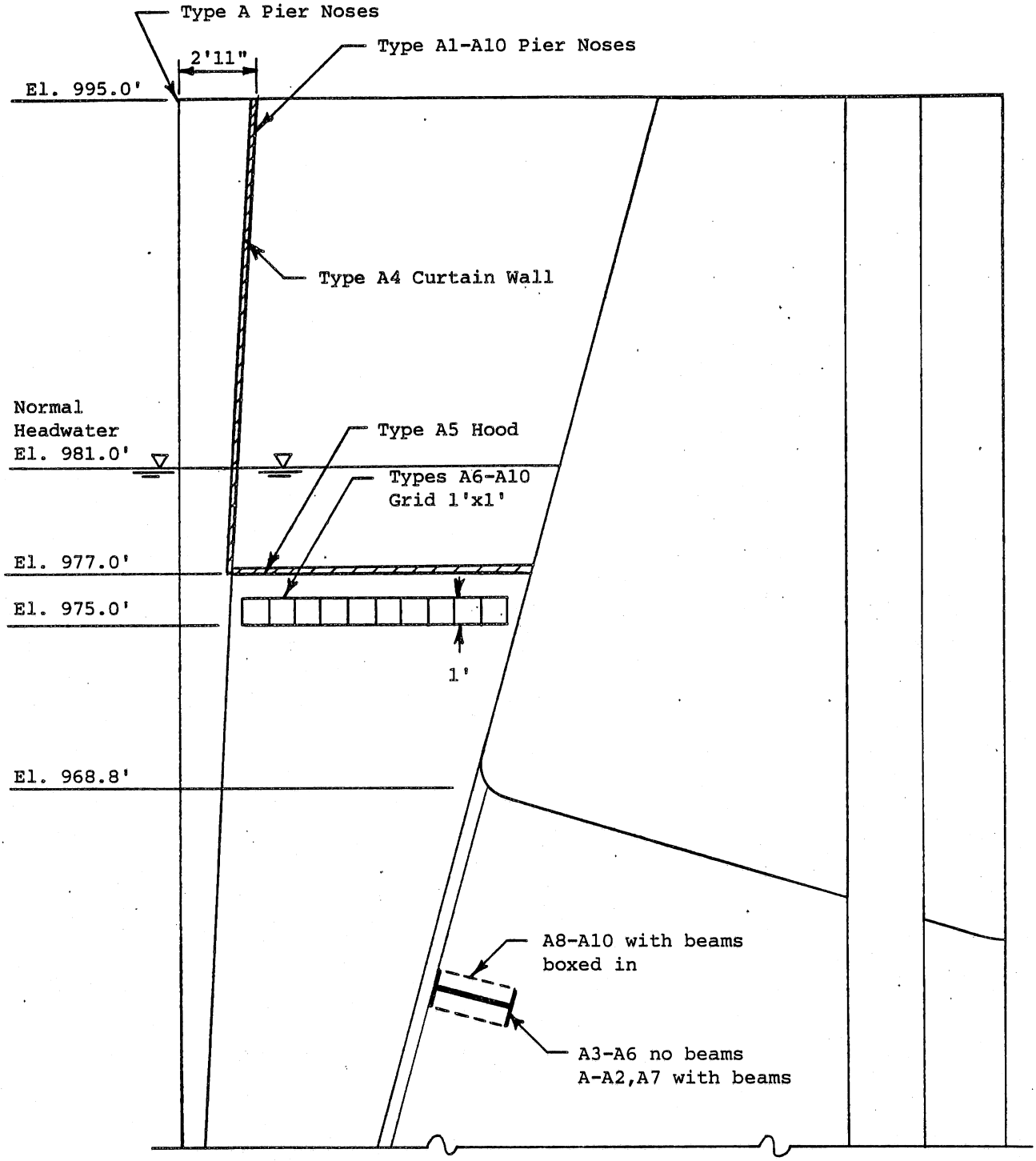

Figure 9
ST. CLOUD HYDROELECTRIC PROJECT
HYDRAULIC MODEL STUDIES
Model Scale 1:24
Geometries Tested

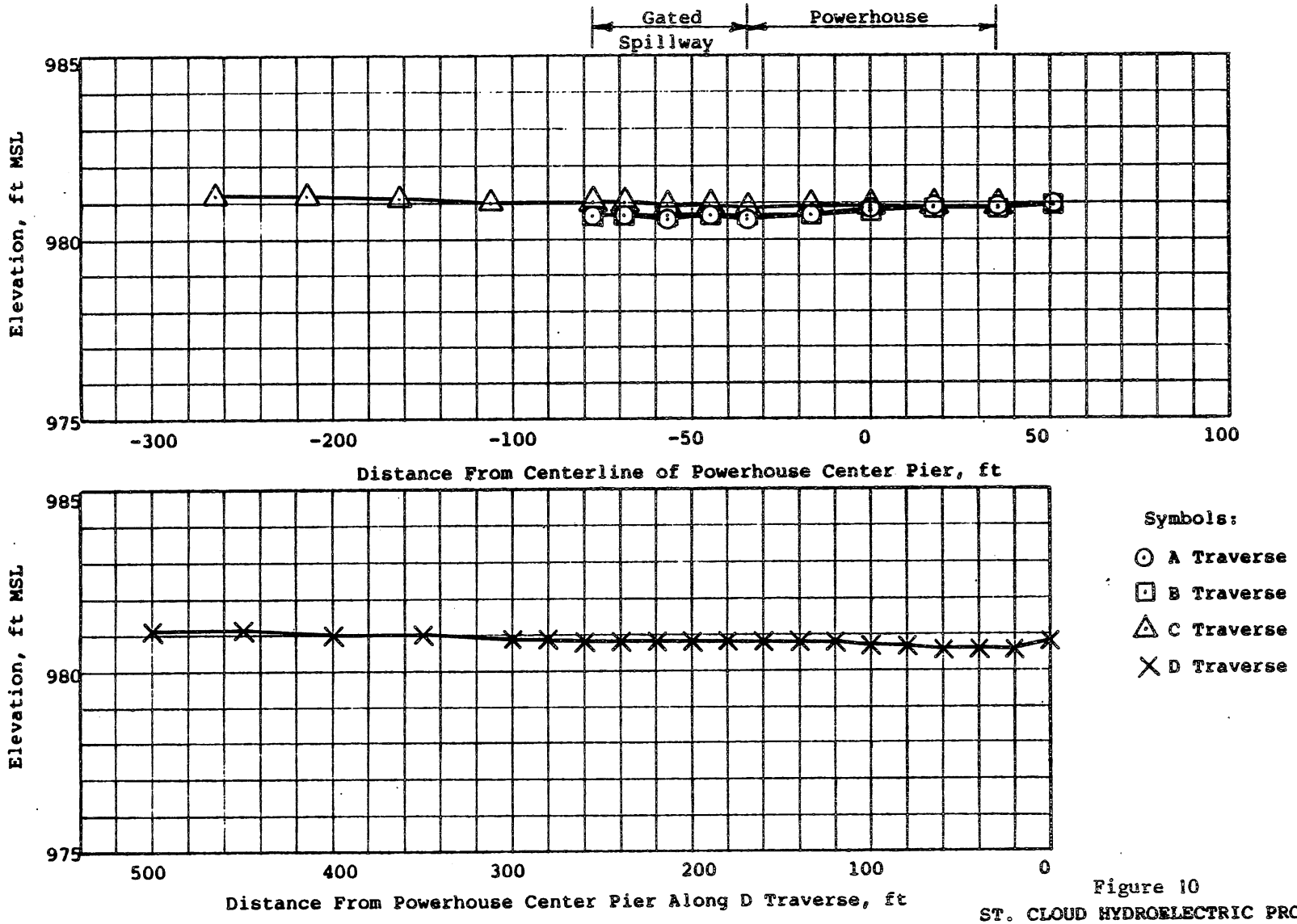

Figure 10

ST. CLOUD HYDROELECTRIC PROJECT
HYDRAULIC MODEL STUDIES
Type A1 , Model Scale 1:24
Q_p = 6500 cfs, Q_{GS} = 0 cfs,
Q_{MS} = 0 cfs, H.W. = 981 ft.
Typical Water Surface Traverses

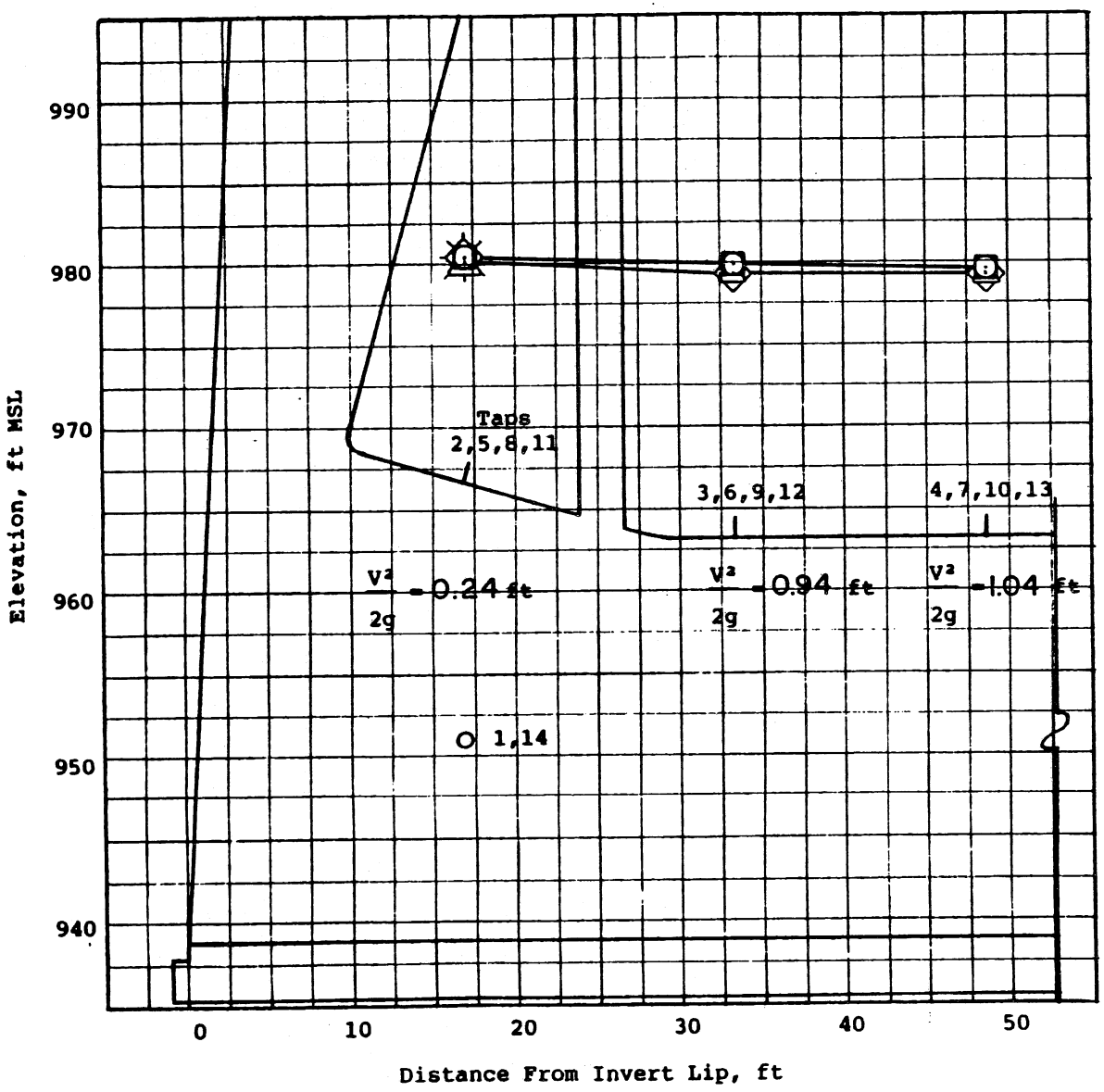

Symbols:

- ⊙ Bay 1 (Right Side)
- ⊡ Bay 2
- △ Bay 3
- ◇ Bay 4 (Left Side)
- + Right Wall Tap
- × Left Wall Tap

Figure 11
ST. CLOUD HYDROELECTRIC PROJECT
HYDRAULIC MODEL STUDIES
Type A1 , Model Scale 1:24
Q_p = 6500 cfs, Q_{GS} = 0 cfs
Q_{MS} = 0 cfs, H.W. = 981 ft

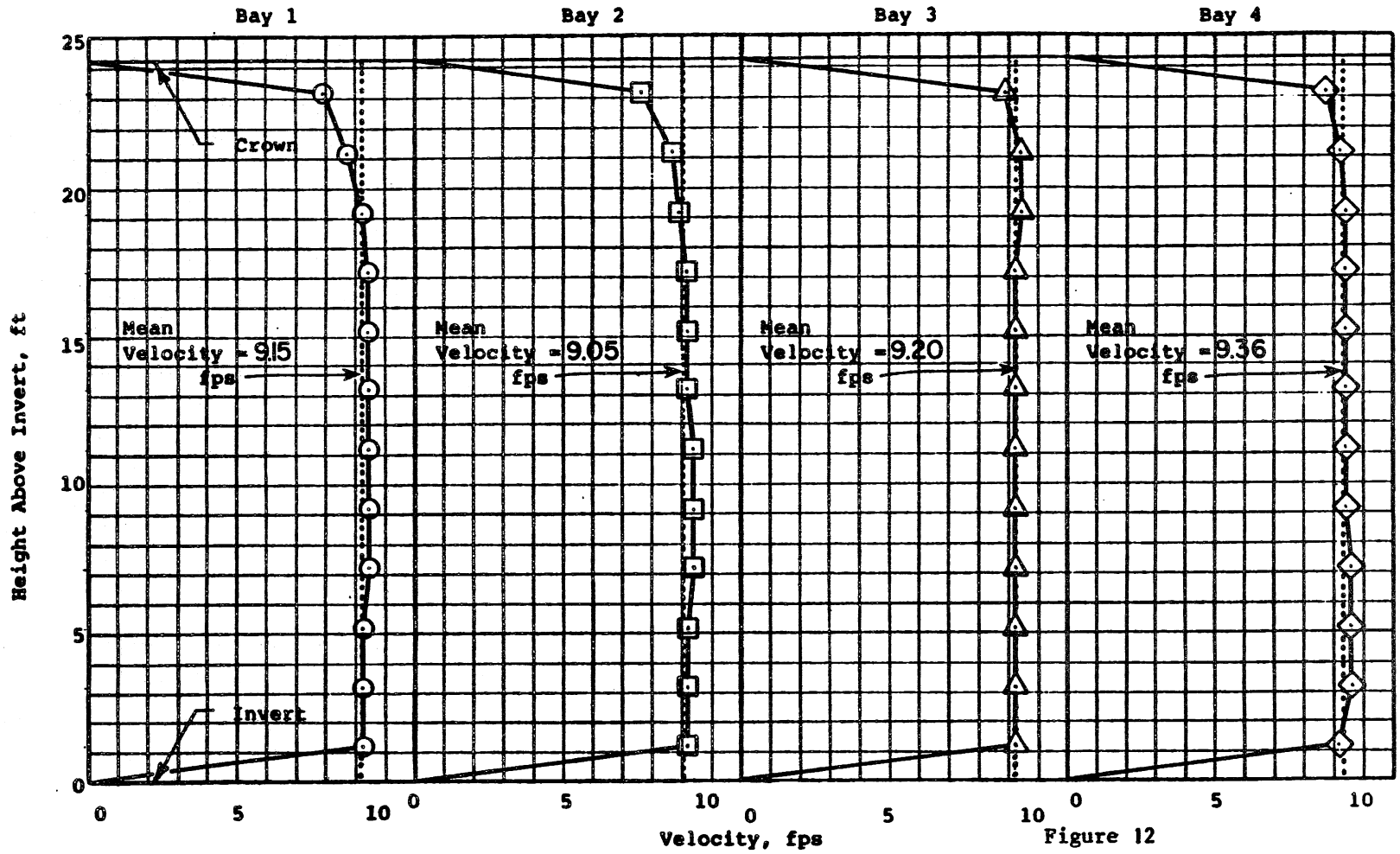

Figure 12

ST. CLOUD HYDROELECTRIC PROJECT
HYDRAULIC MODEL STUDIES
Type Al , Model Scale 1:24
Q_p = 6500 cfs, Q_{GS} = 0 cfs,
Q_{MS} = 0 cfs, H.W. = 981 ft.
Typical Velocity Profiles

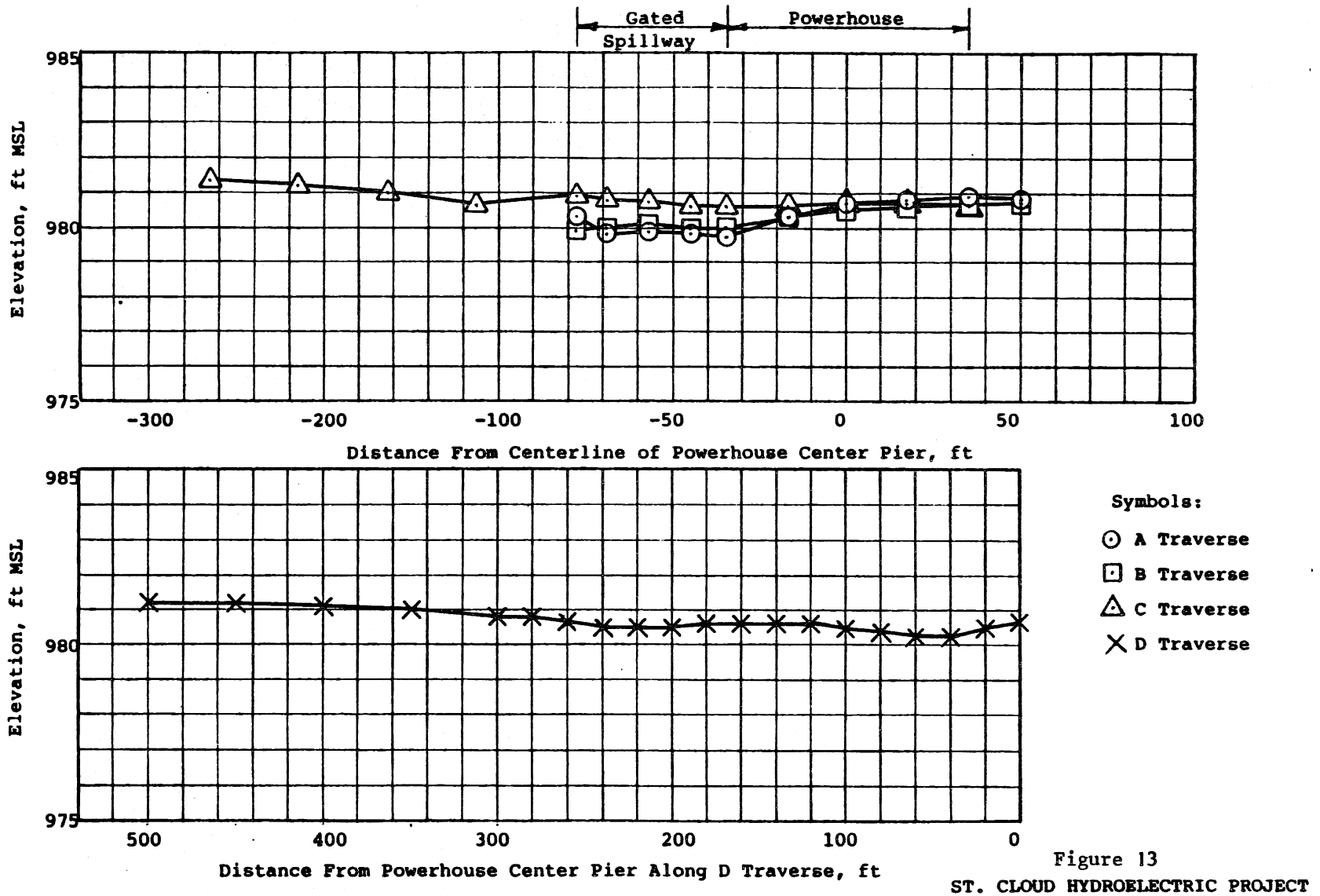

Figure 13

ST. CLOUD HYDROELECTRIC PROJECT
HYDRAULIC MODEL STUDIES
Type A1 , Model Scale 1:24
Q_p =6500 cfs, Q_{GS} =3000 cfs,
Q_{MS} =0 cfs, H.W. =981 ft.
Typical Water Surface Traverses

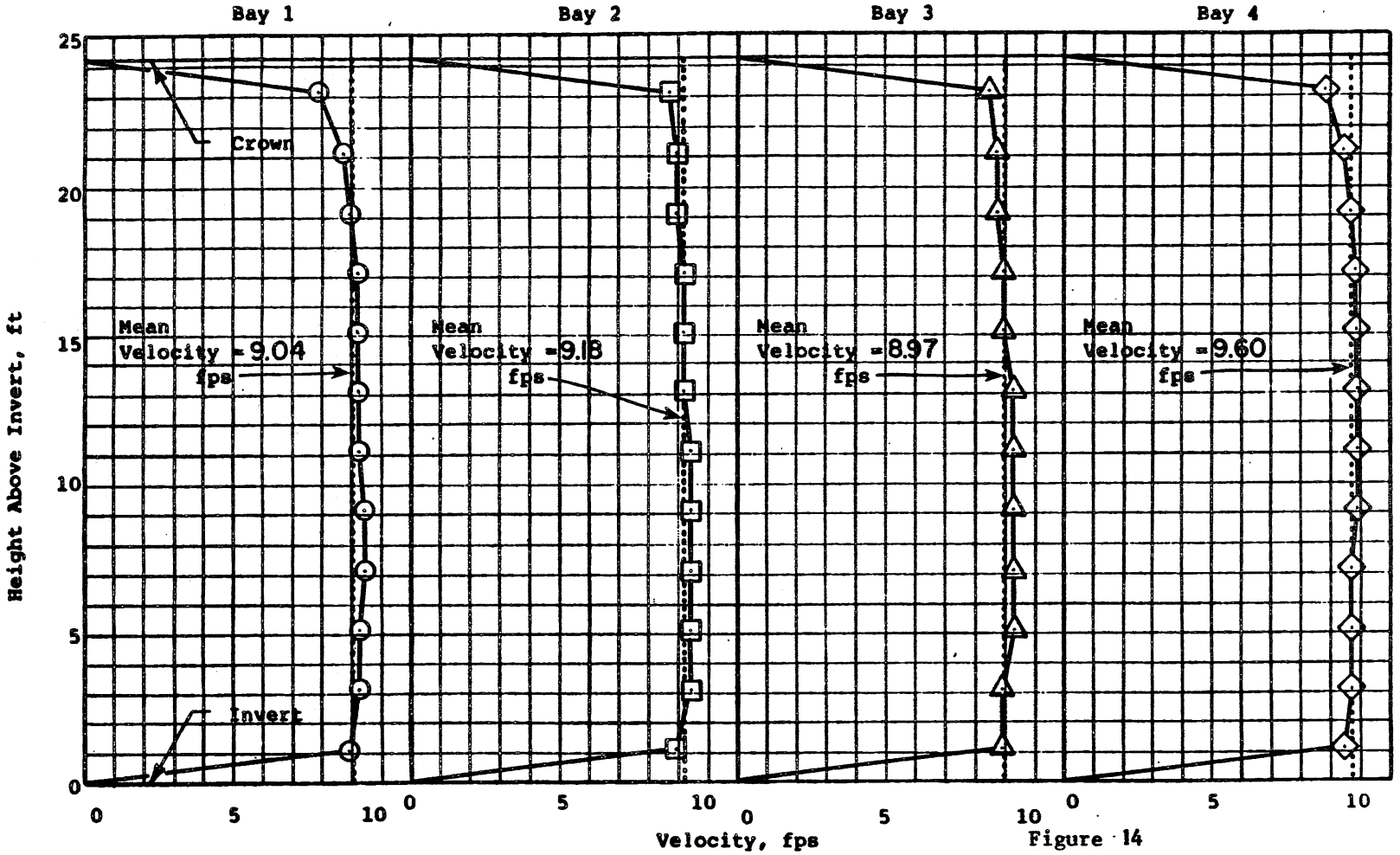

Figure 14

ST. CLOUD HYDROELECTRIC PROJECT
HYDRAULIC MODEL STUDIES
Type AI , Model Scale 1:24
Q_p =6500 cfs, Q_{GS} =3000 cfs,
Q_{MS} = 0 cfs, H.W. = 981 ft.
Typical Velocity Profiles

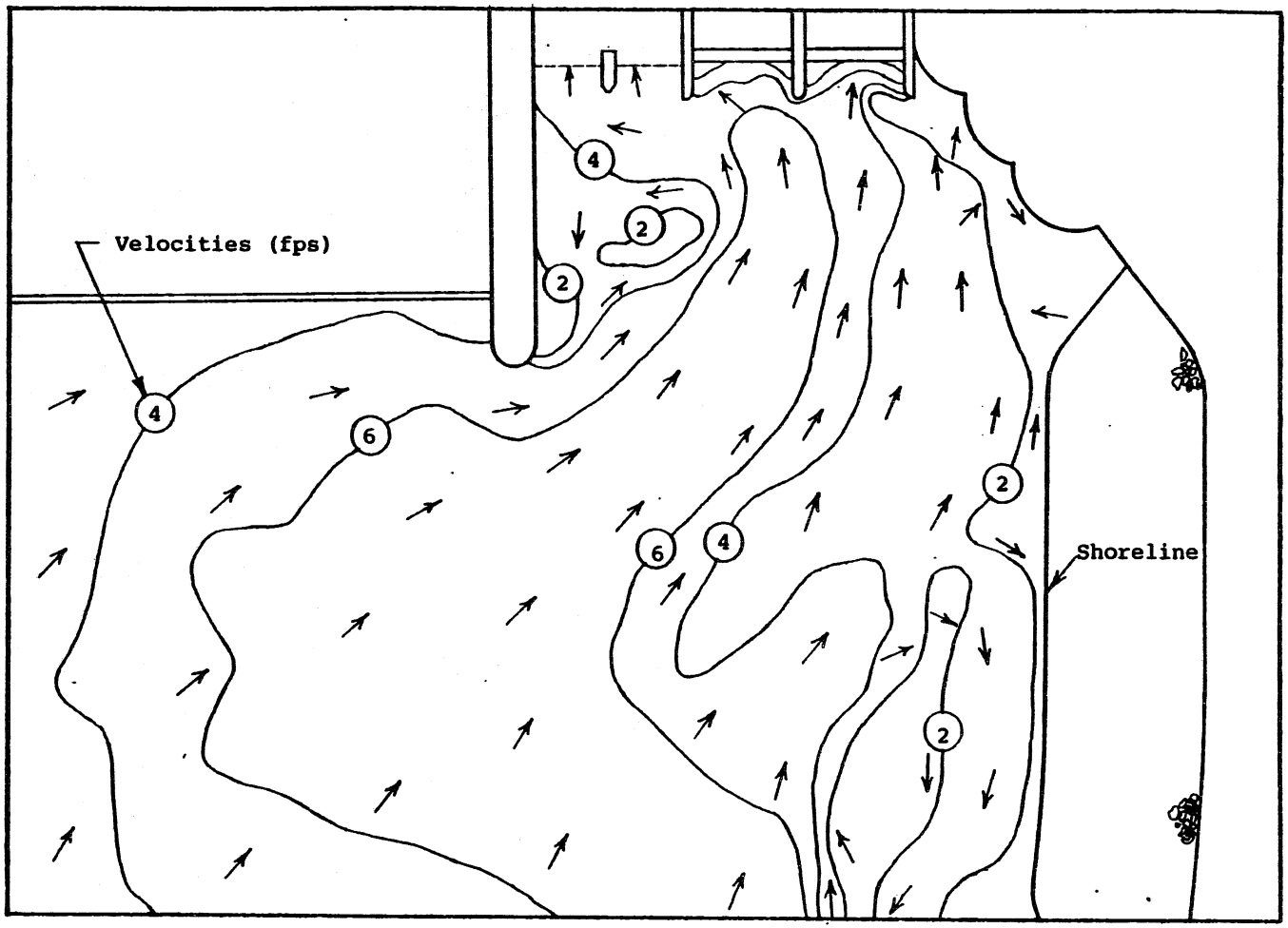

From Photo No. 381-63

Figure 15

ST. CLOUD HYDROELECTRIC PROJECT
HYDRAULIC MODEL STUDIES
Type A1, Model Scale 1:24
Q_p = 6,500 cfs, Q_{GS} = 3000 cfs,
Q_{MS} = 0 cfs, H.W. = 981 ft.
Flow Patterns and Velocities at the Water Surface

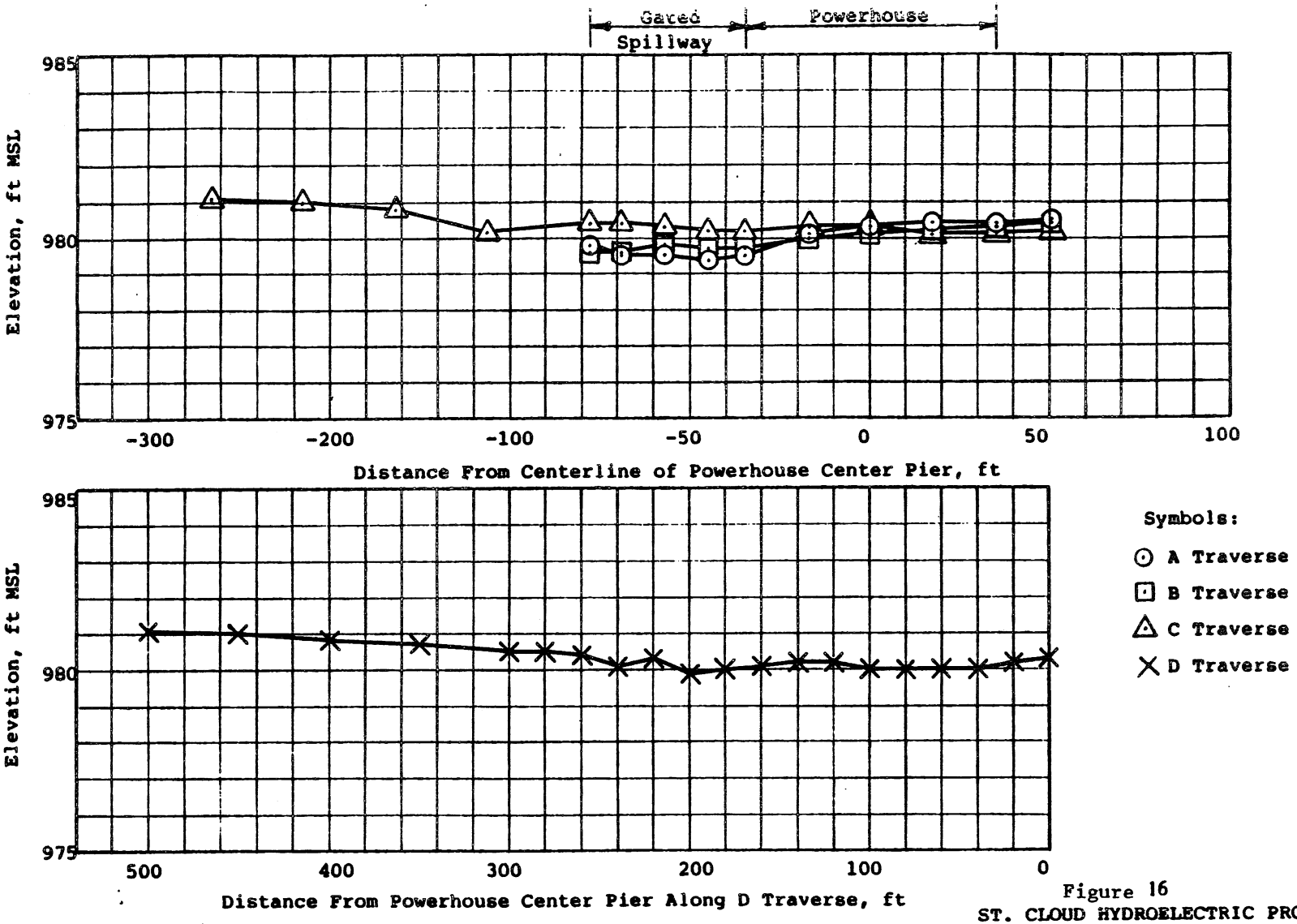

Figure 16

ST. CLOUD HYDROELECTRIC PROJECT
HYDRAULIC MODEL STUDIES
Type Al , Model Scale 1:24
Q_p = 6500 cfs, Q_{GS} = 3000 cfs,
Q_{MS} = 2400 cfs, H.W. = 981 ft.
Typical Water Surface Traverses

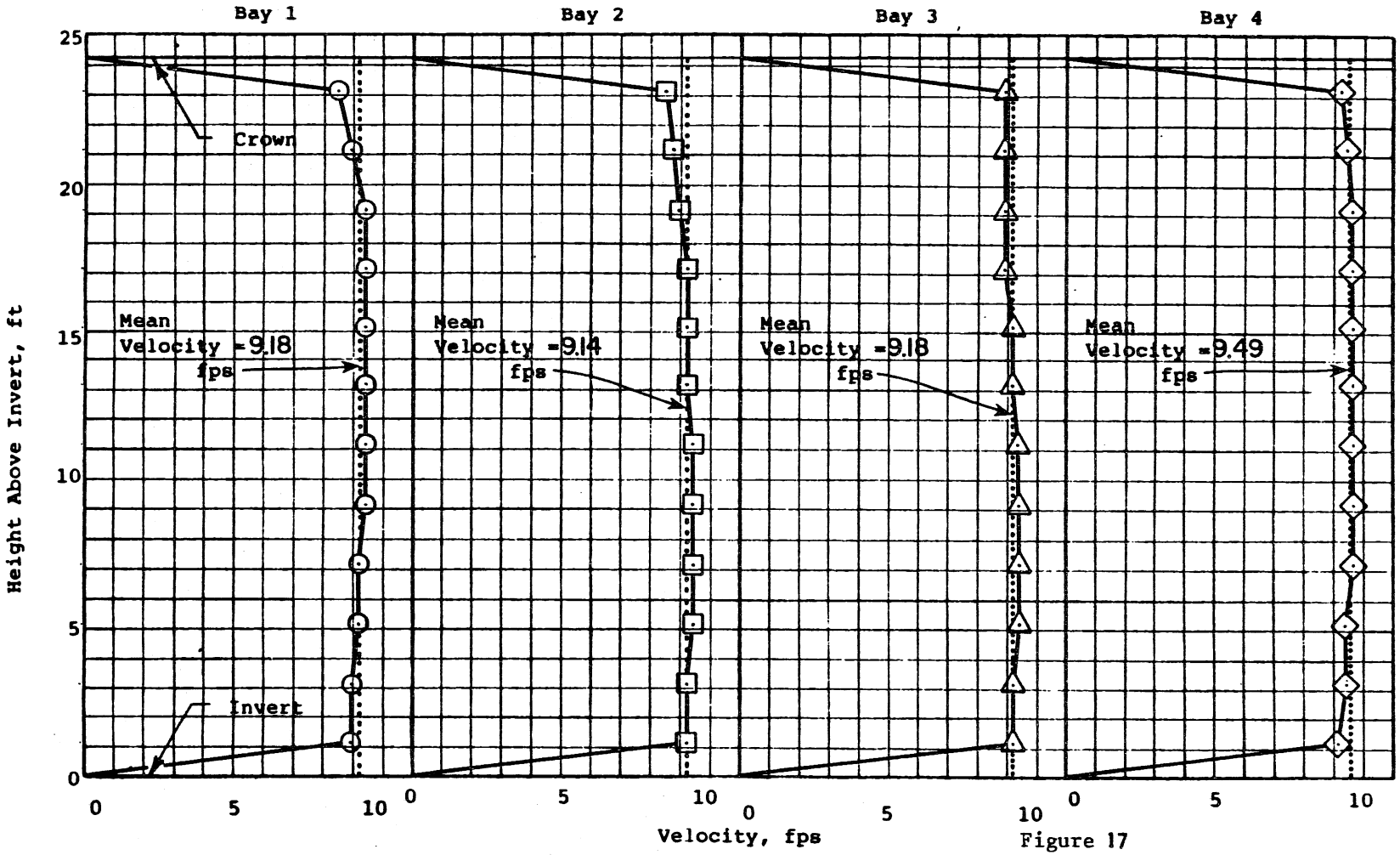

Figure 17

ST. CLOUD HYDROELECTRIC PROJECT
HYDRAULIC MODEL STUDIES
Type AI , Model Scale 1:24
Q_p =6500 cfs, Q_{GS} =3000 cfs,
Q_{MS} =2400 cfs, H.W. =981 ft.
Typical Velocity Profiles

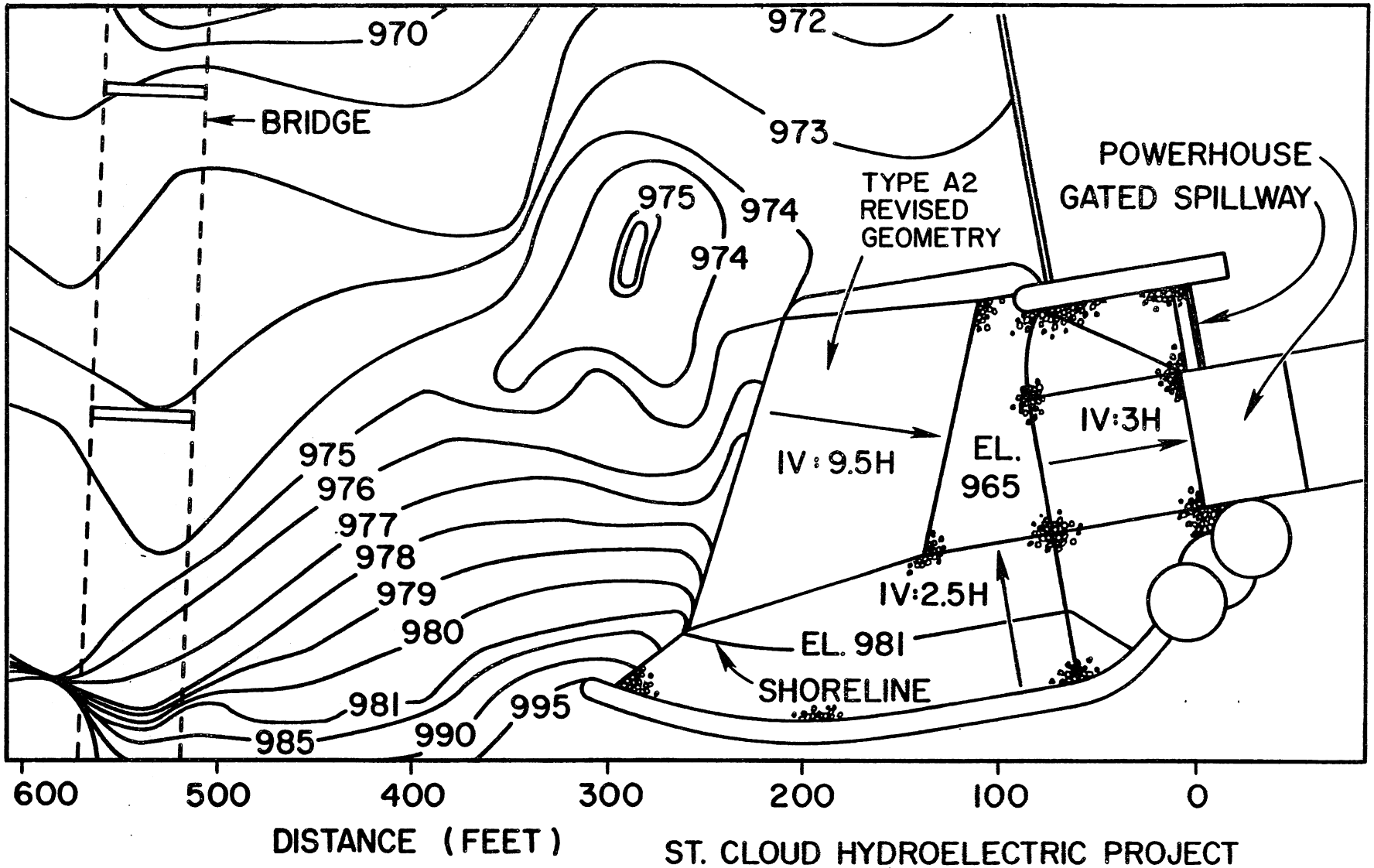

Figure 18

ST. CLOUD HYDROELECTRIC PROJECT
HYDRAULIC MODEL STUDIES
MODEL SCALE 1:24
TYPE A2 REVISED GEOMETRY

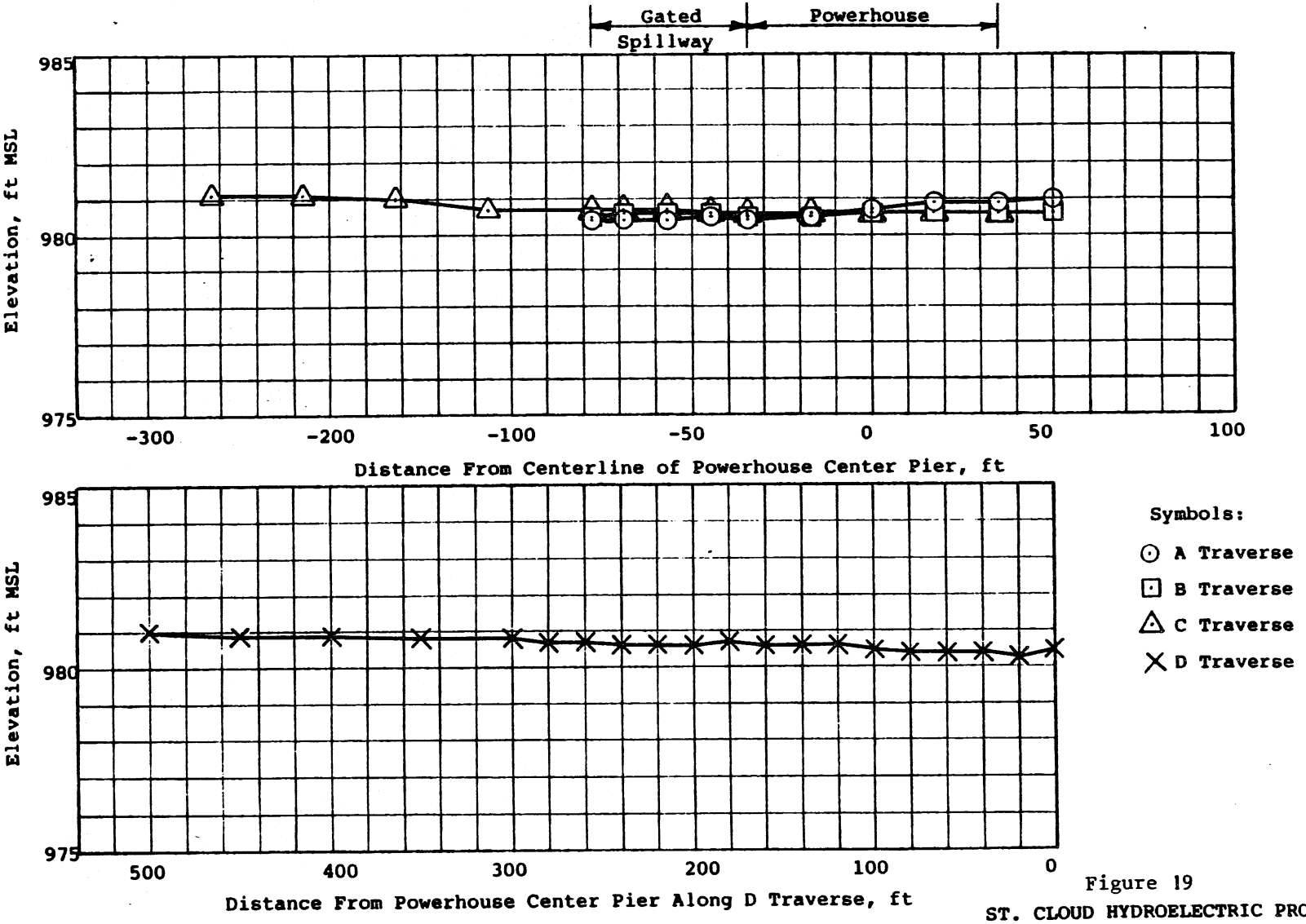

Figure 19

ST. CLOUD HYDROELECTRIC PROJECT
HYDRAULIC MODEL STUDIES
Type A2 , Model Scale 1:24
Q_p =6500 cfs, Q_{GS} =0 cfs,
Q_{MS} =0 cfs, H.W. =981 ft.
Typical Water Surface Traverses

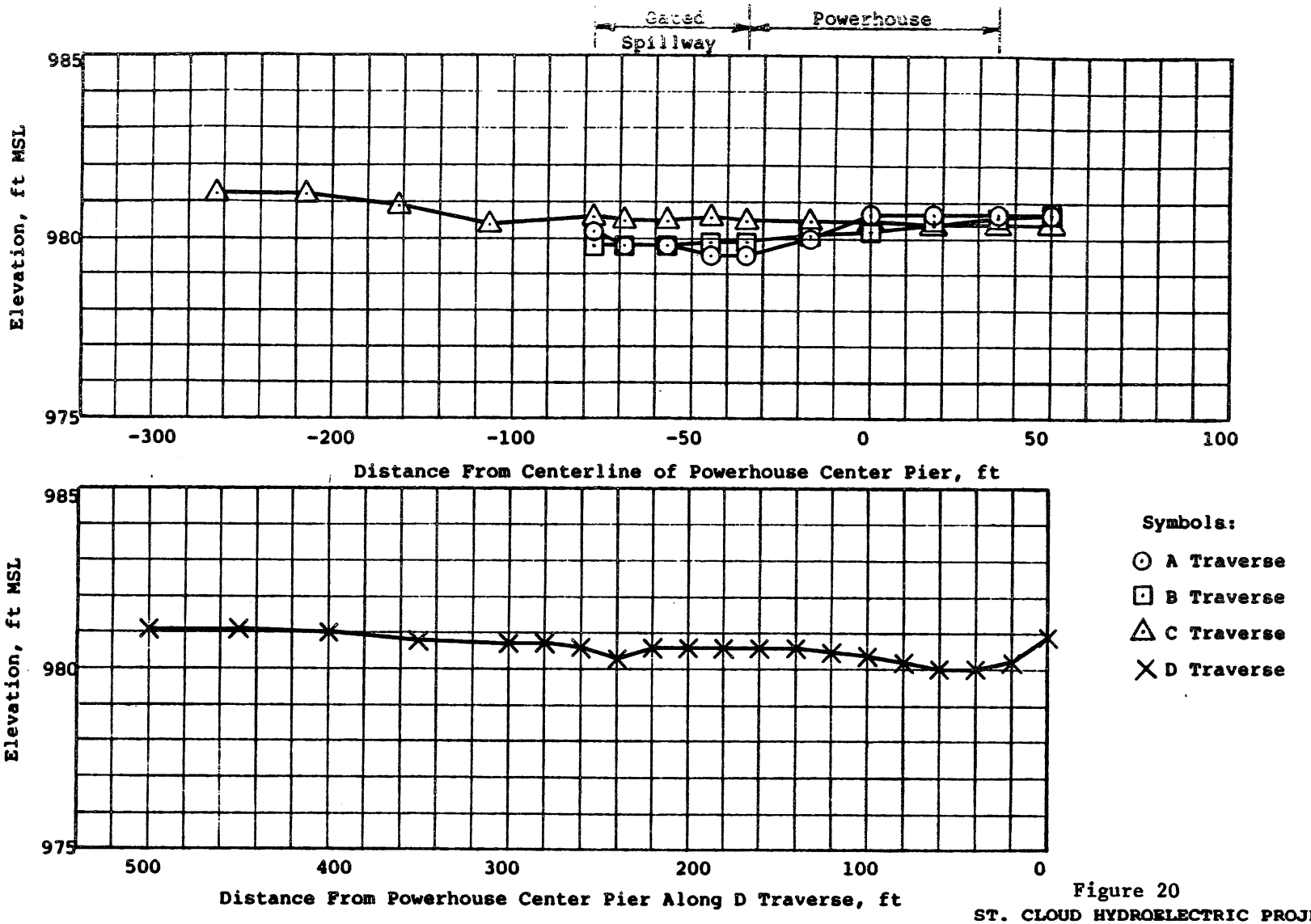

Figure 20

ST. CLOUD HYDROELECTRIC PROJECT
HYDRAULIC MODEL STUDIES
Type A2 , Model Scale 1:24
Q_p = 6500 cfs, Q_{GS} = 3000 cfs,
Q_{MS} = 0 cfs, H.W. = 981 ft.
Typical Water Surface Traverses

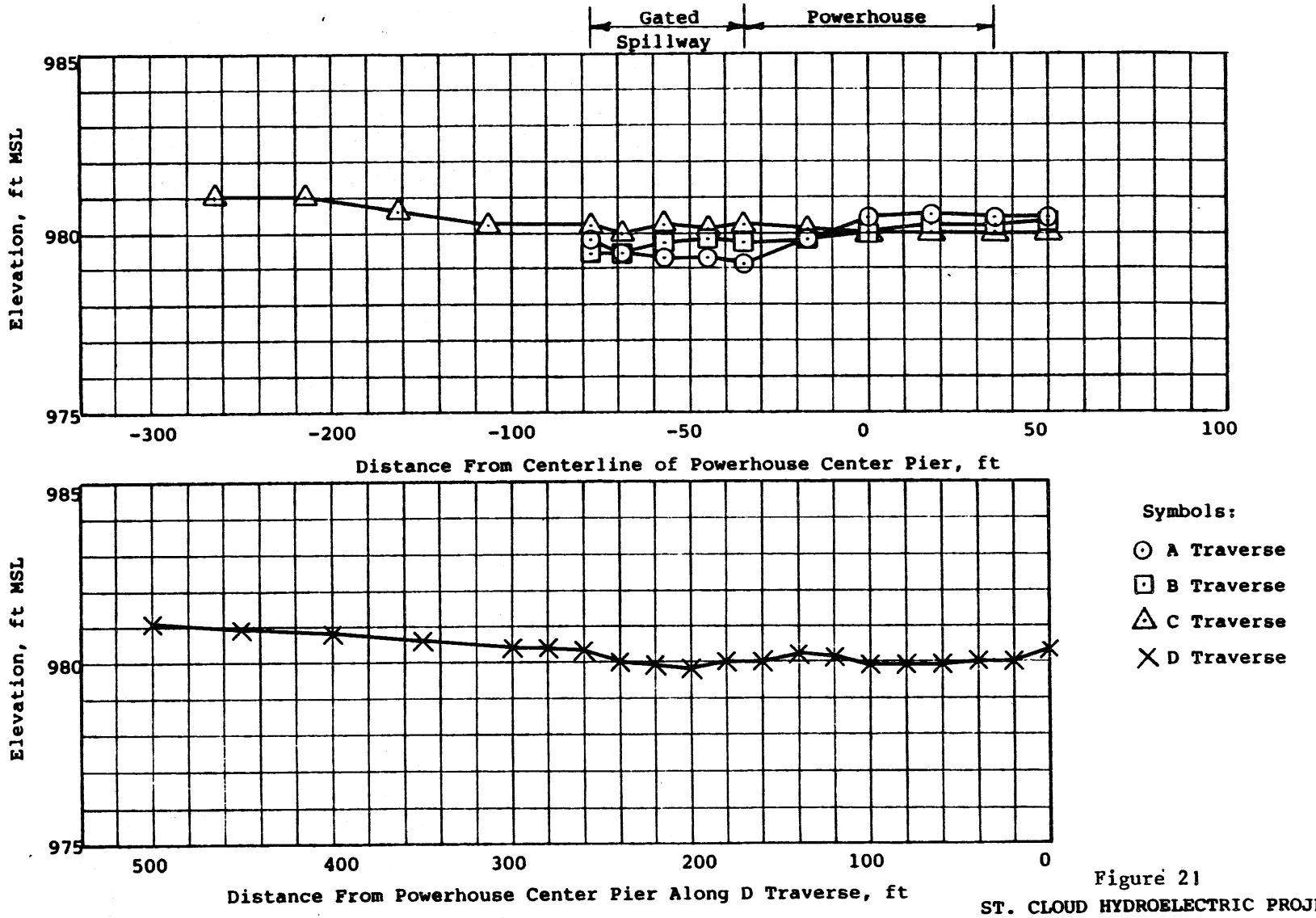

Figure 21

ST. CLOUD HYDROELECTRIC PROJECT
HYDRAULIC MODEL STUDIES
Type A2 , Model Scale 1:24
Q_p =6500 cfs, Q_{GS} =3000 cfs,
Q_{MS} =2400 cfs, H.W. =981 ft.
Typical Water Surface Traverses

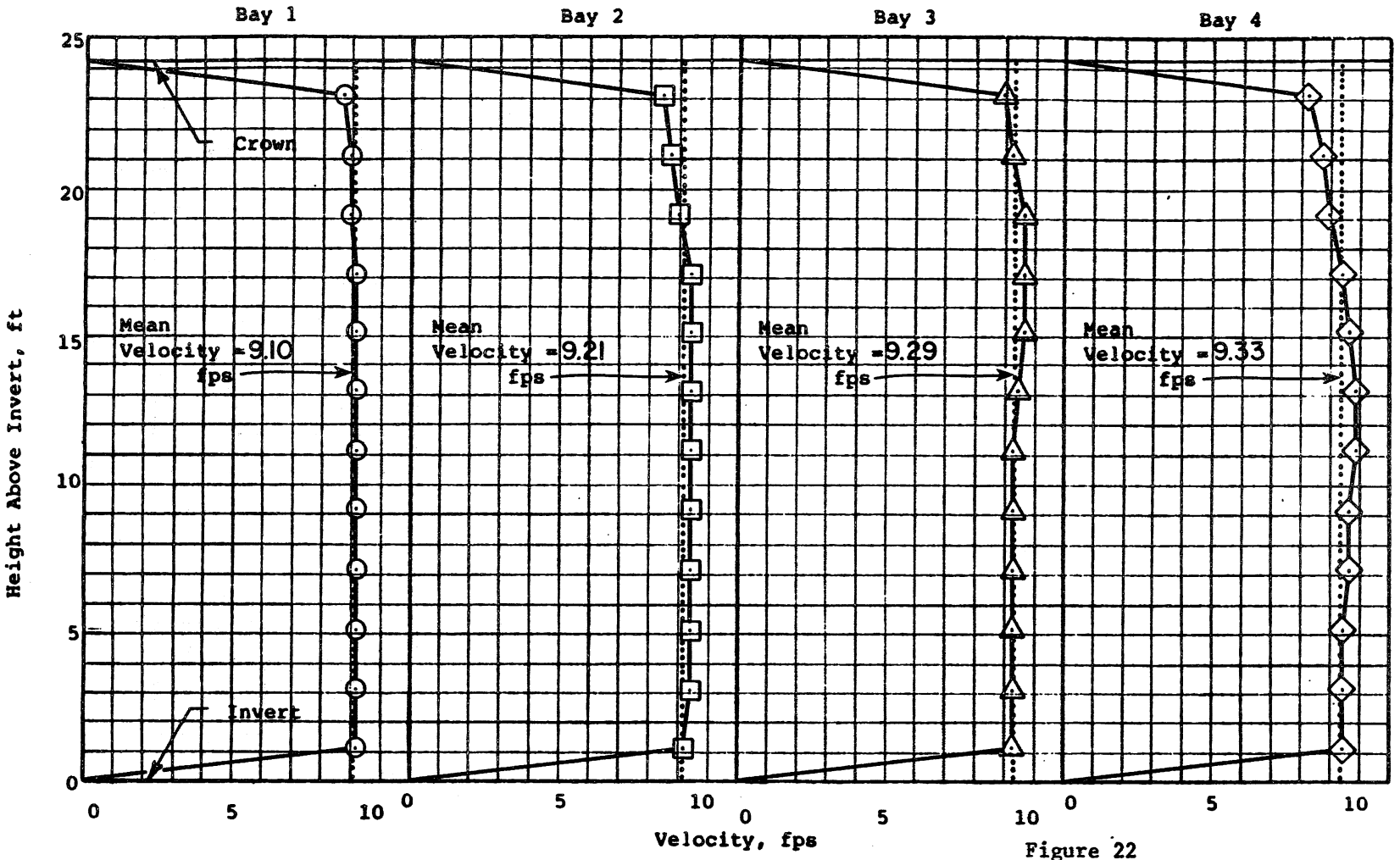

Figure 22

ST. CLOUD HYDROELECTRIC PROJECT
HYDRAULIC MODEL STUDIES
Type A3 , Model Scale 1:24
Q_p = 6500 cfs, Q_{GS} = 0 cfs,
Q_{MS} = 0 cfs, H.W. = 981 ft.
Typical Velocity Profiles

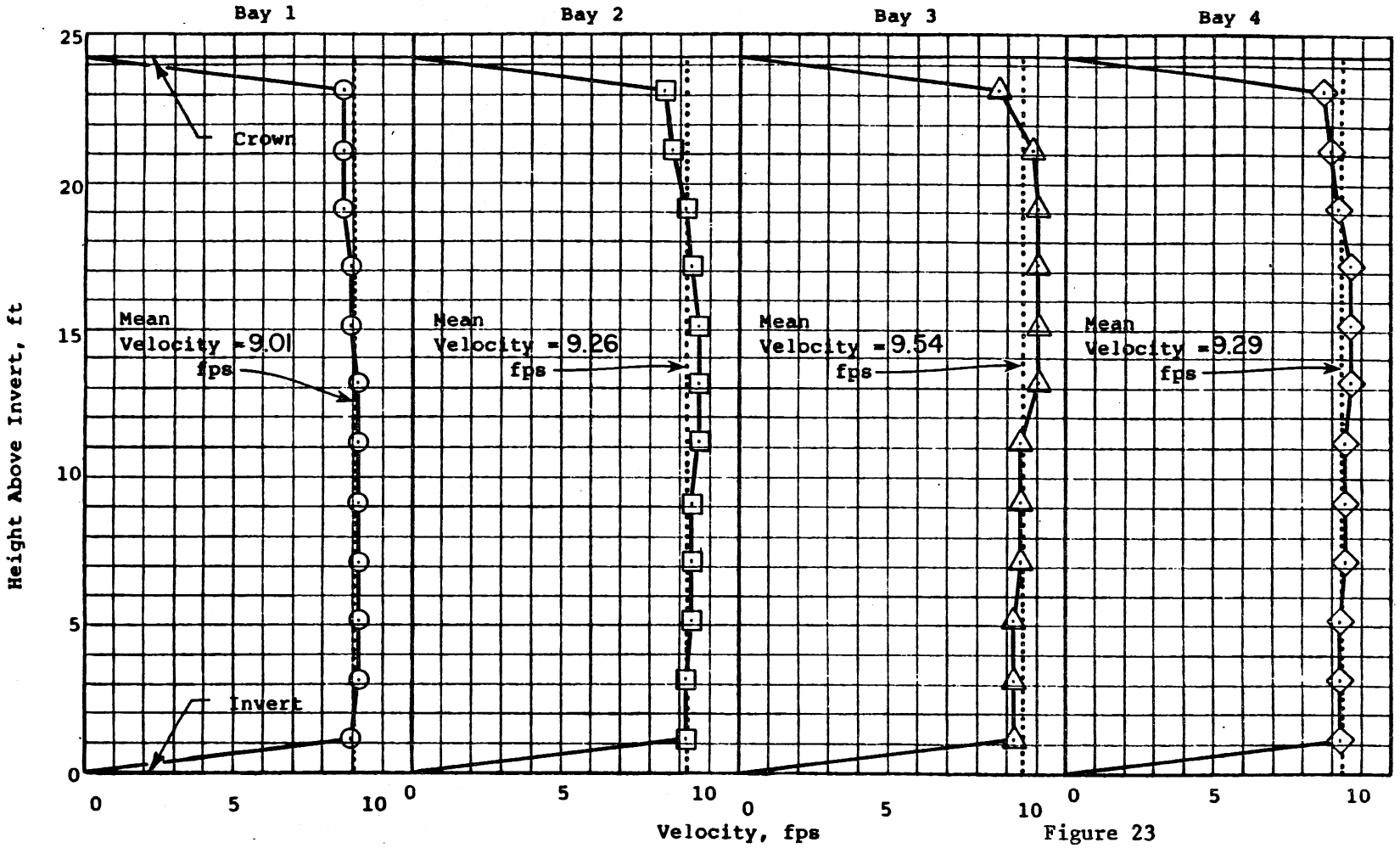

Figure 23

ST. CLOUD HYDROELECTRIC PROJECT
HYDRAULIC MODEL STUDIES
Type A4 , Model Scale 1:24
Q_p = 6500 cfs, Q_{GS} = 0 cfs,
Q_{MS} = 0 cfs, H.W. = 981 ft.
Typical Velocity Profiles

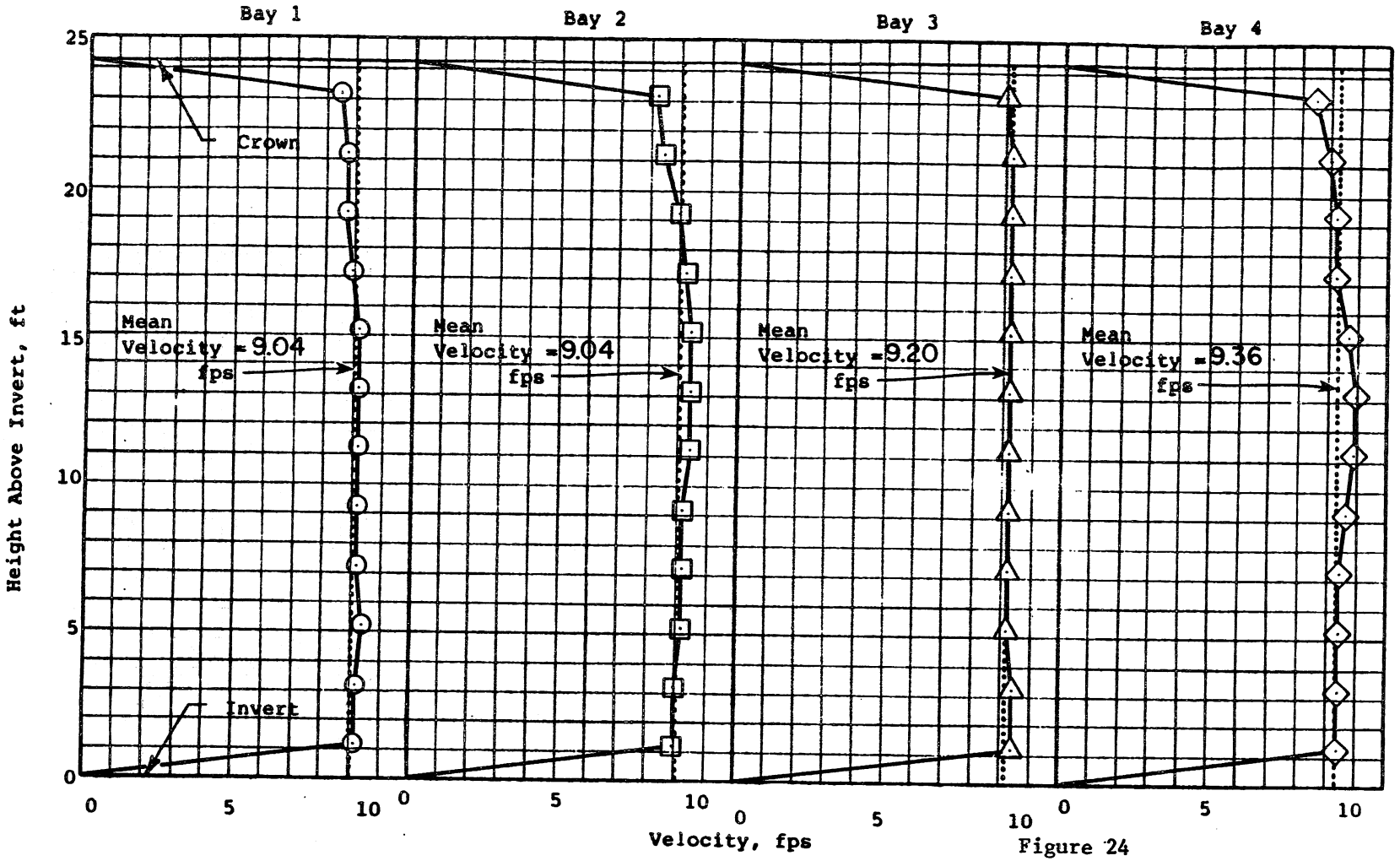

Figure 24

ST. CLOUD HYDROELECTRIC PROJECT
HYDRAULIC MODEL STUDIES
Type A5 , Model Scale 1:24
Q_p = 6500 cfs, Q_{GS} = 0 cfs,
Q_{MS} = 0 cfs, H.W. = 981 ft.
Typical Velocity Profiles

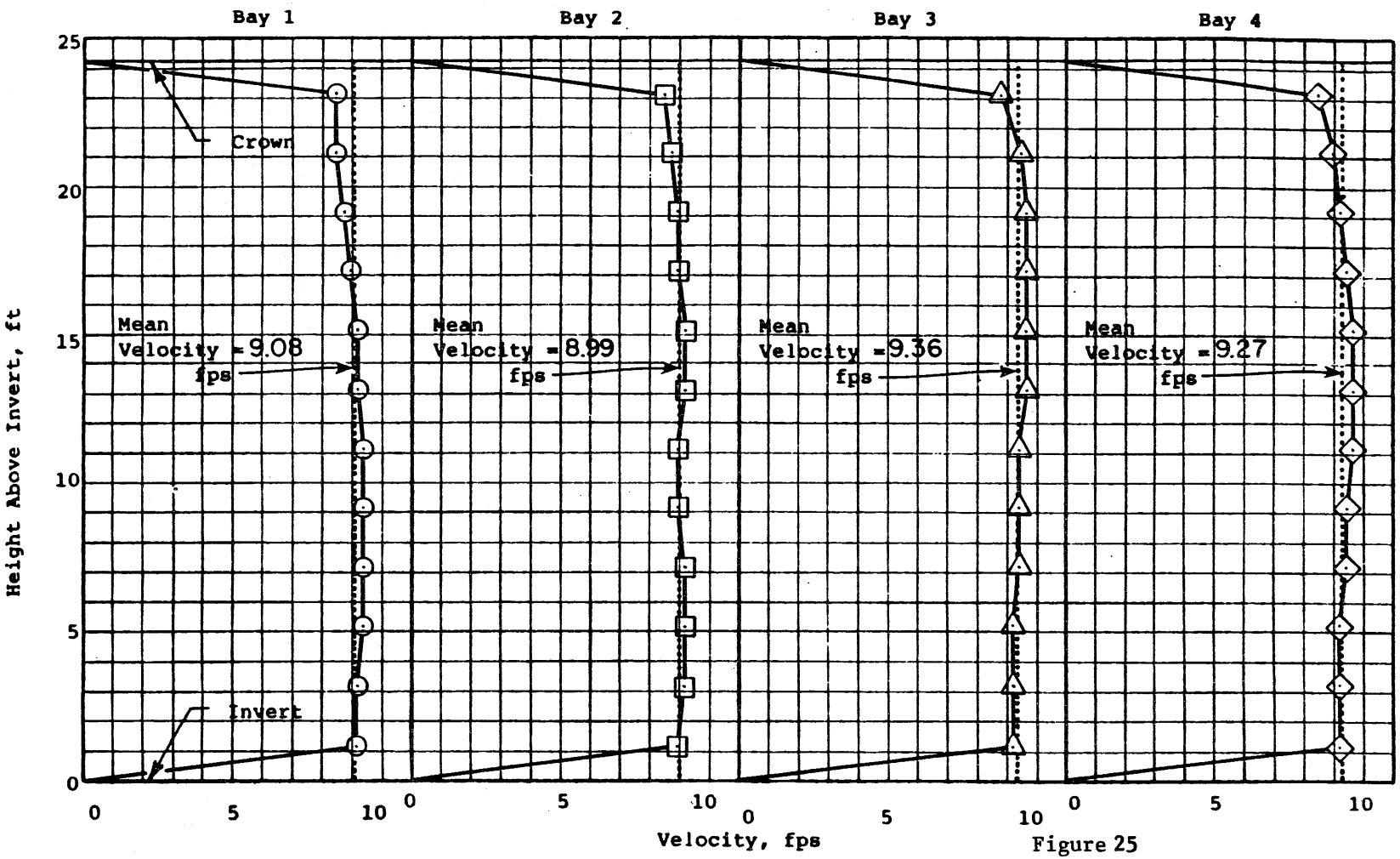

Figure 25

ST. CLOUD HYDROELECTRIC PROJECT
HYDRAULIC MODEL STUDIES
Type A6 , Model Scale 1:24
Q_p = 6500 cfs, Q_{GS} = 0 cfs,
Q_{MS} = 0 cfs, H.W. = 981 ft.
Typical Velocity Profiles

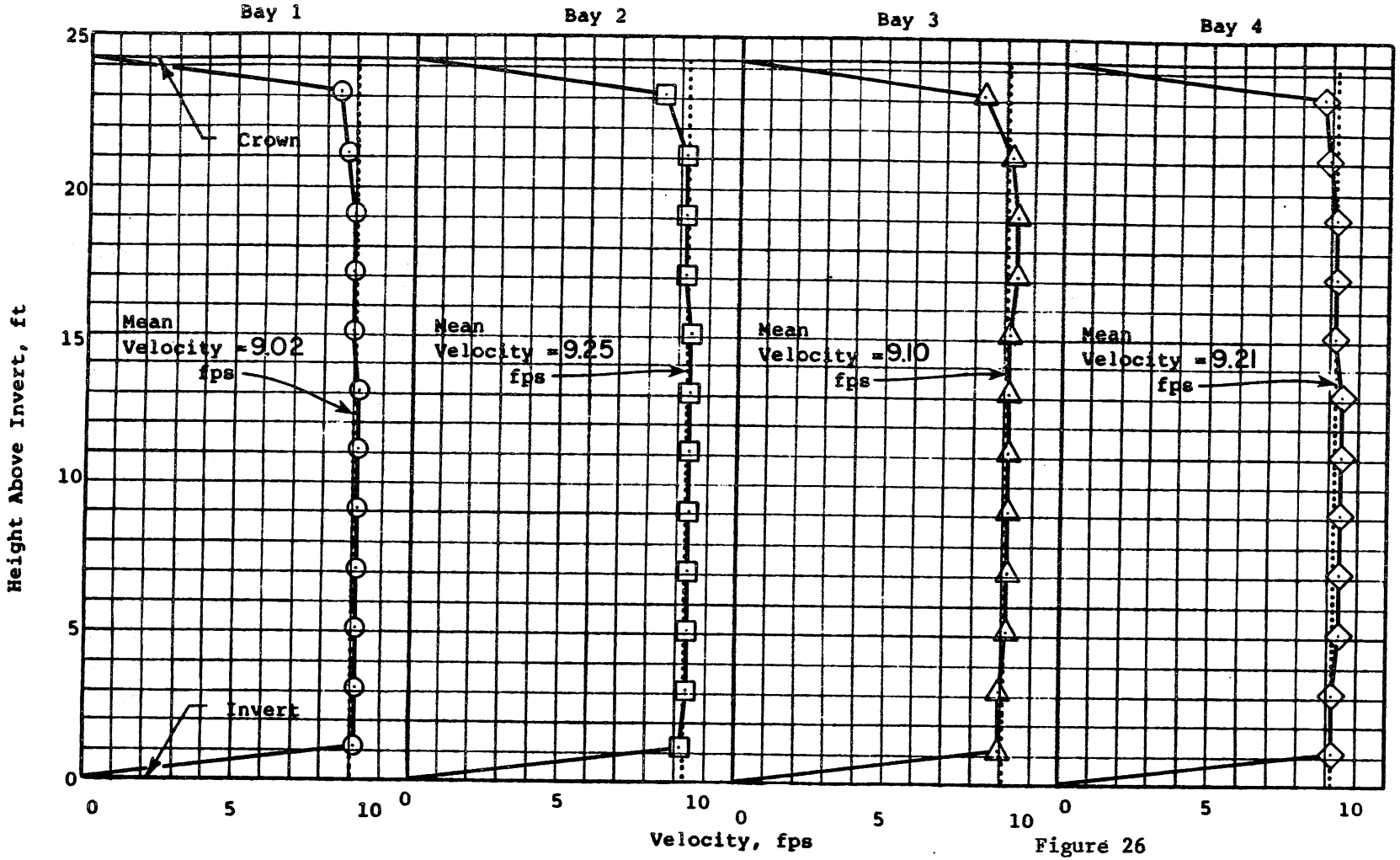

Figure 26

ST. CLOUD HYDROELECTRIC PROJECT
HYDRAULIC MODEL STUDIES

Type A7 , Model Scale 1:24

Q_P = 6500 cfs, Q_{GS} = 0 cfs,

Q_{MS} = 0 cfs, H.W. = 981 ft.

Typical Velocity Profiles

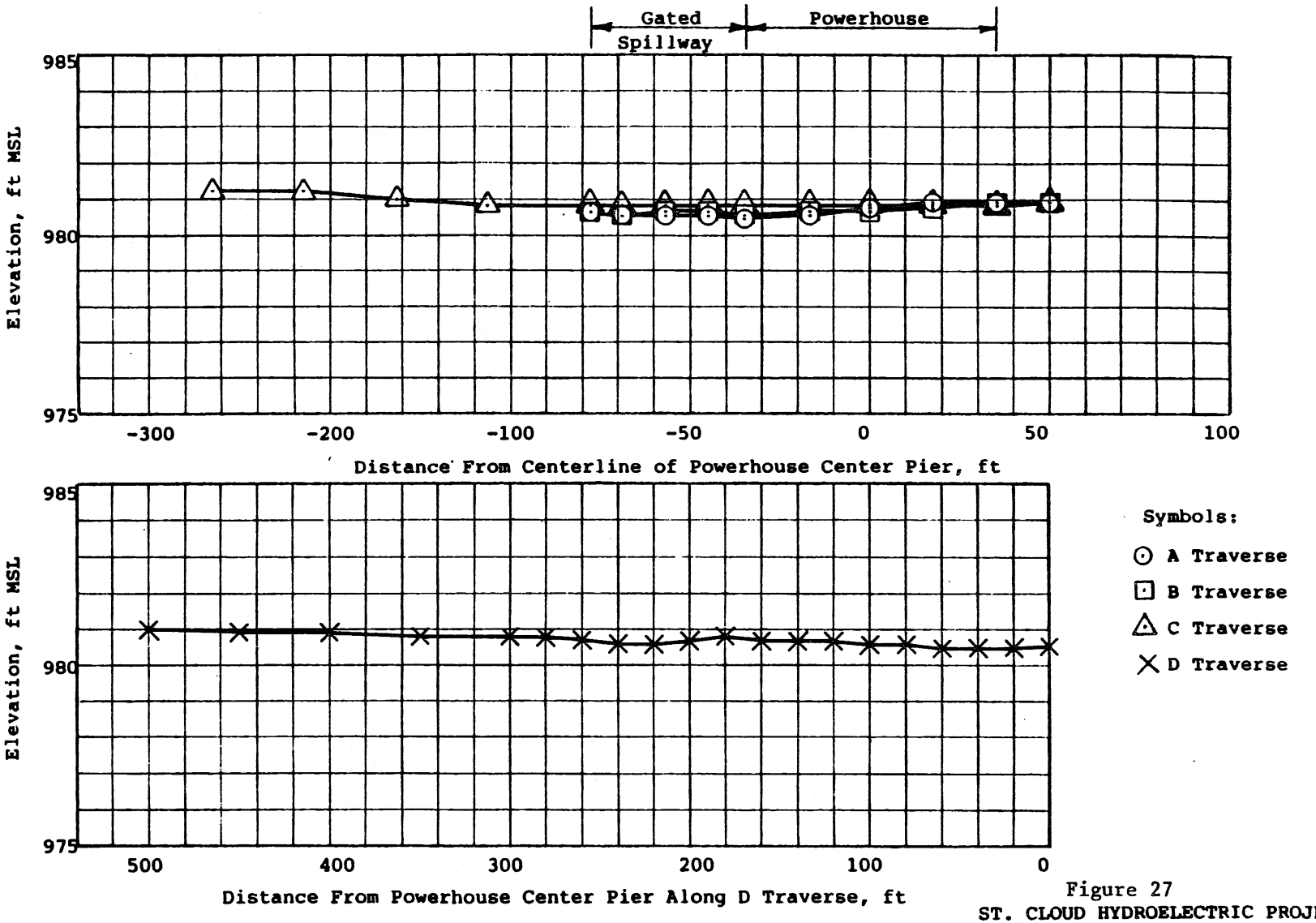

Figure 27
ST. CLOUD HYDROELECTRIC PROJECT
HYDRAULIC MODEL STUDIES
Type A8 , Model Scale 1:24
Q_p =6500 cfs, Q_{GS} = 0 cfs,
Q_{MS} = 0 cfs, H.W. = 981 ft.
Typical Water Surface Traverses

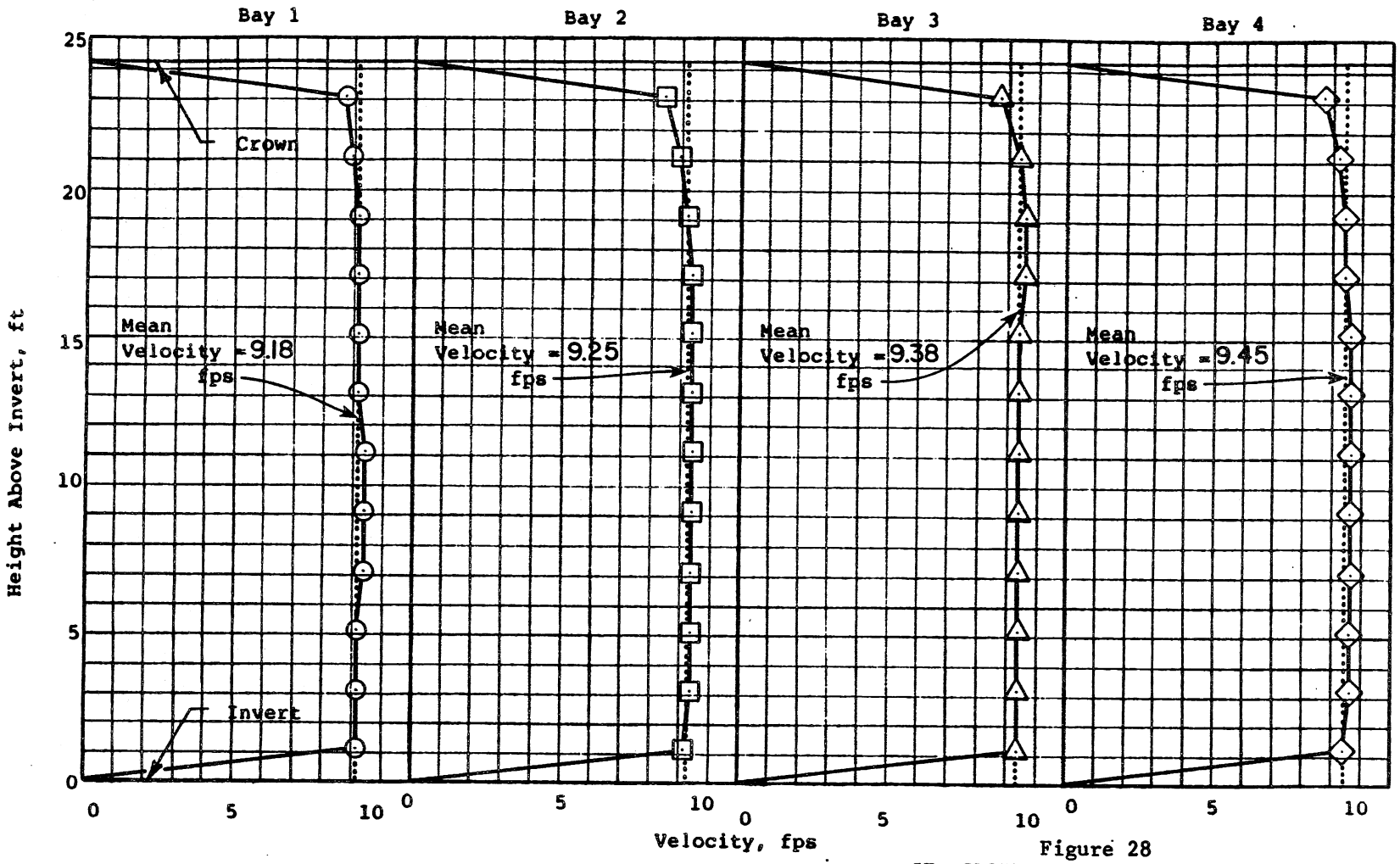

Figure 28

ST. CLOUD HYDROELECTRIC PROJECT
HYDRAULIC MODEL STUDIES

Type A8 , Model Scale 1:24

Q_p = 6500 cfs, Q_{GS} = 0 cfs,

Q_{MS} = 0 cfs, H.W. = 981 ft.

Typical Velocity Profiles

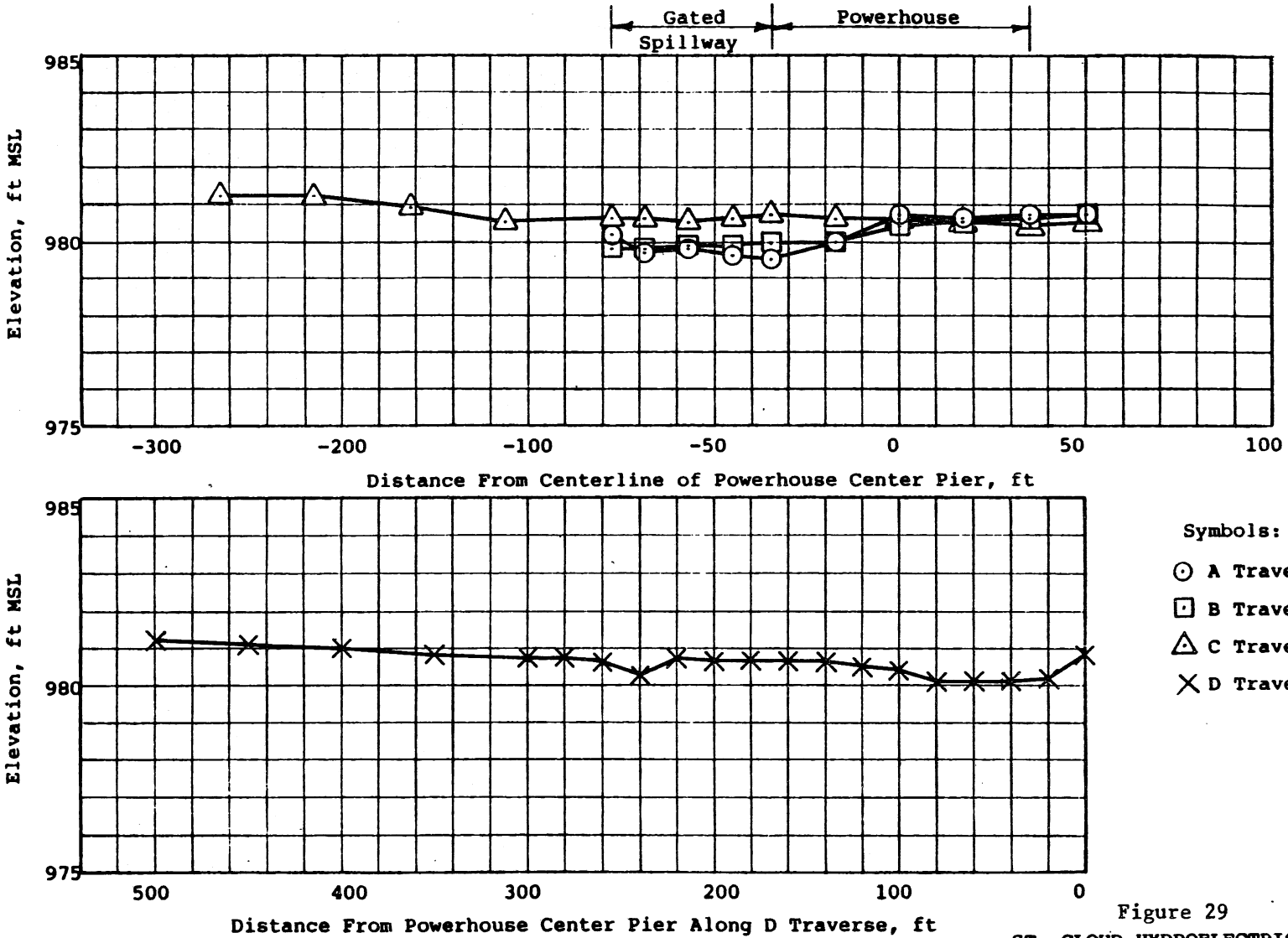

Figure 29

ST. CLOUD HYDROELECTRIC PROJECT
HYDRAULIC MODEL STUDIES
Type A8 , Model Scale 1:24
Q_p = 6500 cfs, Q_{GS} = 3000 cfs,
Q_{MS} = 0 cfs, H.W. = 981 ft.
Typical Water Surface Traverses

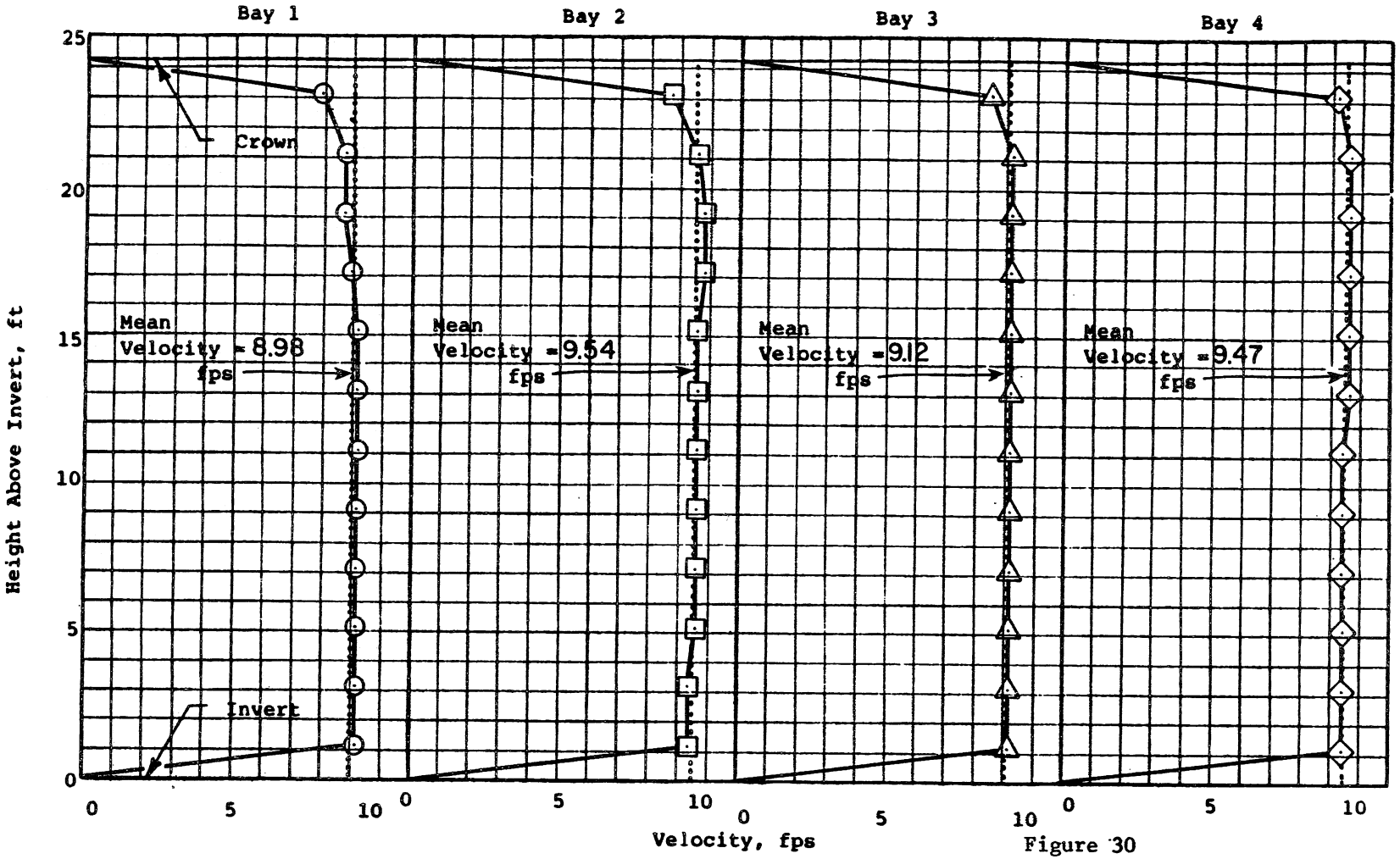

Figure 30

ST. CLOUD HYDROELECTRIC PROJECT
HYDRAULIC MODEL STUDIES
Type A8 , Model Scale 1:24
Q_p = 6500 cfs, Q_{GS} = 3000 cfs,
Q_{MS} = 0 cfs, H.W. = 981 ft.
Typical Velocity Profiles

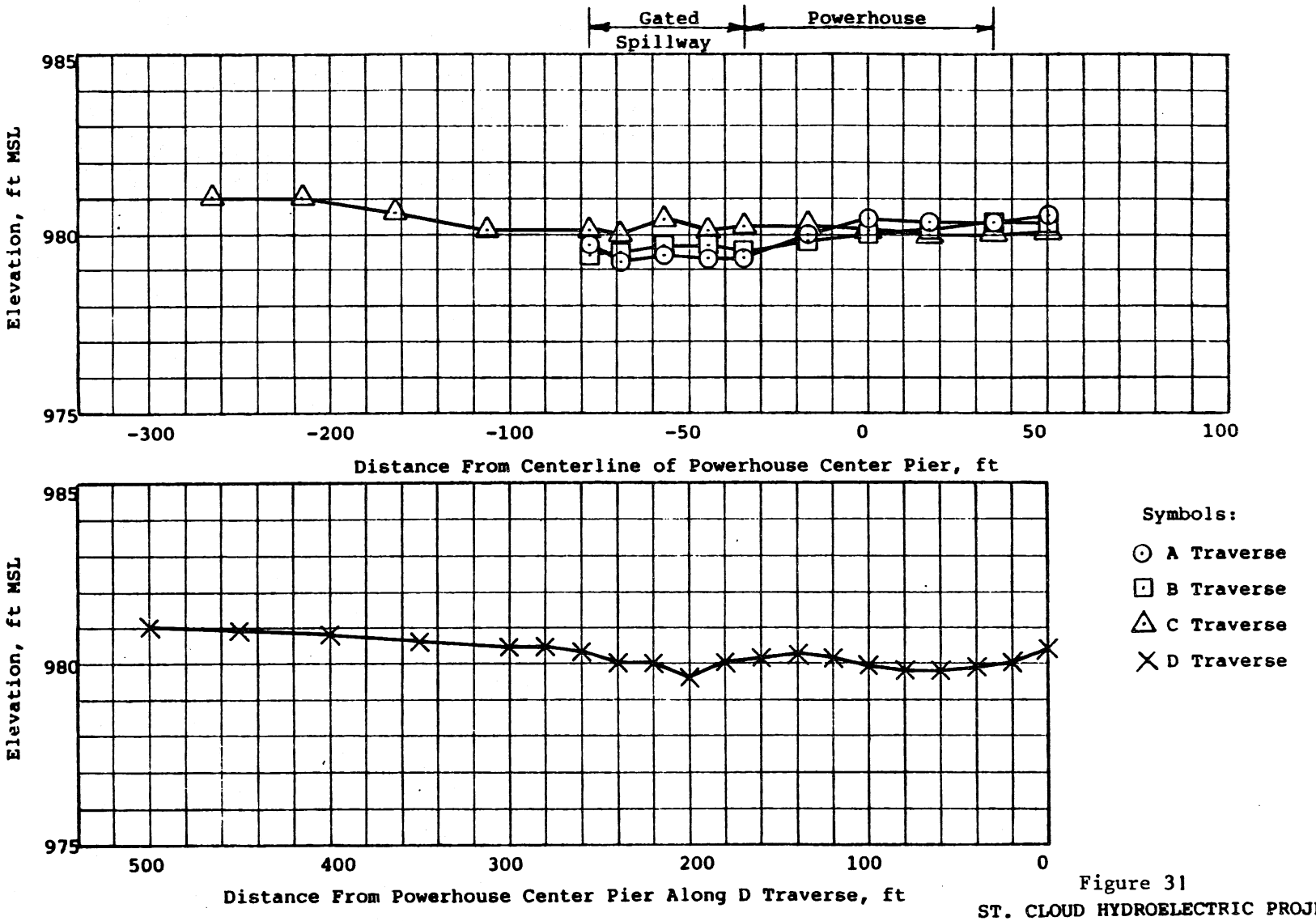

Figure 31

ST. CLOUD HYDROELECTRIC PROJECT
HYDRAULIC MODEL STUDIES
Type A8 , Model Scale 1:24
Q_p =6500 cfs, Q_{GS} =3000 cfs,
Q_{MS} =2400 cfs, H.W. =981 ft.
Typical Water Surface Traverses

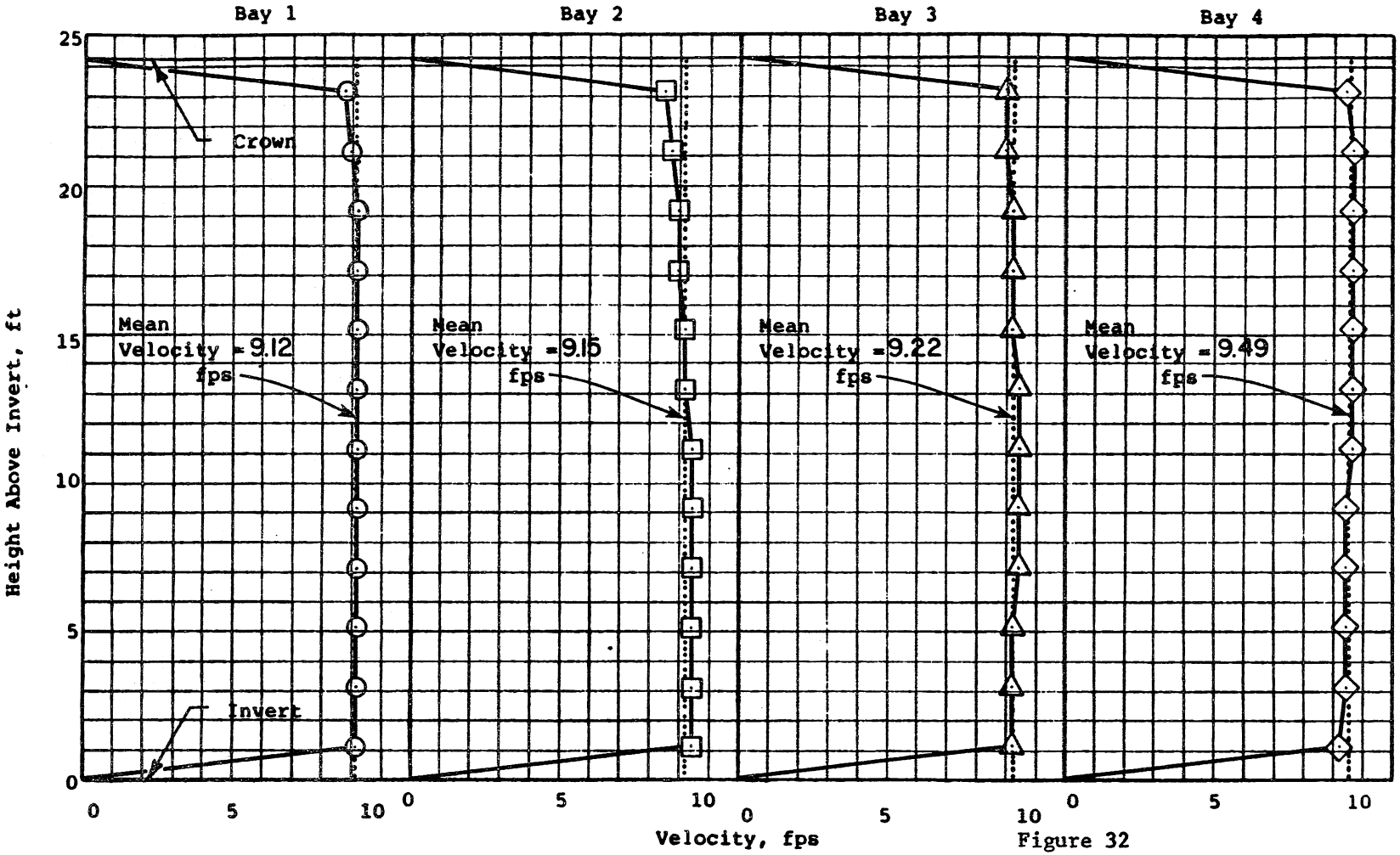

Figure 32

ST. CLOUD HYDROELECTRIC PROJECT
HYDRAULIC MODEL STUDIES

Type A8 , Model Scale 1:24

Q_p = 6500 cfs, Q_{GS} = 3000 cfs,

Q_{MS} = 2400 cfs, H.W. = 981 ft.

Typical Velocity Profiles

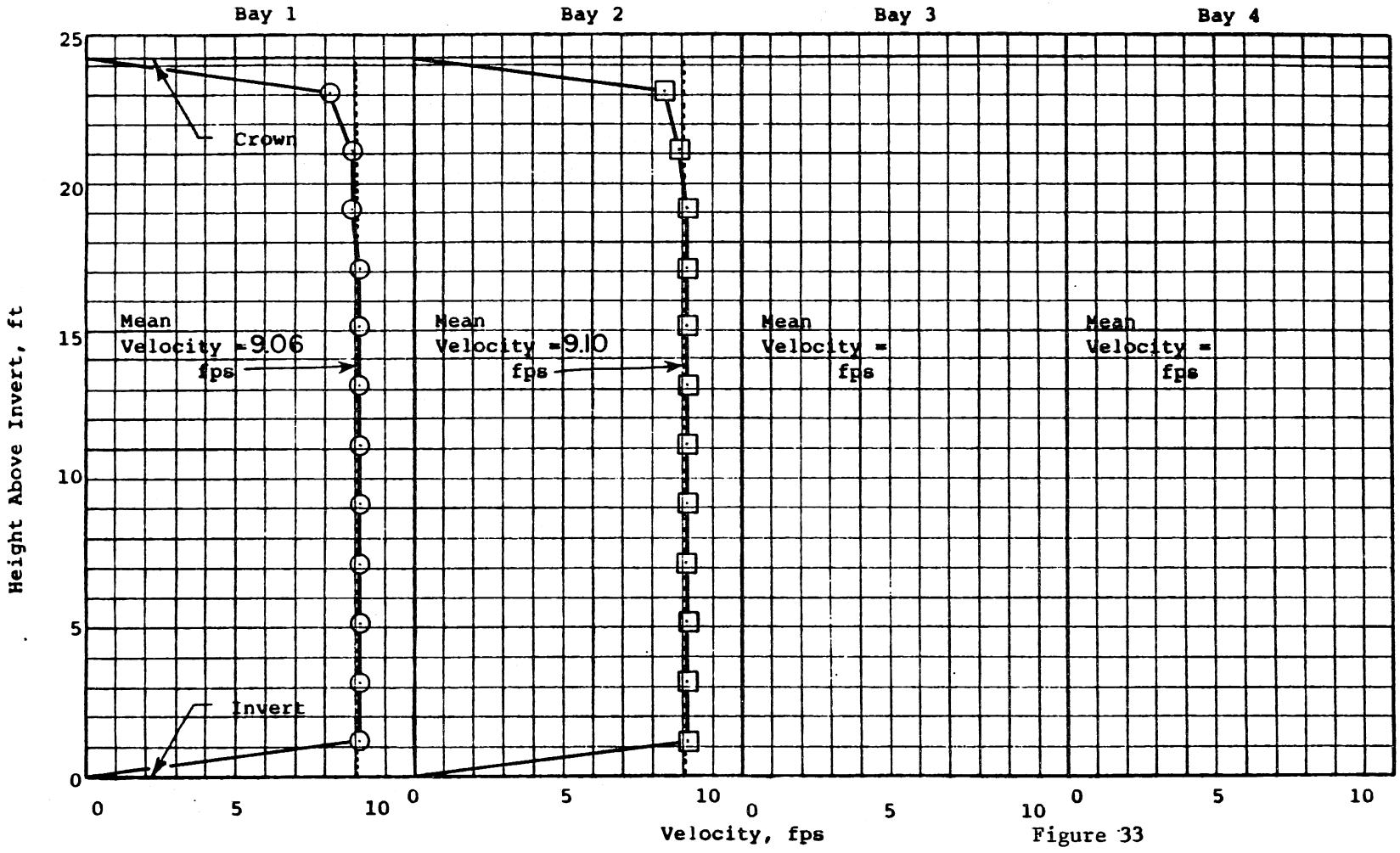

Note: Right powerhouse in operation only.

Figure 33

ST. CLOUD HYDROELECTRIC PROJECT
HYDRAULIC MODEL STUDIES
Type A8 , Model Scale 1:24
Q_{PR} = 3250 cfs, Q_{GS} = 0 cfs,
Q_{MS} = 0 cfs, H.W. = 981 ft.
Typical Velocity Profiles

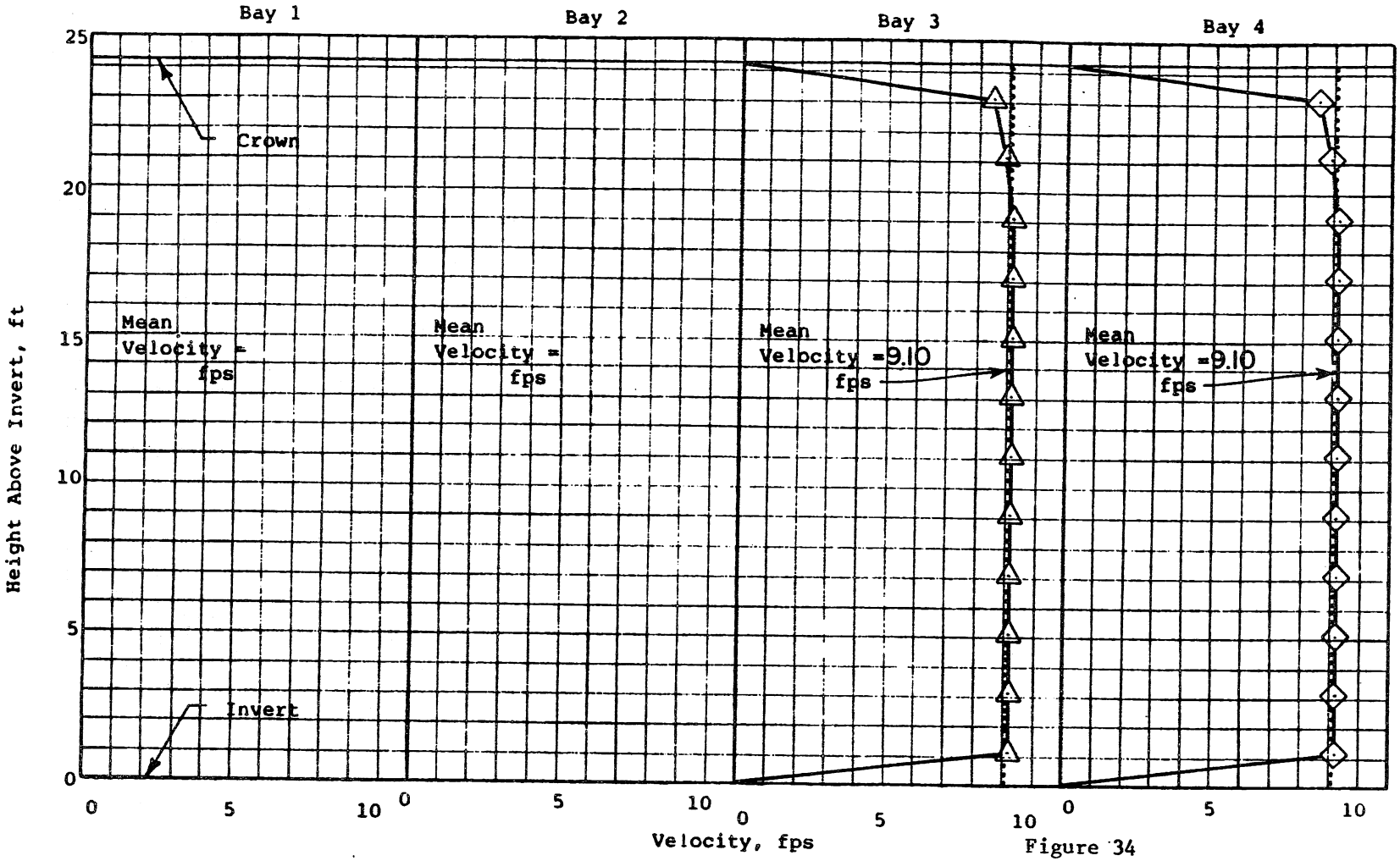

Note: Left powerhouse in operation only.

Figure 34
ST. CLOUD HYDROELECTRIC PROJECT
HYDRAULIC MODEL STUDIES
Type A8 , Model Scale 1:24
Q_{pL} = 3250 cfs, Q_{GS} = 0 cfs,
Q_{MS} = 0 cfs, H.W. = 981 ft.
Typical Velocity Profiles

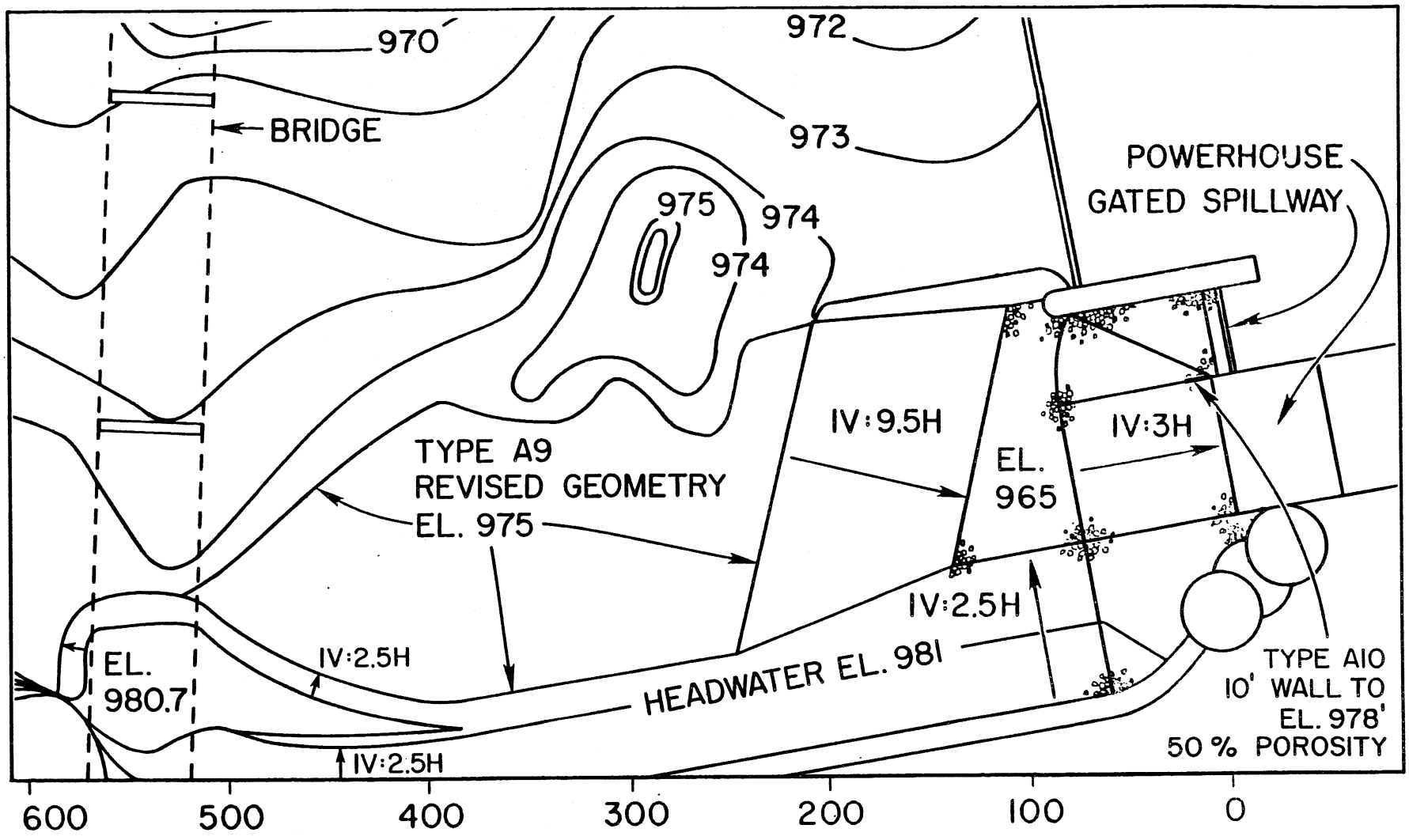

Figure 35

ST. CLOUD HYDROELECTRIC PROJECT
HYDRAULIC MODEL STUDIES
MODEL SCALE 1:24
TYPES A9, AIO REVISED GEOMETRIES

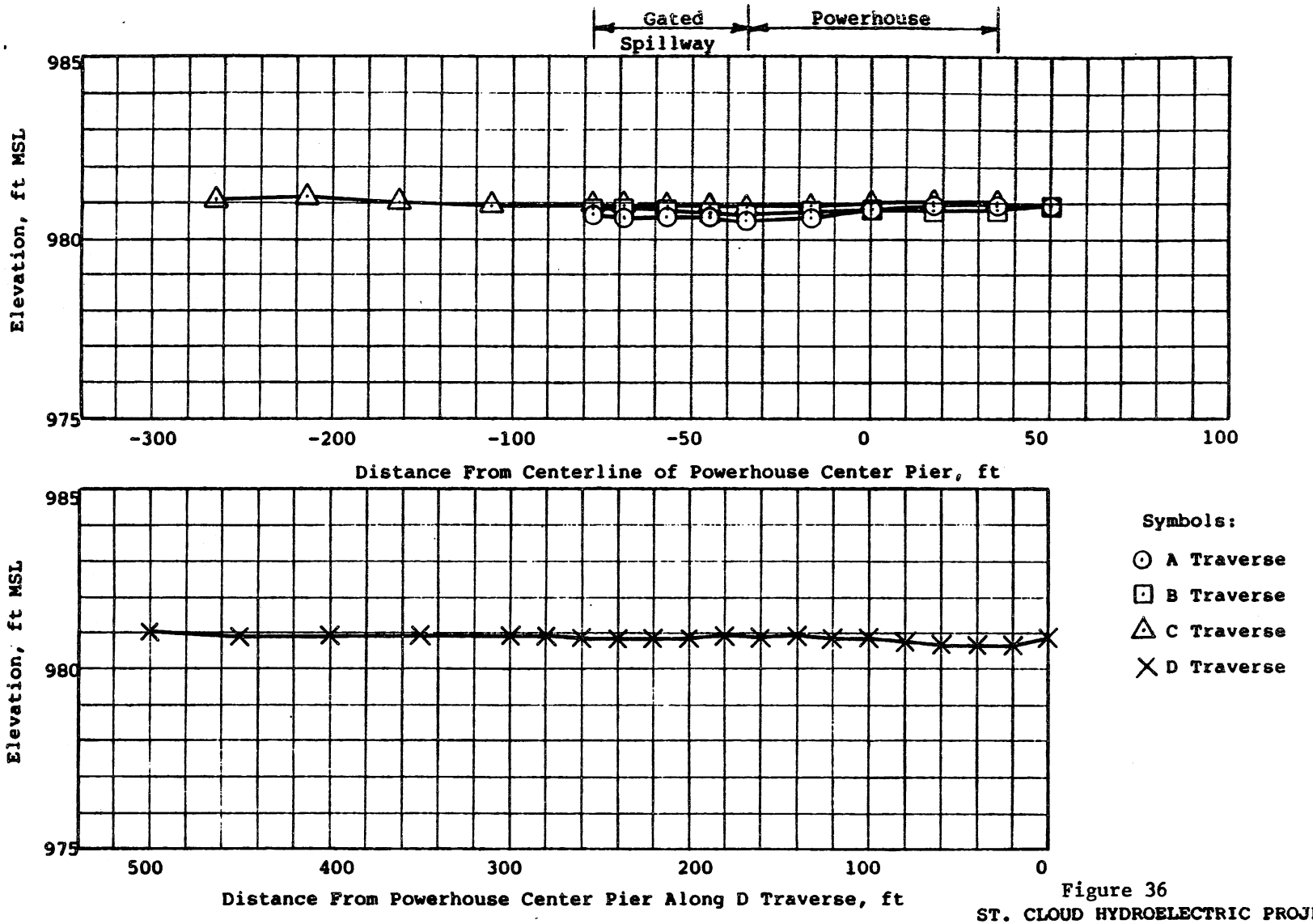

Figure 36
ST. CLOUD HYDROELECTRIC PROJECT
HYDRAULIC MODEL STUDIES
Type A9 , Model Scale 1:24
Q_p = 6500 cfs, Q_{GS} = 0 cfs,
Q_{MS} = 0 cfs, H.W. = 981 ft.
Typical Water Surface Traverses

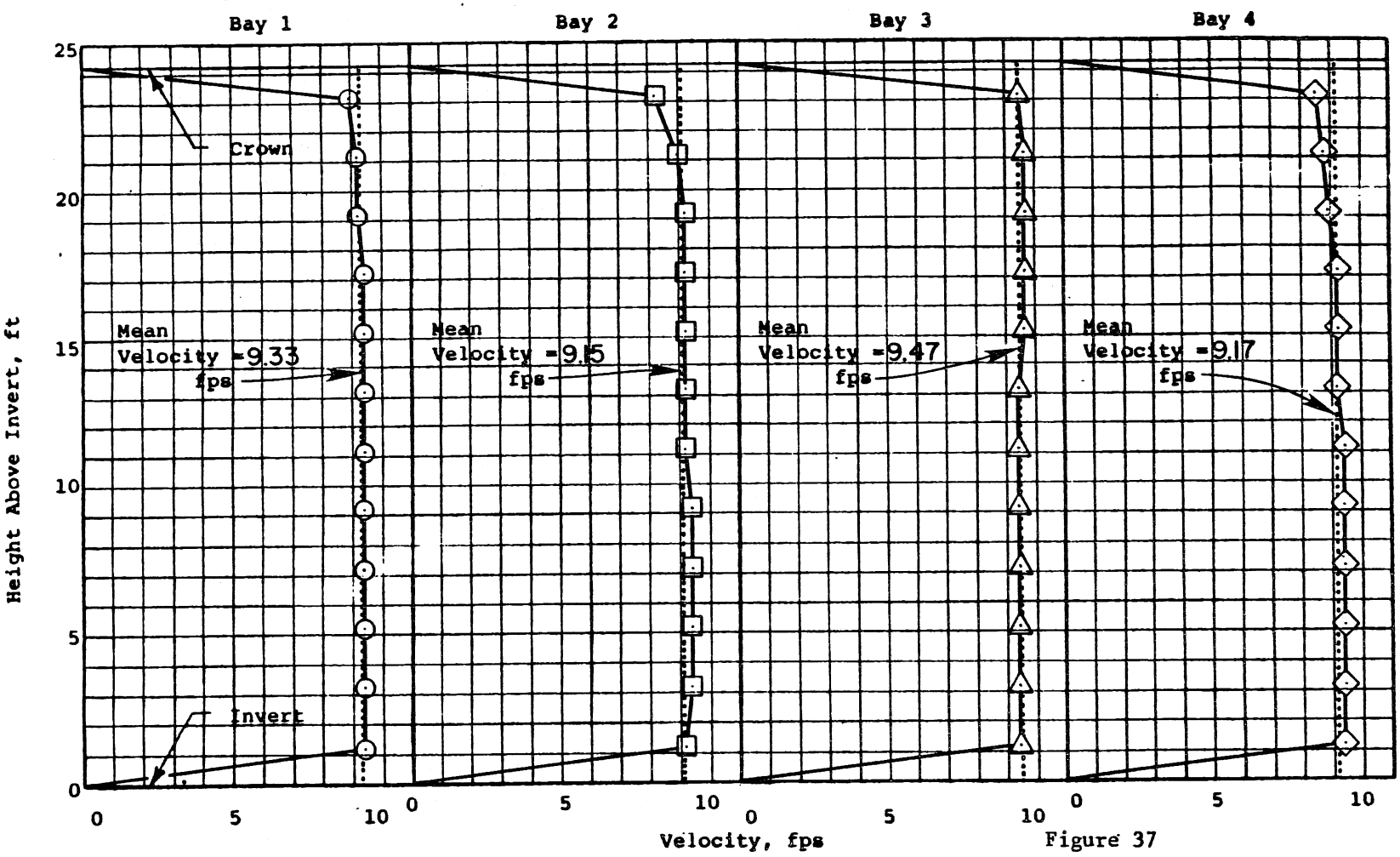

Figure 37

ST. CLOUD HYDROELECTRIC PROJECT
HYDRAULIC MODEL STUDIES
Type A9 , Model Scale 1:24
Q_p = 6500 cfs, Q_{GS} = 0 cfs,
Q_{MS} = 0 cfs, H.W. = 981 ft.
Typical Velocity Profiles

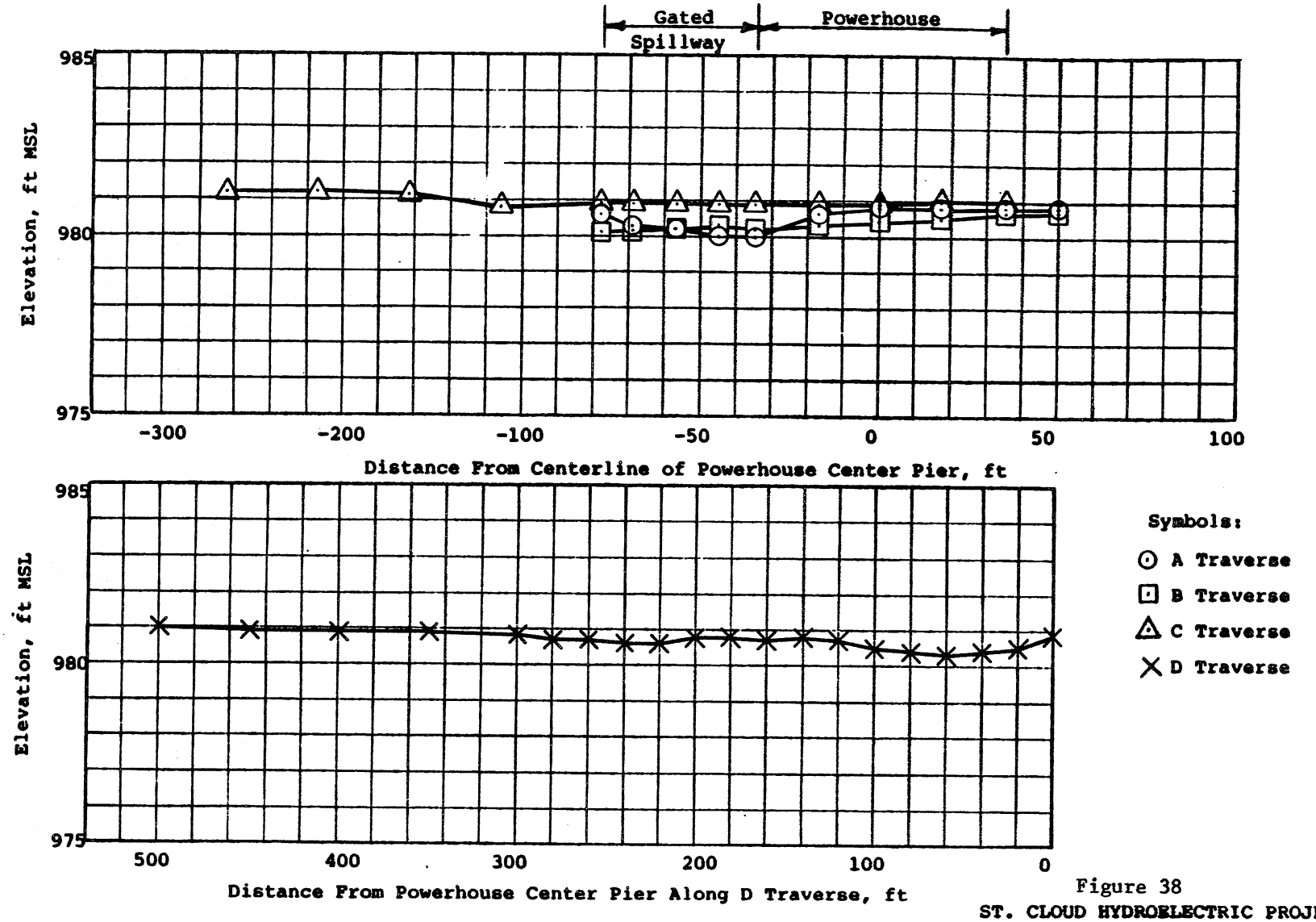

Figure 38

ST. CLOUD HYDROELECTRIC PROJECT
HYDRAULIC MODEL STUDIES

Type A9 , Model Scale 1:24

Q_p = 6500 cfs, Q_{GS} = 3300 cfs,

Q_{MS} = 0 cfs, H.W. = 981 ft.

Typical Water Surface Traverses

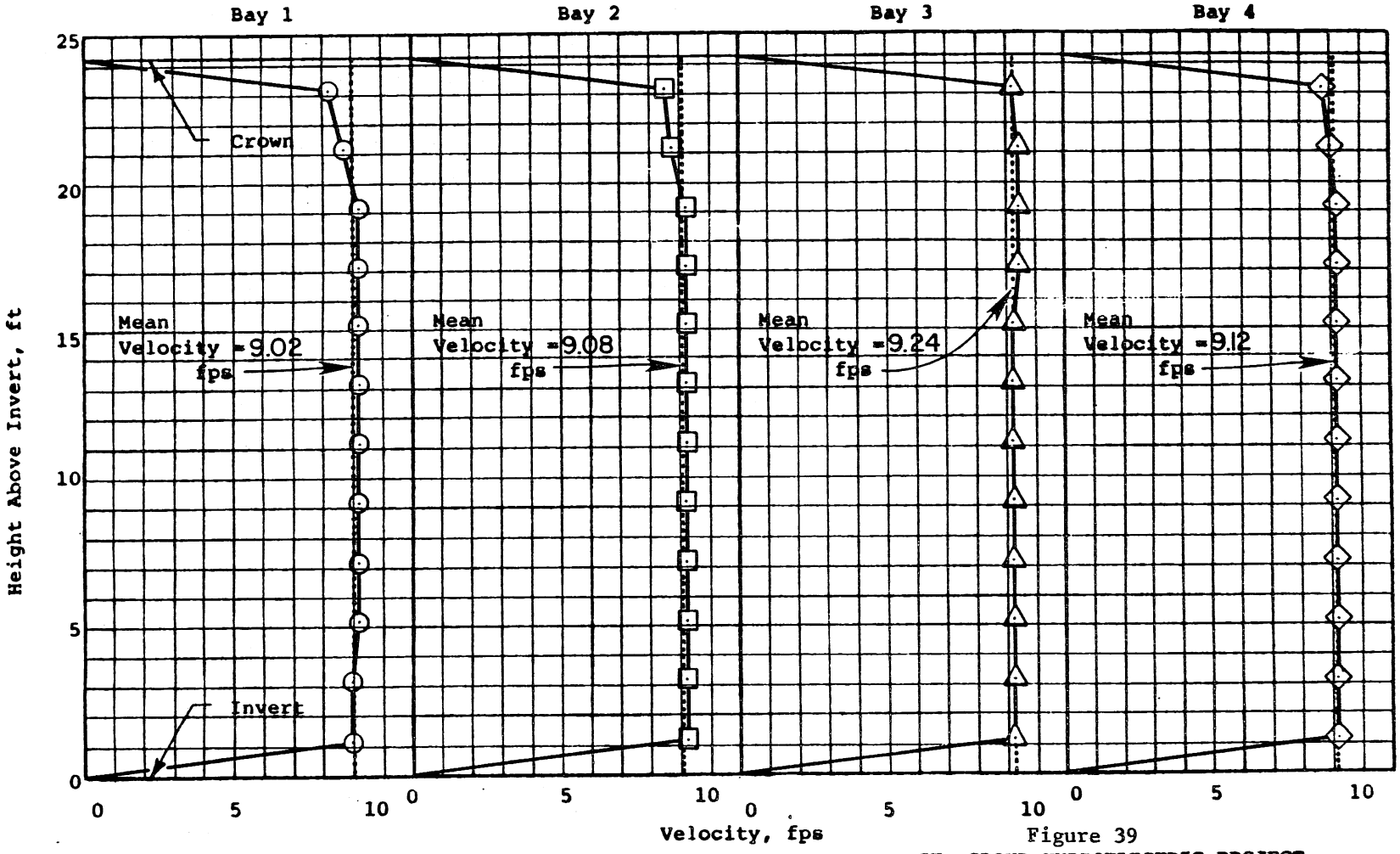

Figure 39

ST. CLOUD HYDROELECTRIC PROJECT
HYDRAULIC MODEL STUDIES
Type A9 , Model Scale 1:24
Q_p = 6500 cfs, Q_{GS} = 3300 cfs,
Q_{MS} = 0 cfs, H.W. = 981 ft.
Typical Velocity Profiles

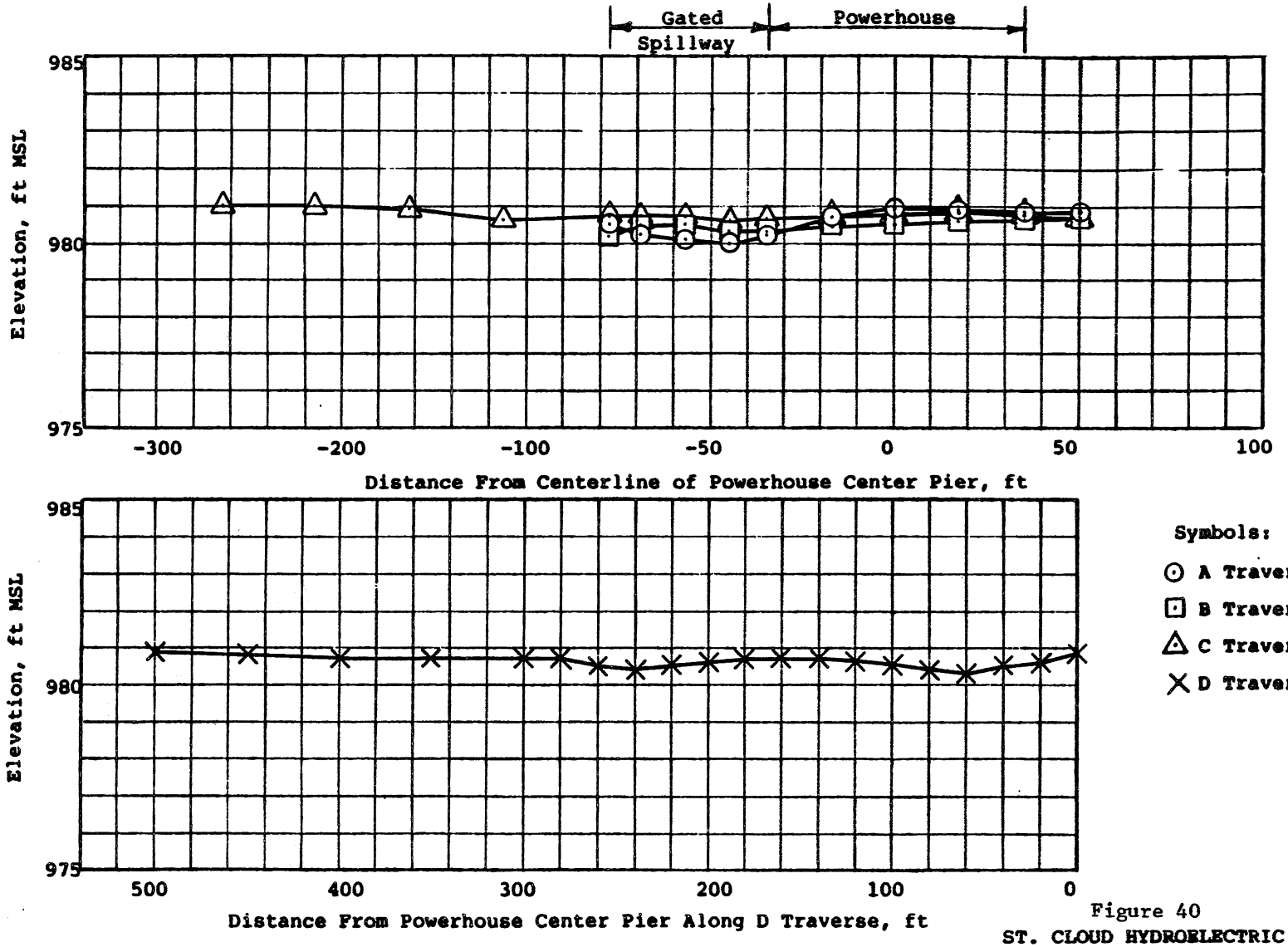

Figure 40

ST. CLOUD HYDROELECTRIC PROJECT
HYDRAULIC MODEL STUDIES
Type A9 , Model Scale 1:24
Q_p = 6500cfs, Q_{GS} = 3300 cfs,
Q_{MS} = 3000 cfs, H.W. = 981 ft.
Typical Water Surface Traverses

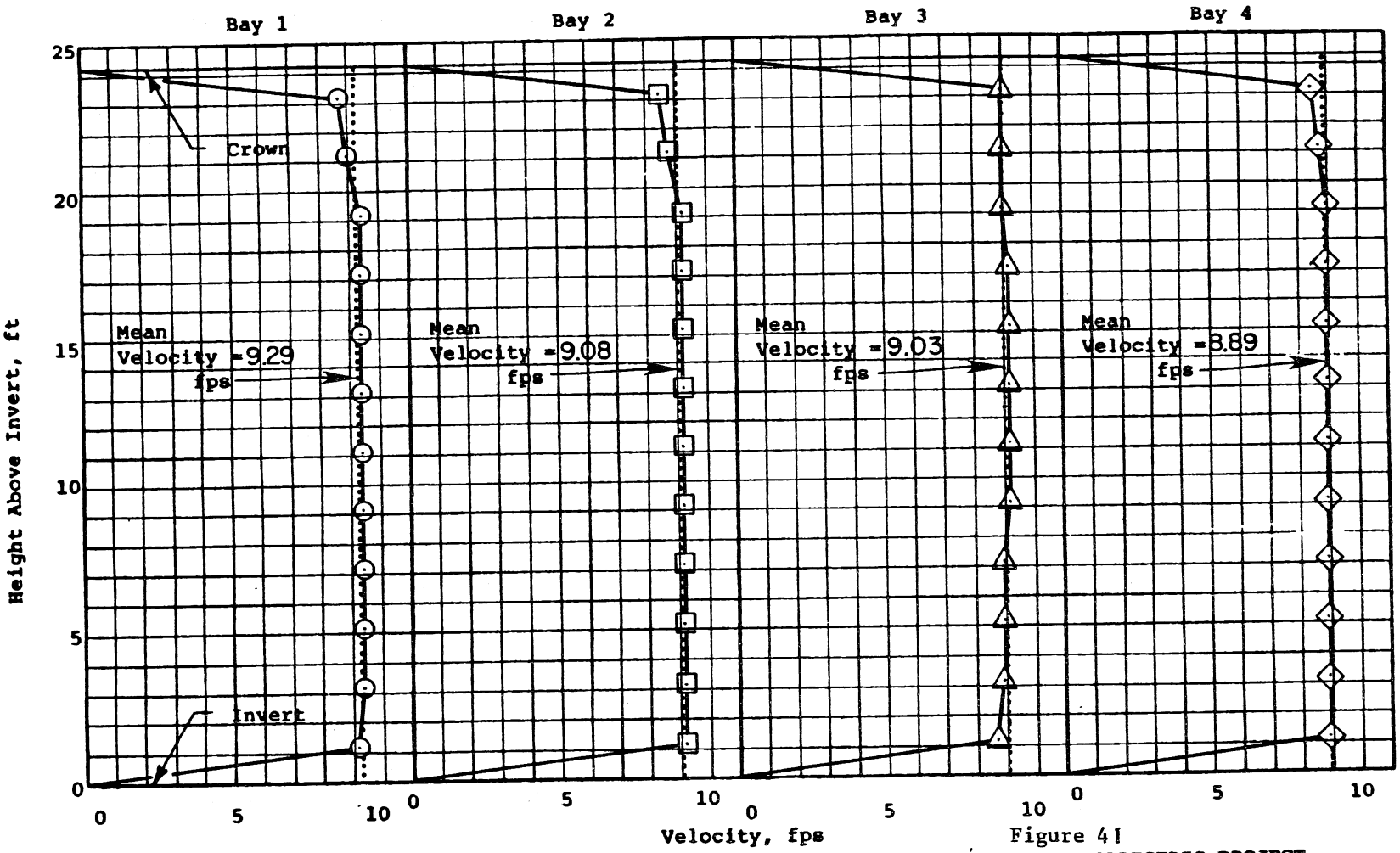

Figure 41

ST. CLOUD HYDROELECTRIC PROJECT
HYDRAULIC MODEL STUDIES
Type A9 , Model Scale 1:24
Q_p = 6500 cfs, Q_{GS} = 3300 cfs,
Q_{MS} = 3000 cfs, H.W. = 981 ft.
Typical Velocity Profiles

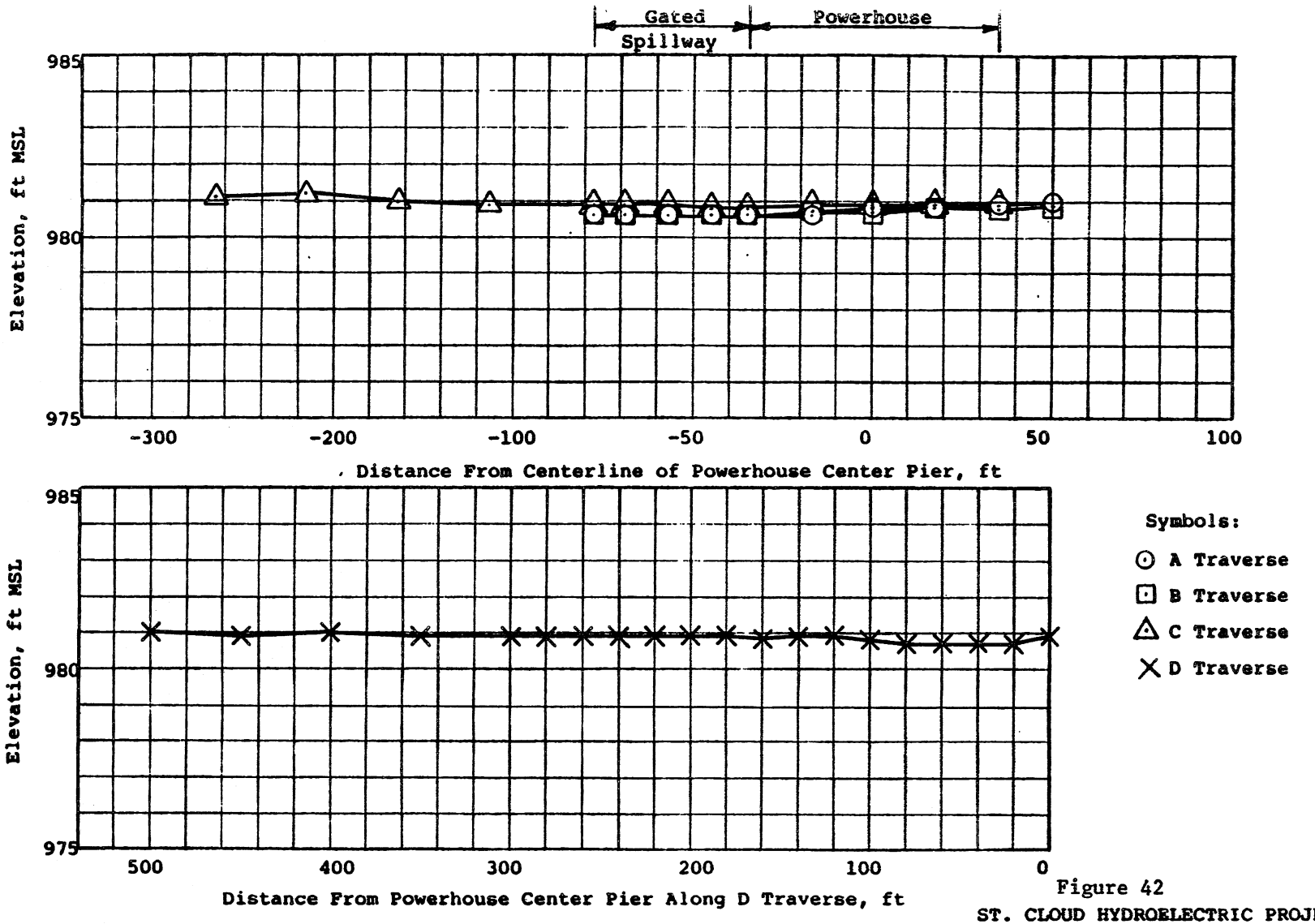

Figure 42

ST. CLOUD HYDROELECTRIC PROJECT
HYDRAULIC MODEL STUDIES
Type A9 , Model Scale 1:24
Q_p = 6500 cfs, Q_{GS} = 0 cfs,
Q_{MS} = 0 cfs, H.W. = 981 ft.
Typical Water Surface Traverses

Sensitivity Test

In this test, the flow in the left side manifold was increased from 40% to 60% and the flow in the upstream manifold reduced from 60% to 40%.

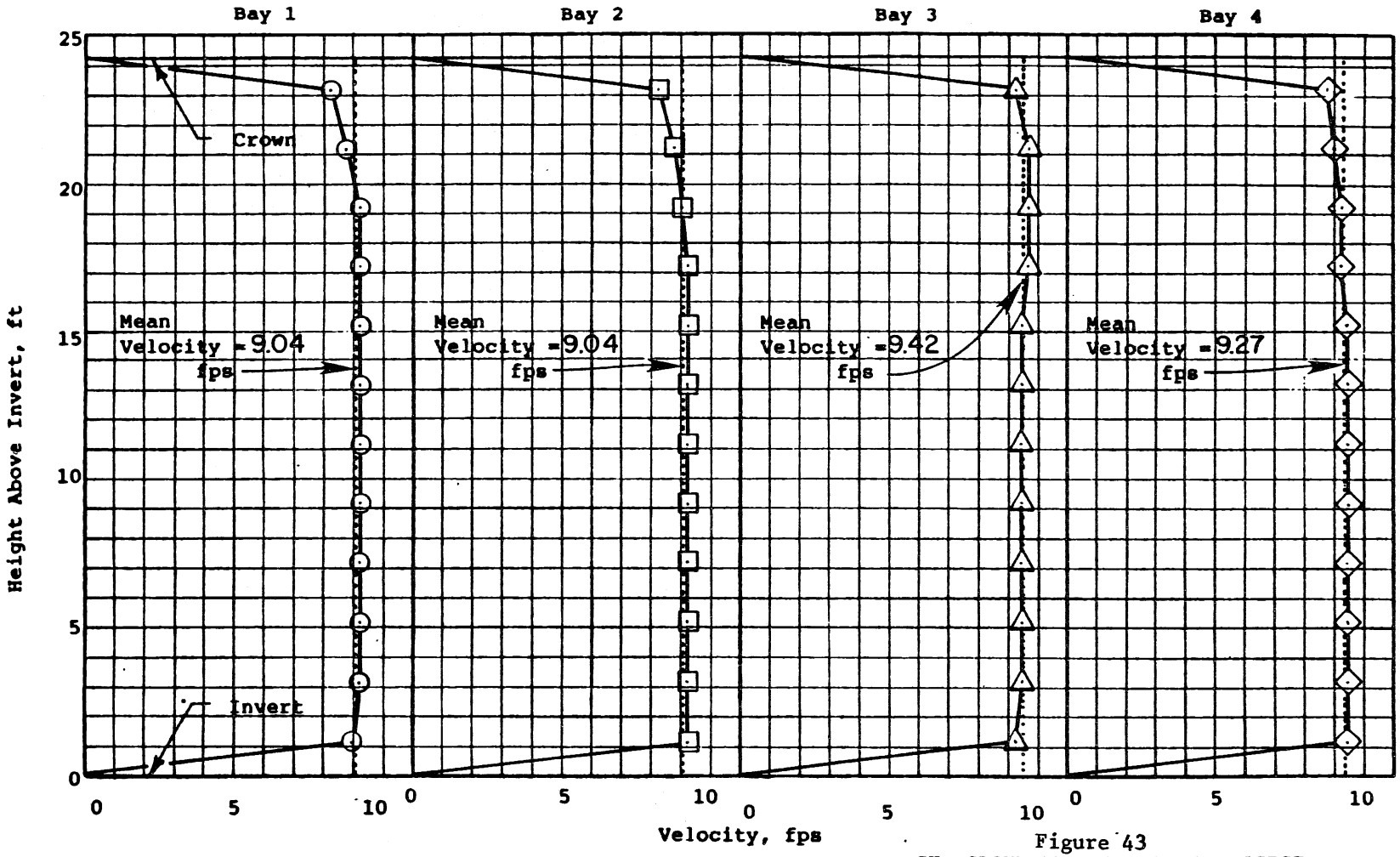

Figure 43

ST. CLOUD HYDROELECTRIC PROJECT
HYDRAULIC MODEL STUDIES
Type A 9 , Model Scale 1:24
Q_p = 6500 cfs, Q_{GS} = 0 cfs,
Q_{MS} = 0 cfs, H.W. = 981 ft.
Typical Velocity Profiles

Sensitivity Test

In this test, the percent of flow in the left manifold was increased from 40% to 60% and the flow in the upstream manifold reduced from 60% to 40%.

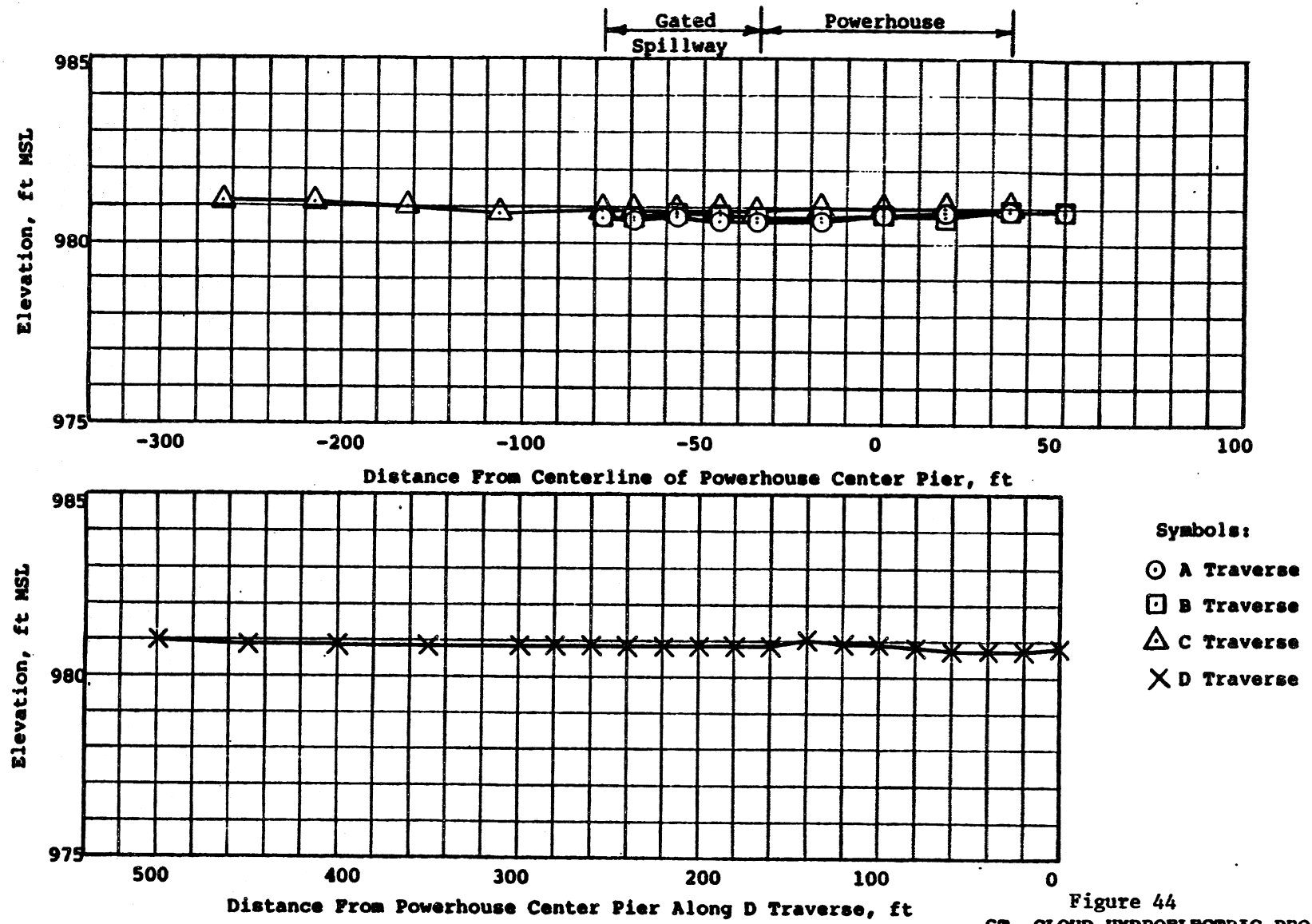

Sensitivity Test

In this test the percent of flow in the left manifold was increased from 40% to 80% and the flow in the upstream manifold reduced from 60% to 20%.

Figure 44

ST. CLOUD HYDROELECTRIC PROJECT
HYDRAULIC MODEL STUDIES

Type A9 , Model Scale 1:24

Q_p = 6500 cfs, Q_{GS} = 0 cfs,

Q_{MS} = 0 cfs, H.W. = 981 ft.

Typical Water Surface Traverses

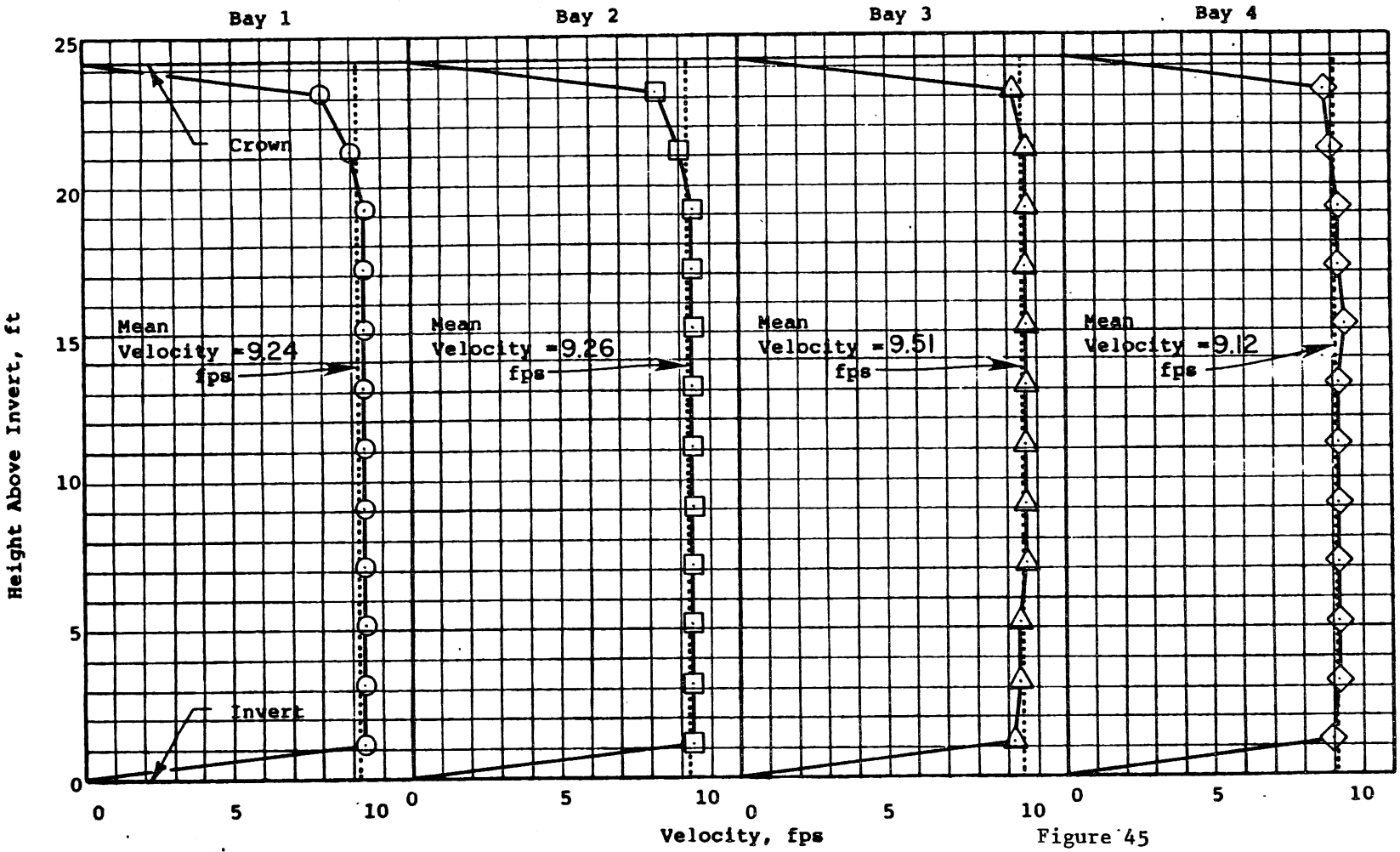

Figure 45

ST. CLOUD HYDROELECTRIC PROJECT
HYDRAULIC MODEL STUDIES
Type A9 , Model Scale 1:24
Q_p = 6500 cfs, Q_{GS} = 0 cfs,
Q_{MS} = 0 cfs, H.W. = 981 ft.
Typical Velocity Profiles

Sensitivity Test

In this test, the percent of flow in the left side manifold was increased from 40% to 80% and the flow in the upstream manifold reduced from 60% to 20%.

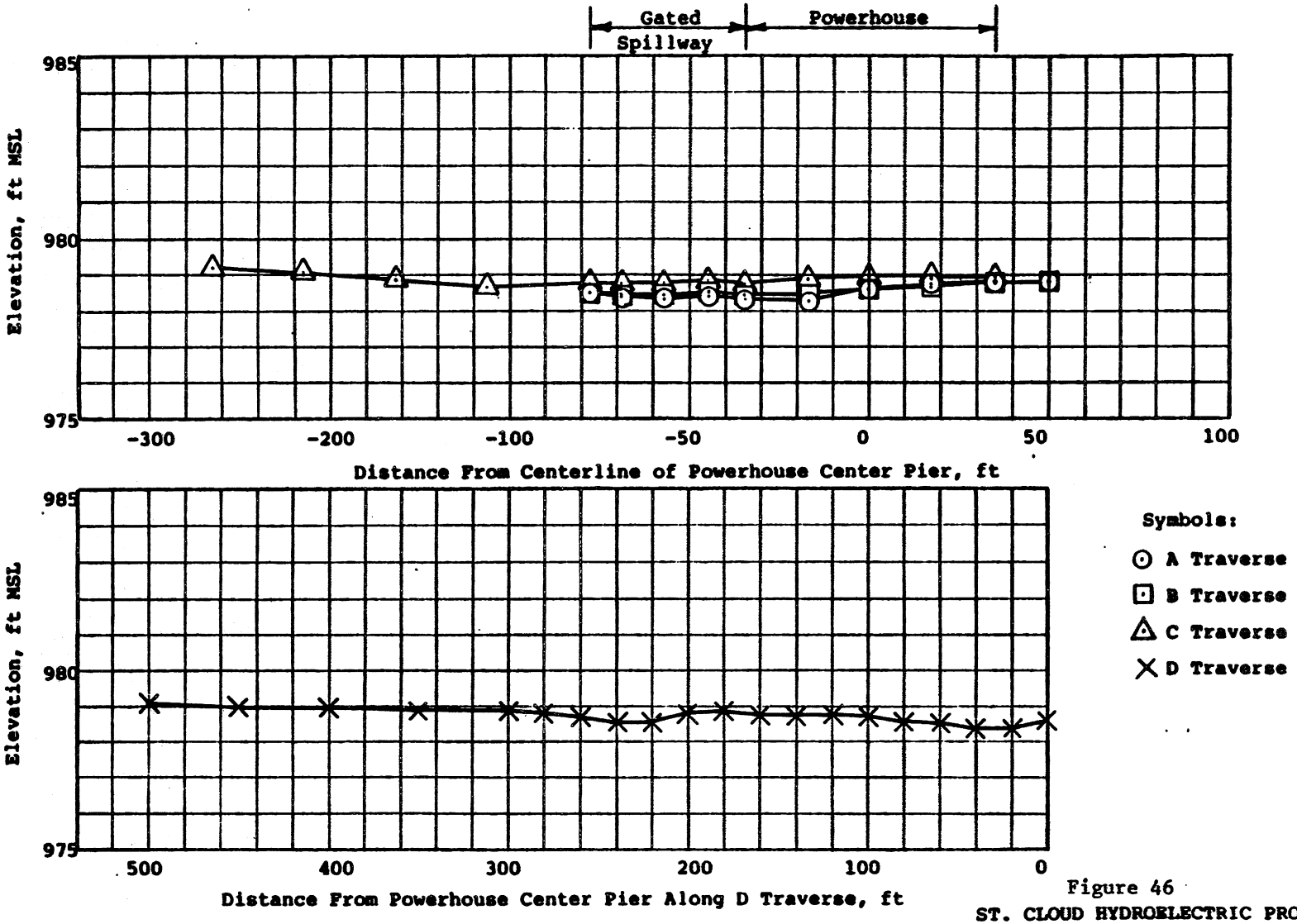

Figure 46

ST. CLOUD HYDROELECTRIC PROJECT
HYDRAULIC MODEL STUDIES
Type A9 , Model Scale 1:24
Q_p = 6500 cfs, Q_{GS} = 0 cfs,
Q_{WR} = 0 cfs, H.W. = 979 ft.
Typical Water Surface Traverses

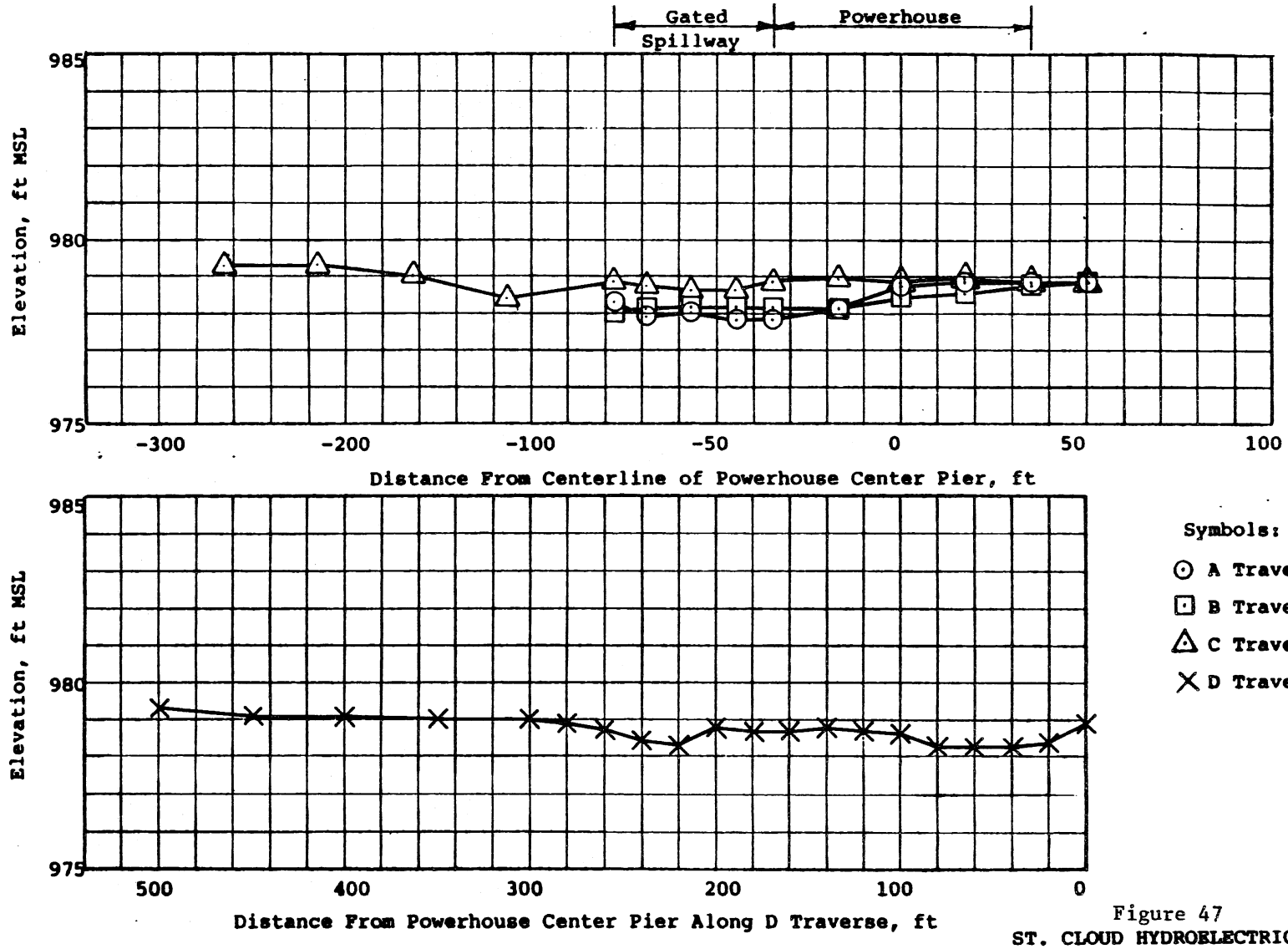

Figure 47

ST. CLOUD HYDROELECTRIC PROJECT
HYDRAULIC MODEL STUDIES

Type A9 , Model Scale 1:24

Q_p = 6500 cfs, Q_{GS} = 2200 cfs,

Q_{MS} = 0 cfs, H.W. = 979 ft.

Typical Water Surface Traverses

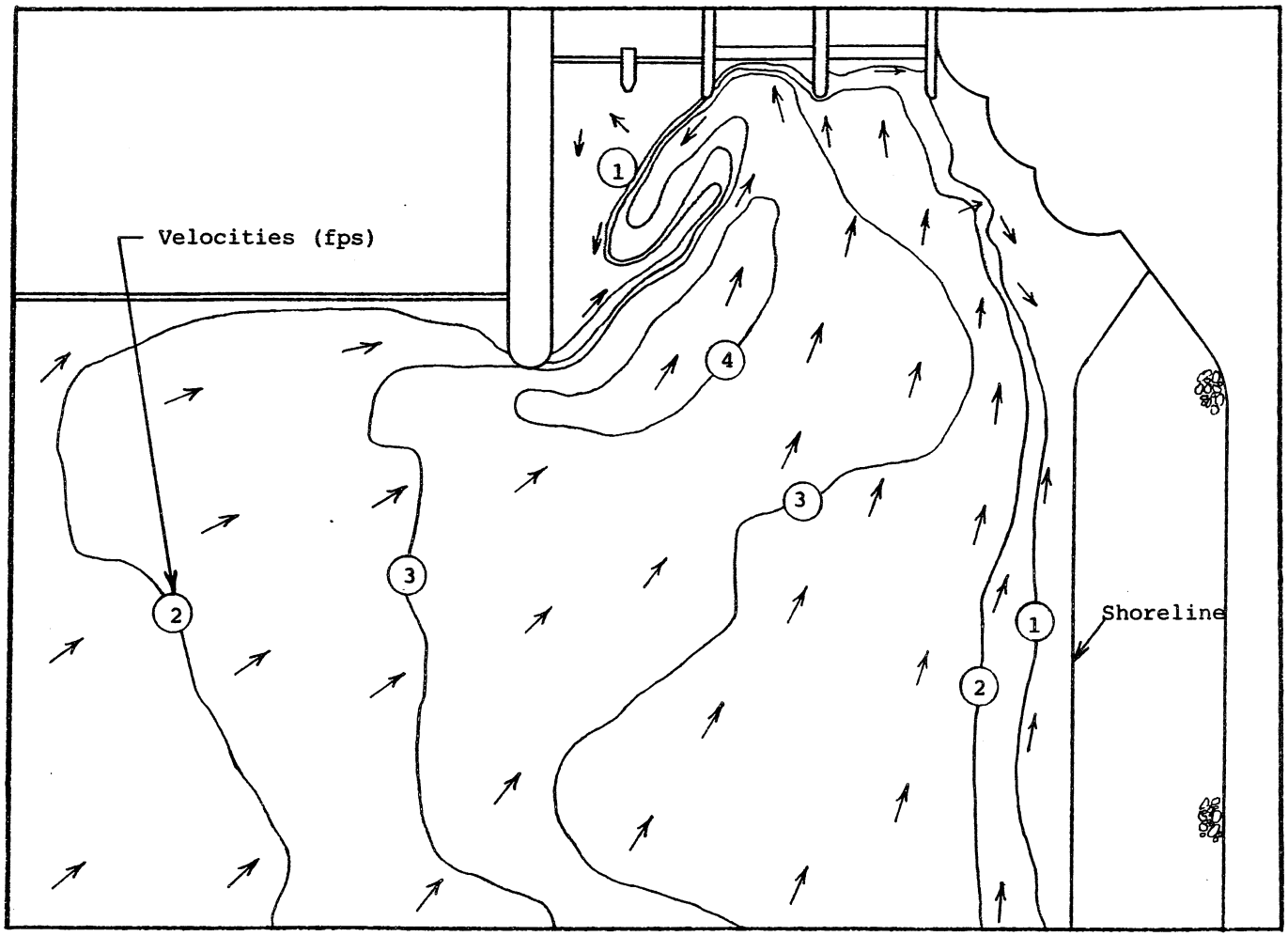

From Photo No. 381-90

Figure 48

ST. CLOUD HYDROELECTRIC PROJECT
HYDRAULIC MODEL STUDIES
Type A9, Model Scale 1:24
Q_p = 6,500 cfs, Q_{GS} = 0 cfs
Q_{MS} = 0 cfs, H.W. = 981 ft
Flow Patterns and Velocities at the Water Surface

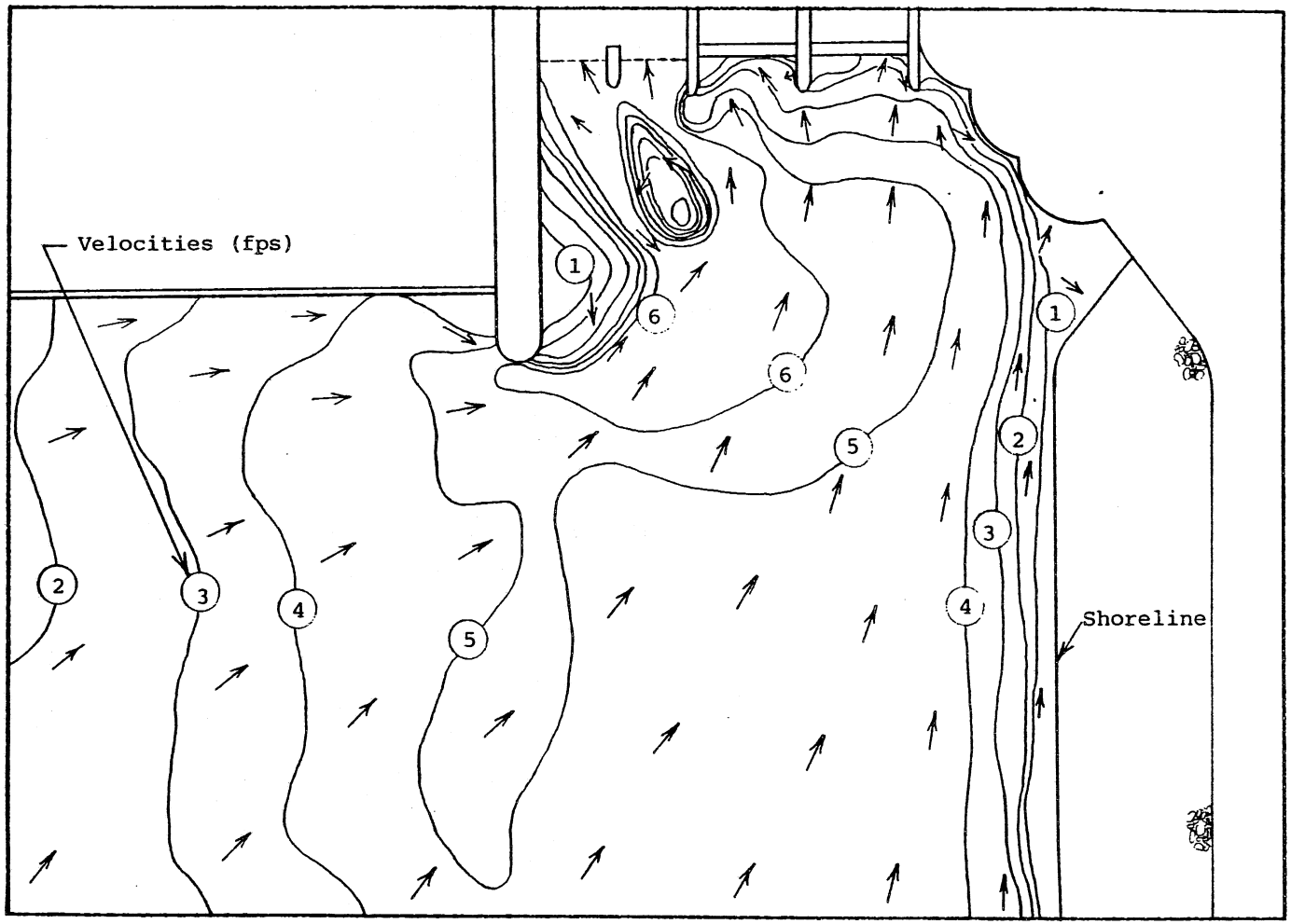

From Photo No. 381-103

0 50

Scale (feet)

Figure 49

ST. CLOUD HYDROELECTRIC PROJECT
HYDRAULIC MODEL STUDIES
Type A9, Model Scale 1:24
Q_p = 6,500 cfs, Q_{GS} = 3,300 cfs
Q_{MS} = 0 cfs, H.W. = 981 ft
Flow Patterns and Velocities at the Water Surface

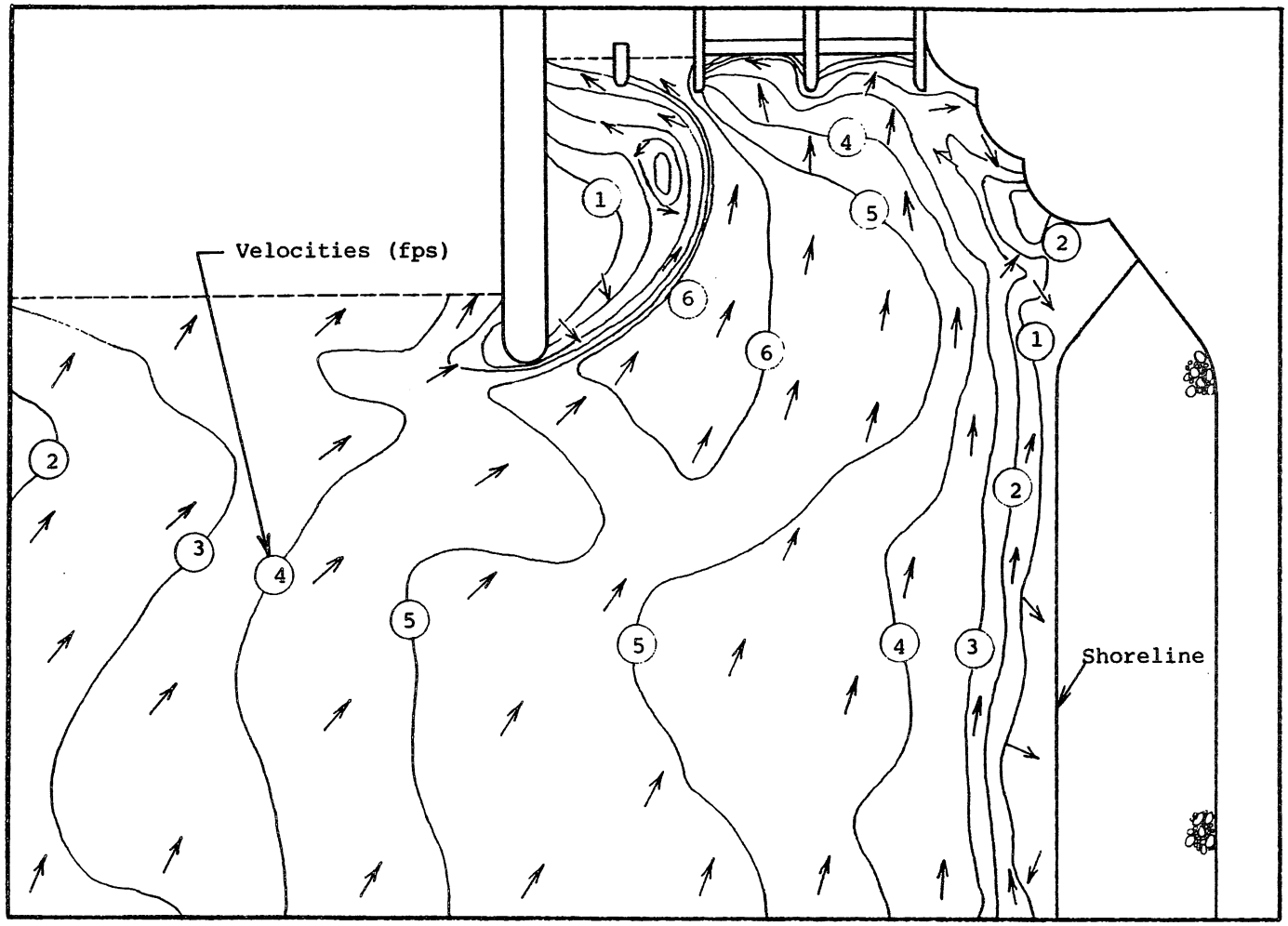

From Photo No. 381-116

Figure 50

ST. CLOUD HYDROELECTRIC PROJECT
HYDRAULIC MODEL STUDIES
Type A9, Model Scale 1:24
Q_P = 6,500 cfs, Q_{GS} = 3,300 cfs
Q_{MS} = 3,000 cfs, H.W. = 981 ft
Flow Patterns and Velocities at the Water Surface

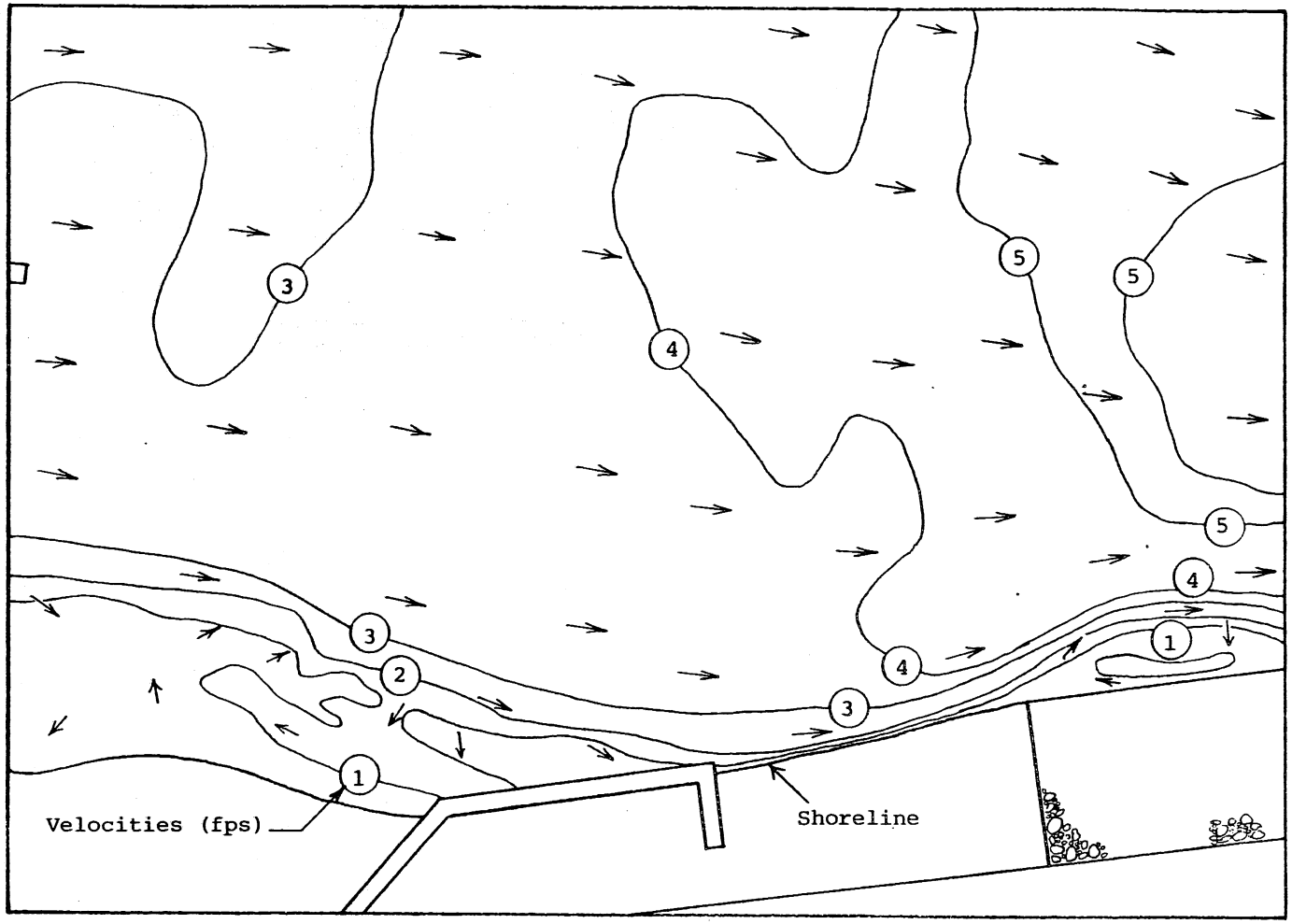

0 50

Scale (feet)

From Photo No. 381-120

Figure 51

ST. CLOUD HYDROELECTRIC PROJECT
HYDRAULIC MODEL STUDIES
Type A9, Model Scale 1:24
Q_P = 6,500 cfs, Q_{GS} = 3,300 cfs
Q_{MS} = 3,000 cfs, H.W. = 981 ft
Flow Patterns and Velocities at the Water Surface
along shoreline.

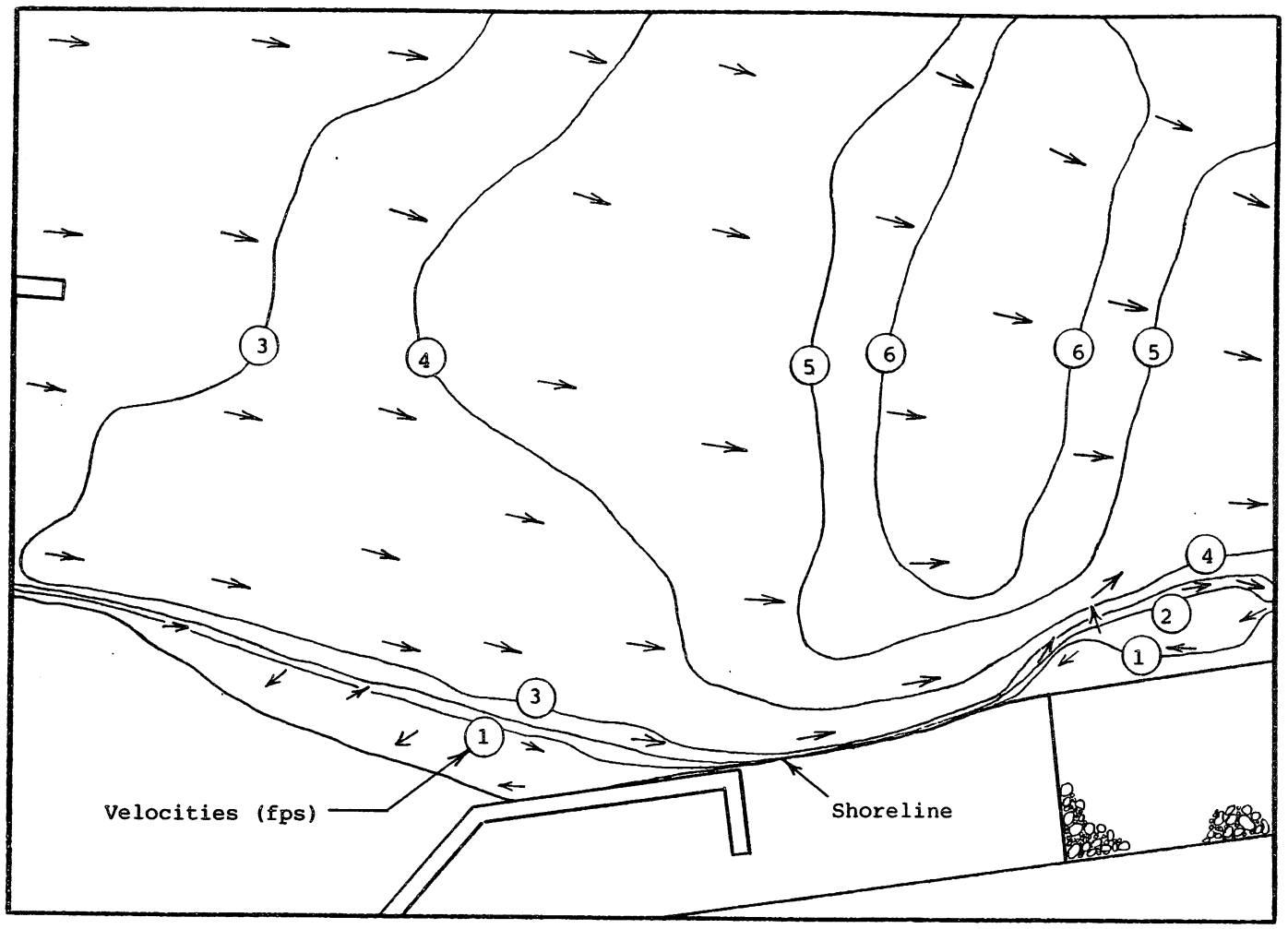

0 50
Scale (feet)

From Photo No. 381-132

Figure 52

ST. CLOUD HYDROELECTRIC PROJECT
HYDRAULIC MODEL STUDIES
Type A9, Model Scale 1:24
Q_p = 6,500 cfs, Q_{GS} = 2,200 cfs
Q_{MS} = 0 cfs, H.W. = 979 ft
Flow Patterns and Velocities at the Water Surface along shoreline.

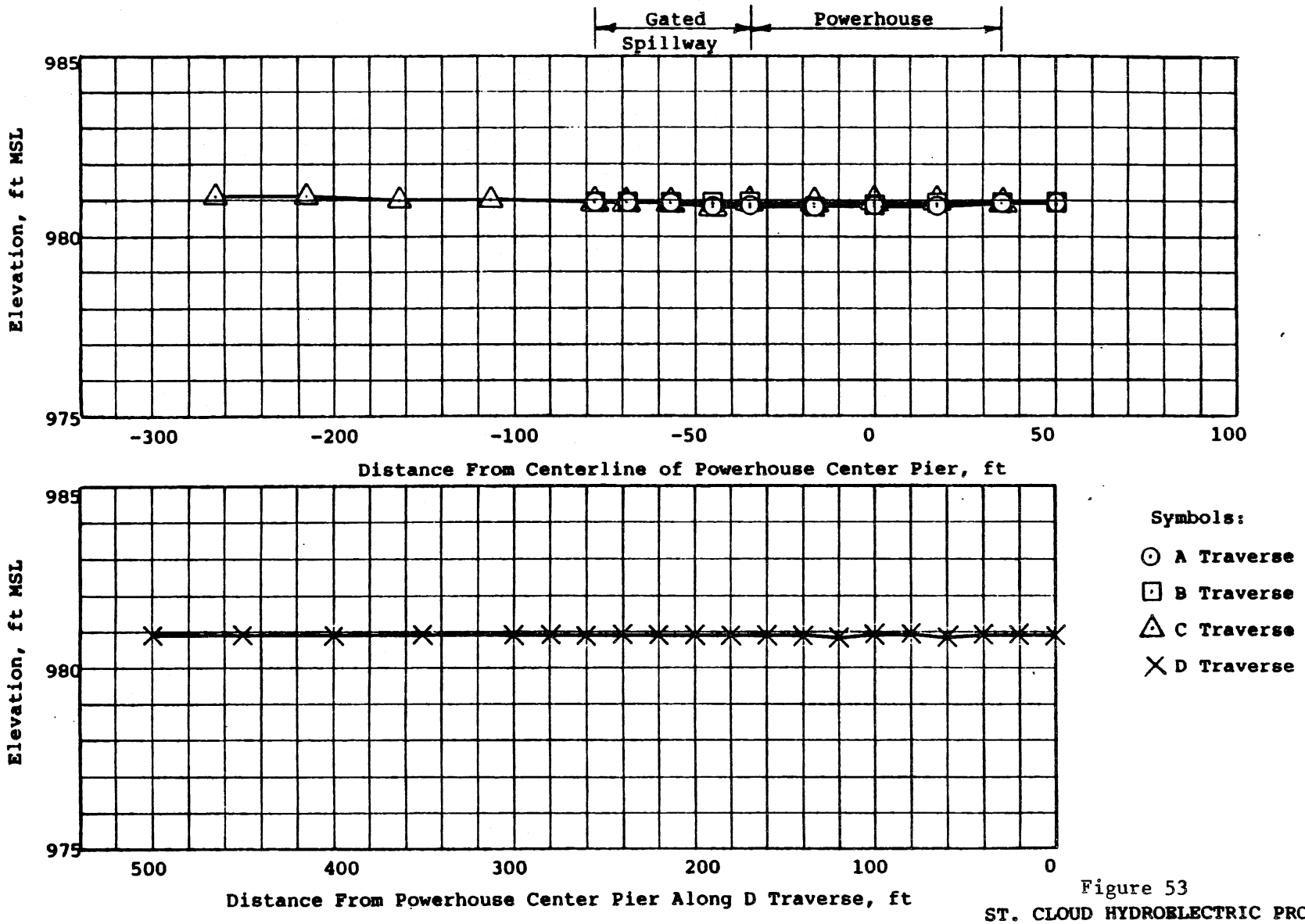

Note: Right powerhouse in operation only.

Figure 53

ST. CLOUD HYDROELECTRIC PROJECT
HYDRAULIC MODEL STUDIES
Type A9 , Model Scale 1:24
Q_{pR} = 3250 cfs, Q_{GS} = 0 cfs,
Q_{MS} = 0 cfs, H.W. = 981 ft.
Typical Water Surface Traverses

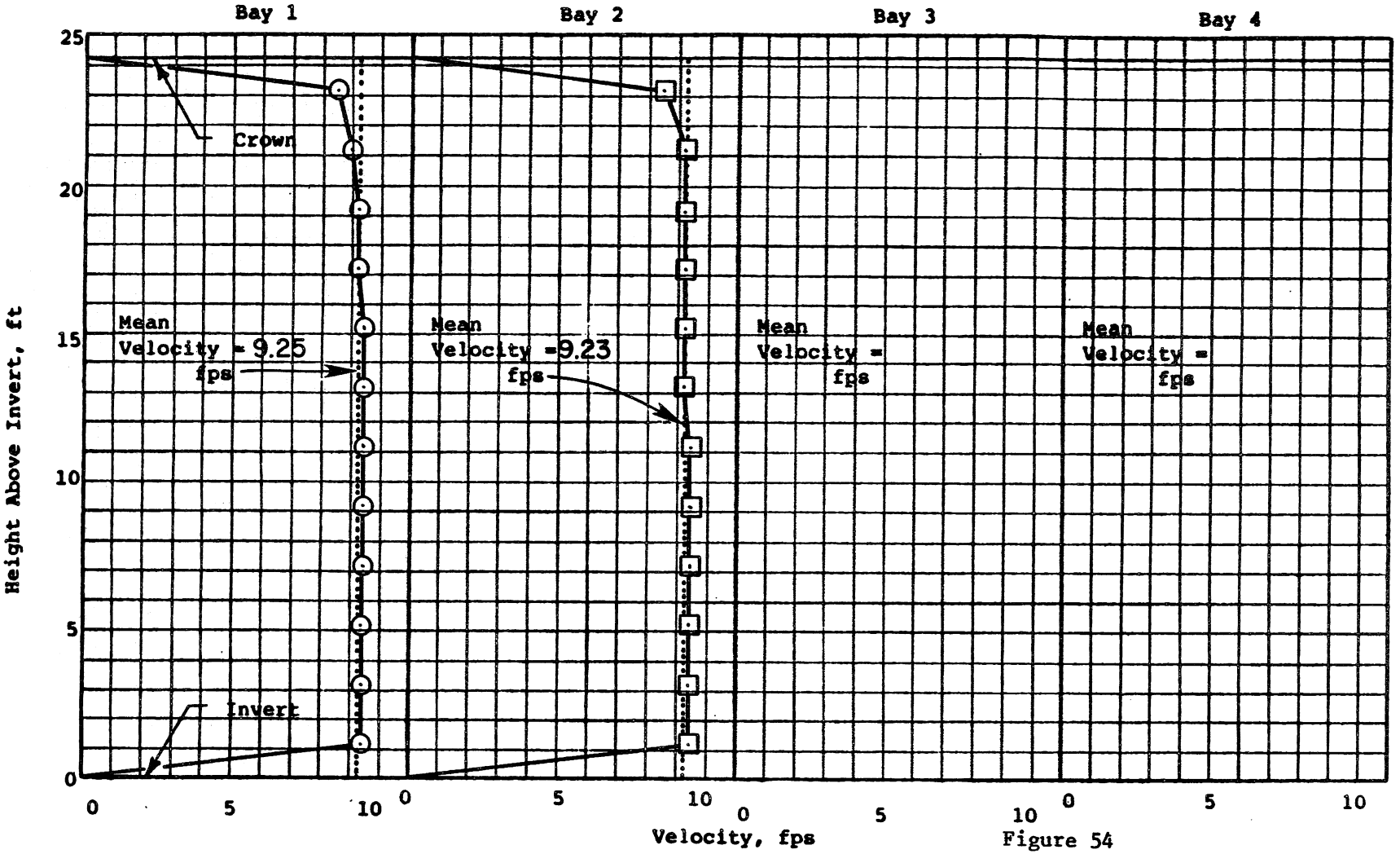

Note: Right powerhouse in operation only.

Figure 54

ST. CLOUD HYDROELECTRIC PROJECT
HYDRAULIC MODEL STUDIES
Type A9 , Model Scale 1:24
Q_{PR} = 3250 cfs, Q_{GS} = 0 cfs,
Q_{MS} = 0 cfs, H.W. = 981 ft.
Typical Velocity Profiles

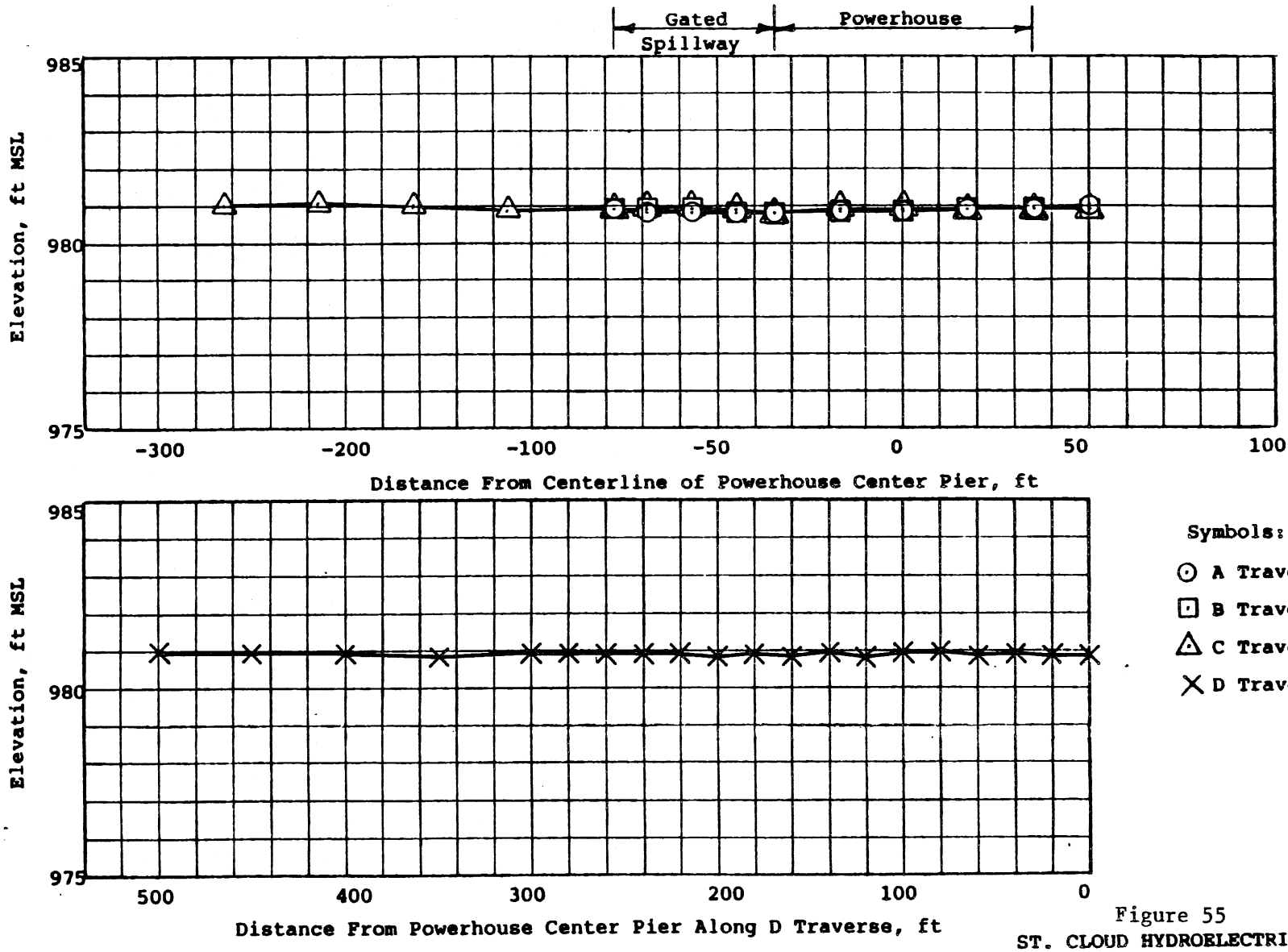

Note: Left powerhouse in operation only.

Figure 55
ST. CLOUD HYDROELECTRIC PROJECT
HYDRAULIC MODEL STUDIES
Type A9 , Model Scale 1:24
Q_{pL} = 3250 cfs, Q_{GS} = 0 cfs,
Q_{MS} = 0 cfs, H.W. = 981 ft.
Typical Water Surface Traverses

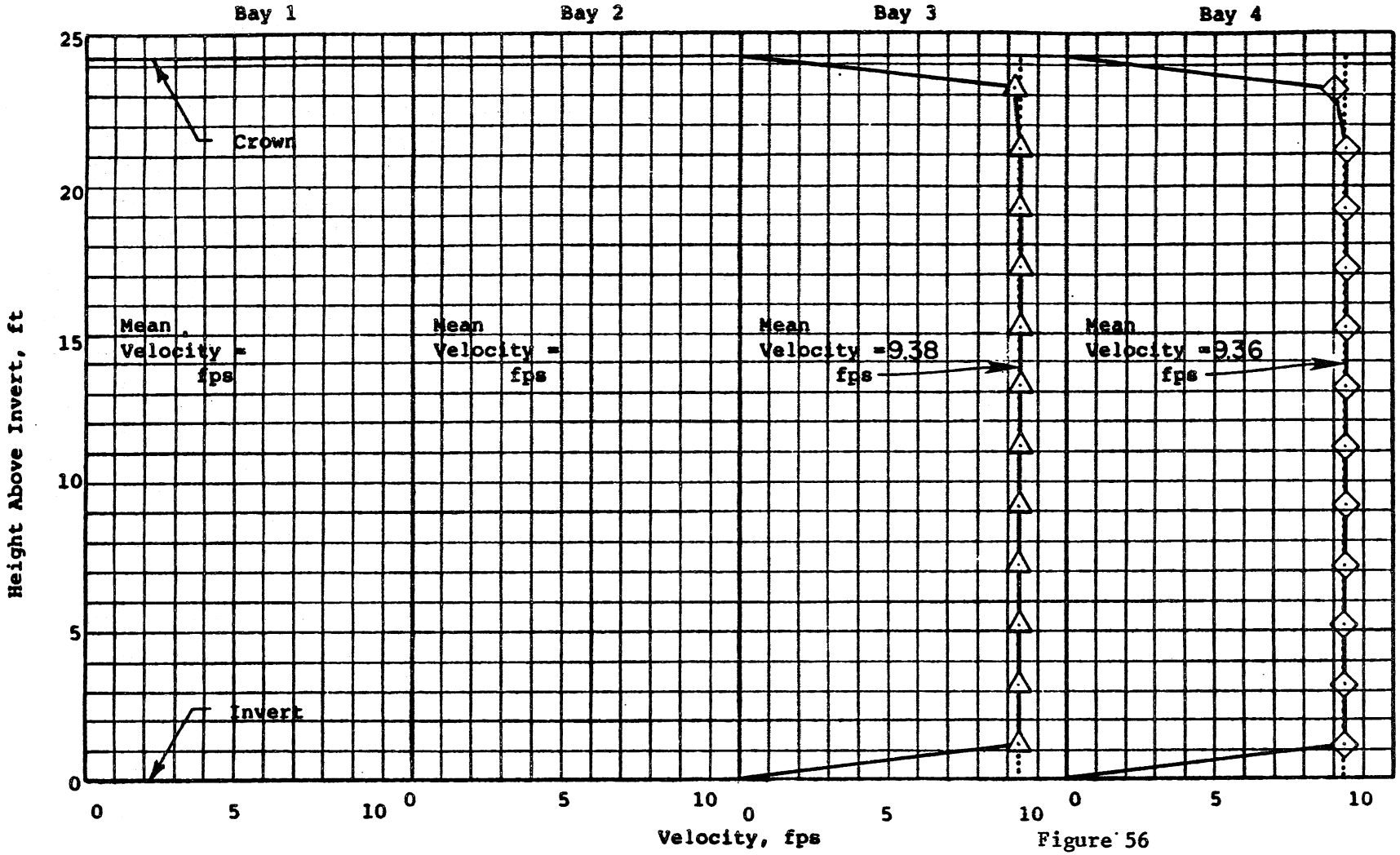

Figure 56

ST. CLOUD HYDROELECTRIC PROJECT
HYDRAULIC MODEL STUDIES
Type A9 , Model Scale 1:24
Q_{pL}=3250 cfs, Q_{GS} = 0 cfs,
Q_{MS} = 0 cfs, H.W. = 981 ft.
Typical Velocity Profiles

Note: Left powerhouse in operation only.

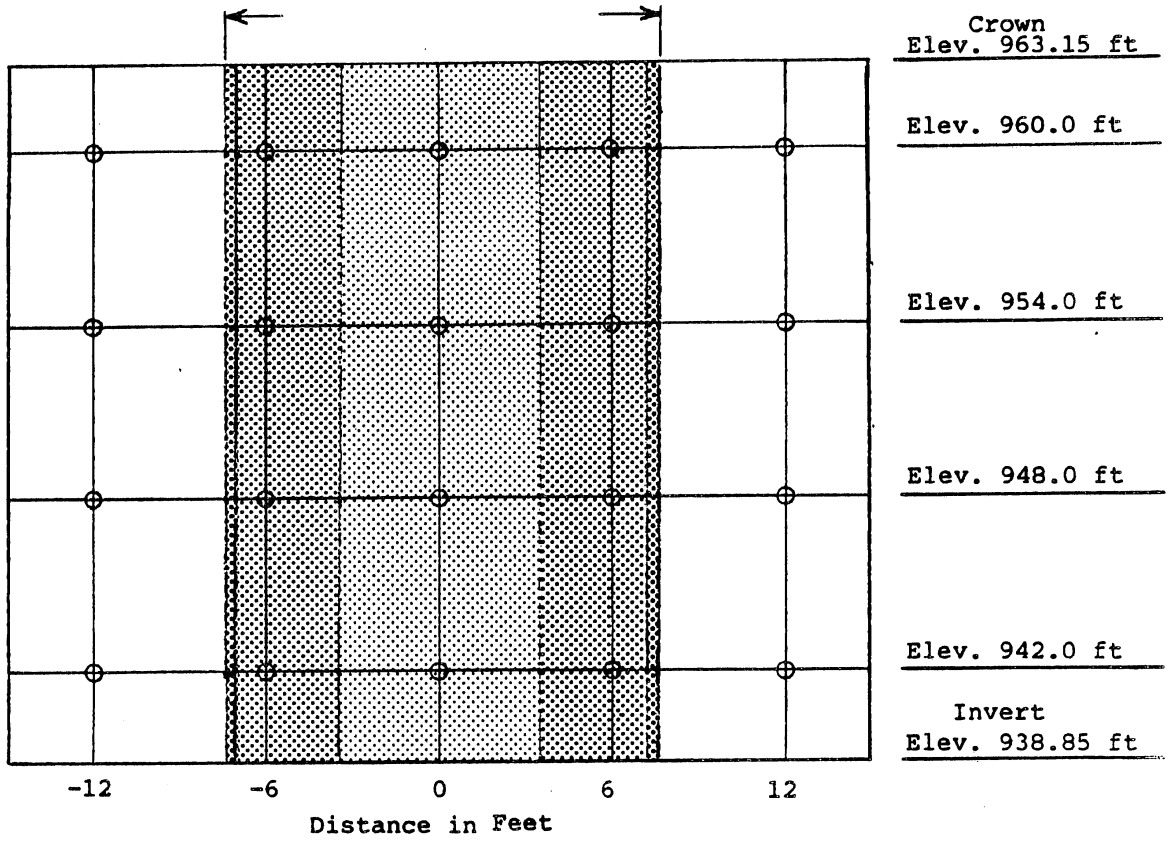

Section View at Bulkhead Slot Looking Downstream
Locations of Velocity Measurements

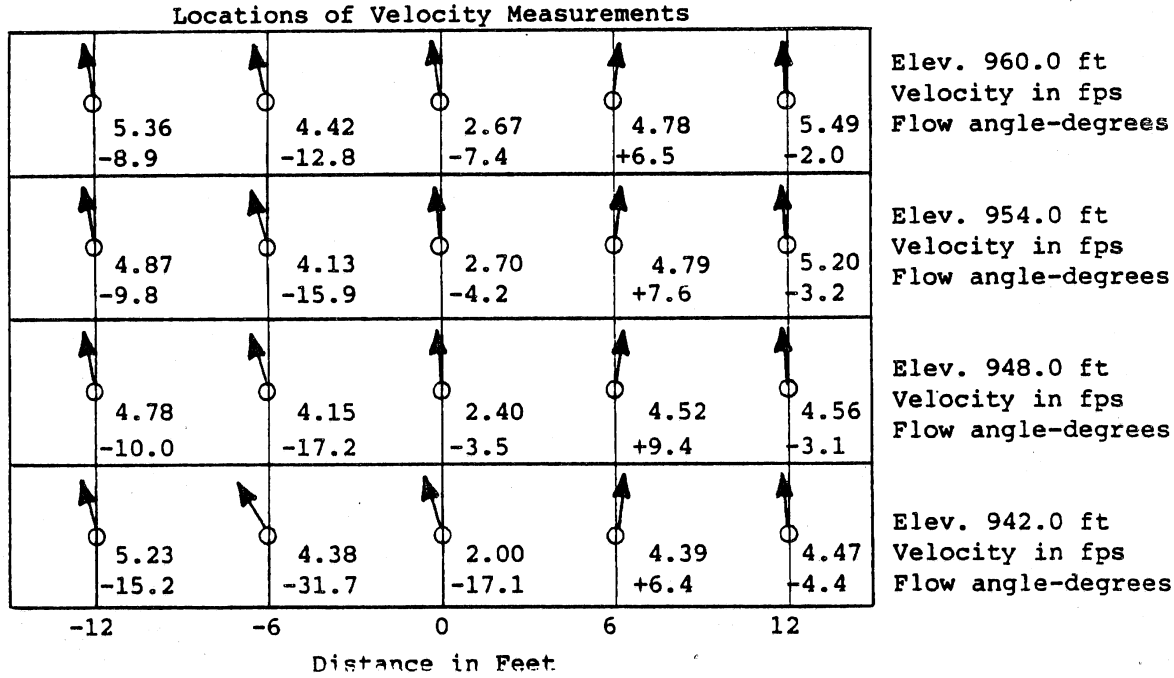

Figure 57. Plan View at Bulkhead Slots
Velocities and Direction of Flow

ST. CLOUD HYDROELECTRIC PROJECT
HYDRAULIC MODEL STUDIES
Type A9 Model Scale 1:24
Q_{PR} = 3250 cfs, Q_{GS} = 0 cfs, Q_{MS} = 0 cfs, H.W. = 981 ft
Typical Velocities and Flow Directions in Right Unit

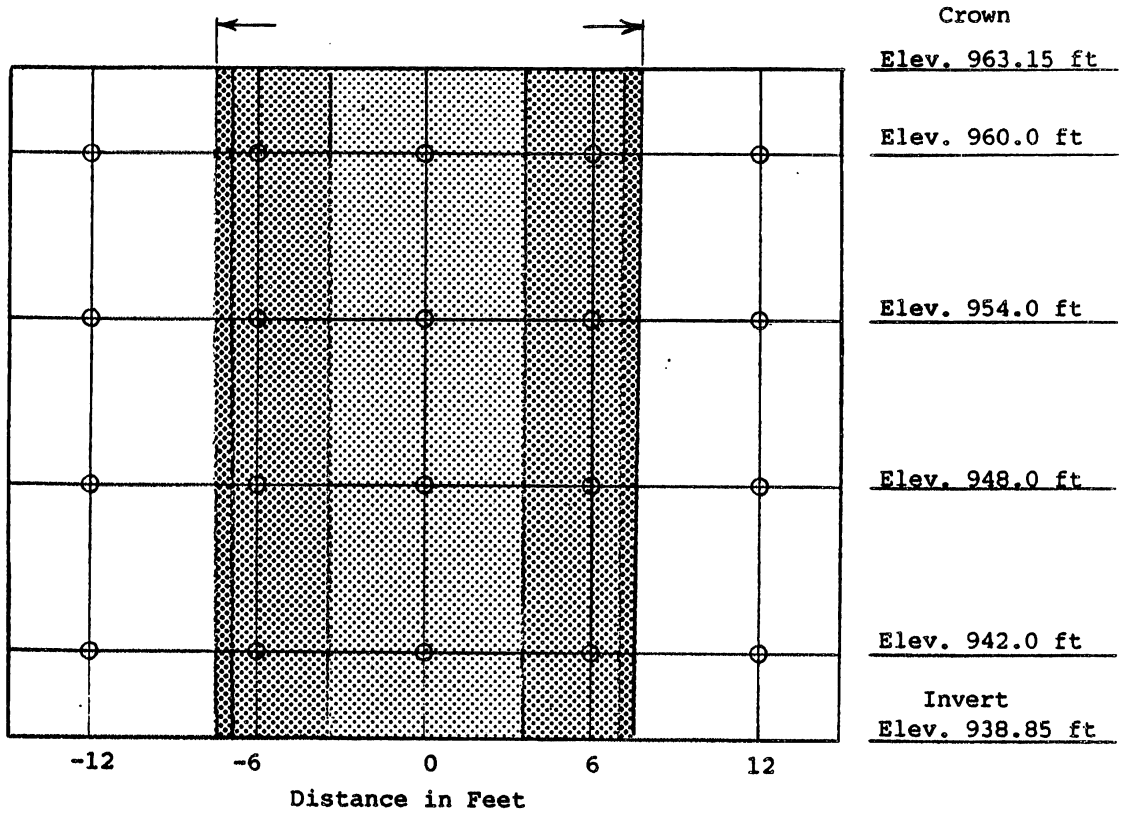

Section View at Bulkhead Slot Looking Downstream

Locations of Velocity Measurements

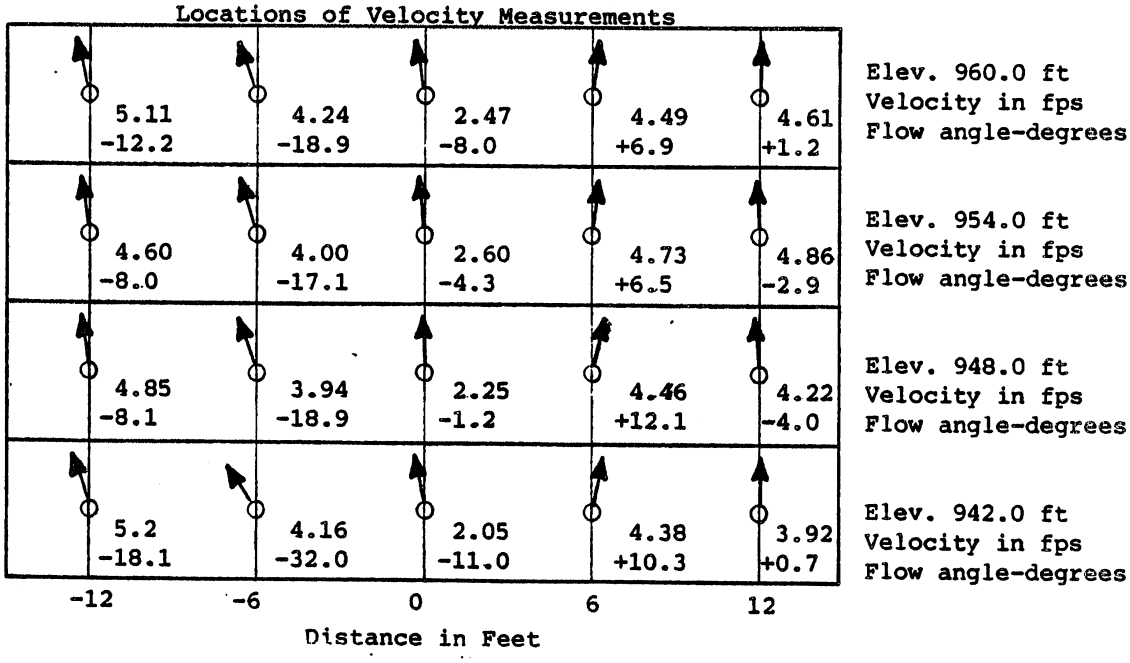

Figure 58. Plan View of Bulkhead Slots
Velocities and Direction of Flow

ST. CLOUD HYDROELECTRIC PROJECT
HYDRAULIC MODEL STUDIES
Type A9 Model Scale 1:24

Q_{PL} = 3250 cfs, Q_{GS} = 0 cfs, Q_{MS} = 0 cfs, H.W. = 981 ft
Typical Velocities and Flow Directions in Left Unit

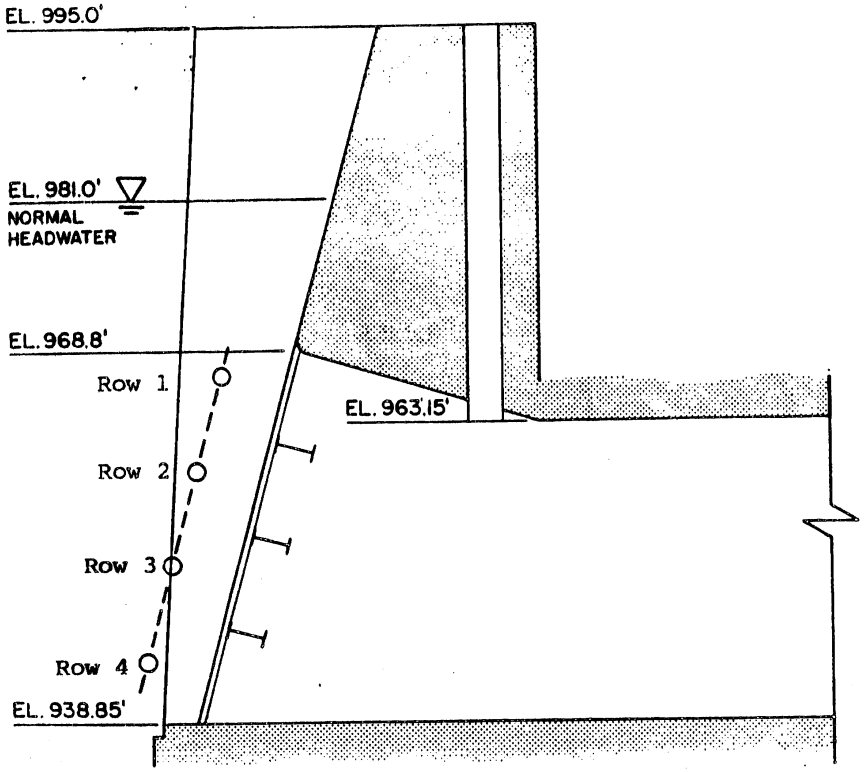

Locations of Flow Direction Observations

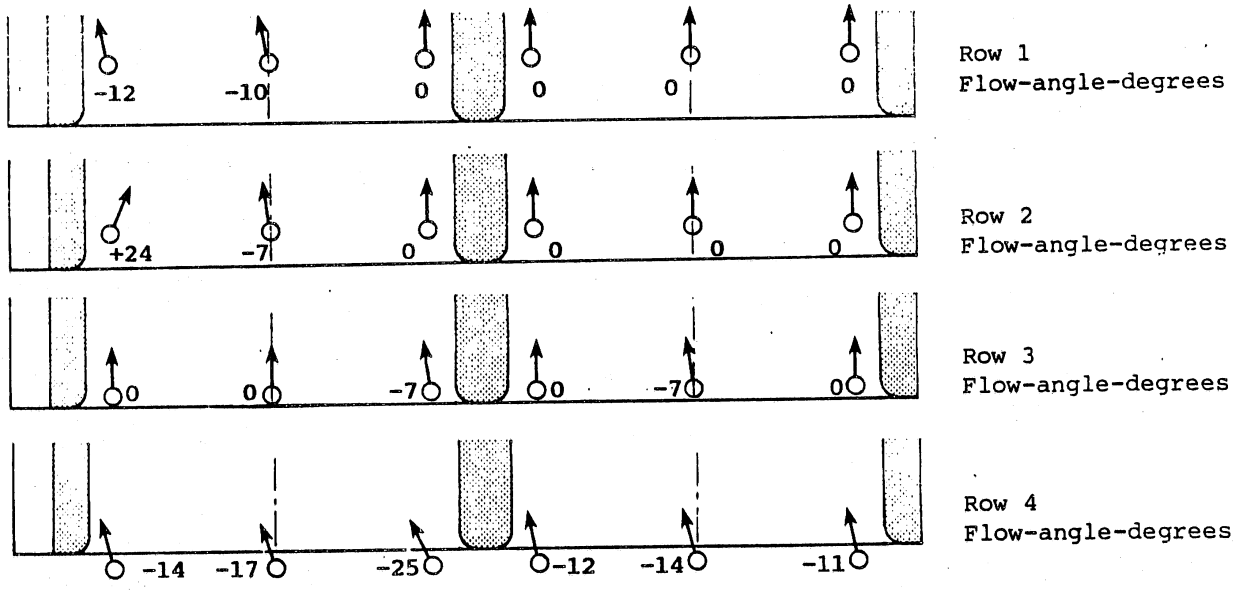

Plan Views
Directions of Flow

Figure 59
ST. CLOUD HYDROELECTRIC PROJECT
HYDRAULIC MODEL STUDIES
Type A9, Model Scale 1:24
Q_P = 6,500 cfs, Q_{GS} = 0 cfs
Q_{MS} = 0 cfs, H.W. = 981 ft
Typical Flow Directions